AFRL-VA-WP-TR-2004-3073

SMOOTHING, INTERPOLATING, AND MODELING COMPLEX MODULUS DATA FOR VISCOELASTIC DAMPING MATERIALS, INCLUDING A NEW APPROACH TO TEMPERATURE SHIFT FUNCTIONS

Lynn Rogers

Structural Mechanics Branch (AFRL/VASM)
Structures Division
Air Vehicles Directorate
Air Force Research Laboratory, Air Force Materiel Command
Wright-Patterson Air Force Base, OH 45433-7542

Bryce Fowler

CSA Engineering, Inc.
2565 Leghorn Street
Mountain View, CA 94043-1613

JULY 2004

Final Report for 01 July 2003 – 30 June 2004

STINFO FINAL REPORT

AIR VEHICLES DIRECTORATE
AIR FORCE MATERIEL COMMAND
AIR FORCE RESEARCH LABORATORY
WRIGHT-PATTERSON AIR FORCE BASE, OH 45433-7542

NOTICE

Using Government drawings, specifications, or other data included in this document for any purpose other than Government procurement does not in any way obligate the U.S. Government. The fact that the Government formulated or supplied the drawings, specifications, or other data does not license the holder or any other person or corporation; or convey any rights or permission to manufacture, use, or sell any patented invention that may relate to them.

This report has been reviewed by the Air Force Research Laboratory Wright Site Office of Public Affairs (AFRL/WS/PA) and is releasable to the National Technical Information Service (NTIS). At NTIS, it will be available to the general public, including foreign nationals.

This technical report has been reviewed and is approved for publication.

/s/
Lynn C. Rogers, P.E., Ph.D.
Aerospace Engineer, Emeritus
Structural Mechanics Branch

/s/
James W. Rogers Jr., Major, USAF
Chief, Structural Mechanics Branch
Structures Division

/s/
John Bowlus
Chief, Structures Division
Air Vehicles Directorate

This report is published in the interest of scientific and technical information exchange and does not constitute approval or disapproval of its ideas or findings

Do not return copies of this report unless contractual obligations or notice on a specific document requires its return.

REPORT DOCUMENTATION PAGE

Form Approved
OMB No. 0704-0188

1. REPORT DATE *(DD-MM-YY)*	2. REPORT TYPE	3. DATES COVERED *(From - To)*
July 2004	Final	07/01/2003 – 06/30/2004

4. TITLE AND SUBTITLE

SMOOTHING, INTERPOLATING, AND MODELING COMPLEX MODULUS DATA FOR VISCOELASTIC DAMPING MATERIALS, INCLUDING A NEW APPROACH TO TEMPERATURE SHIFT FUNCTIONS

5a. CONTRACT NUMBER
In-house

5b. GRANT NUMBER

5c. PROGRAM ELEMENT NUMBER
62201F

6. AUTHOR(S)
Lynn Rogers (AFRL/VASM)
Bryce Fowler (CSA Engineering, Inc.)

5d. PROJECT NUMBER
10A0

5e. TASK NUMBER
1F

5f. WORK UNIT NUMBER
0J

7. PERFORMING ORGANIZATION NAME(S) AND ADDRESS(ES)

Structural Mechanics Branch (AFRL/VASM)
Structures Division
Air Vehicles Directorate
Air Force Research Laboratory, Air Force Materiel Command
Wright-Patterson Air Force Base, OH 45433-7542

CSA Engineering, Inc.
2565 Leghorn Street
Mountain View, CA 94043-1613

8. PERFORMING ORGANIZATION REPORT NUMBER
AFRL-VA-WP-TR-2004-3073

9. SPONSORING/MONITORING AGENCY NAME(S) AND ADDRESS(ES)

Air Vehicles Directorate
Air Force Research Laboratory
Air Force Materiel Command
Wright-Patterson Air Force Base, OH 45433-7542

10. SPONSORING/MONITORING AGENCY ACRONYM(S)
AFRL/VASM

11. SPONSORING/MONITORING AGENCY REPORT NUMBER(S)
AFRL-VA-WP-TR-2004-3073

12. DISTRIBUTION/AVAILABILITY STATEMENT
Approved for public release; distribution is unlimited.

13. SUPPLEMENTARY NOTES
Report contains color.

14. ABSTRACT

The present theory and implementation methodology for the smoothing, interpolation, and modeling of complex modulus data for viscoelastic damping materials has achieved a substantial level of maturity, accuracy, and efficiency; moreover, interconversion among any of the dynamic mechanical properties, the display of relaxation and retardation spectra, and estimated relative molecular weight distribution are greatly facilitated. One key aspect of the approach is to use a ratio (where the order of the numerator and denominator are equal) of polynomials of first order factors to model the complex modulus; this guarantees intrinsically that the required properties of linear systems are satisfied, while also providing an ease of numerical convergence and of interconversion. A second key aspect is the use of the Wicket Plot to 1) edit and perform a quality check on the data, 2) smooth and interpolate the data, 3) map its arc length onto reduced radian frequency, thereby intrinsically defining the complex valued modulus as a function of the reduced radian frequency, and 4) determine the value of the temperature shift function for each experimental data point, an entirely new procedure.

15. SUBJECT TERMS
viscoelastic, vibration, noise, control, damping, complex modulus

16. SECURITY CLASSIFICATION OF:			17. LIMITATION OF ABSTRACT:	18. NUMBER OF PAGES	19a. NAME OF RESPONSIBLE PERSON (Monitor)
a. REPORT	b. ABSTRACT	c. THIS PAGE			Lynn Rogers
Unclassified	Unclassified	Unclassified	SAR	96	19b. TELEPHONE NUMBER *(Include Area Code)* (937) 902-2489

Standard Form 298 (Rev. 8-98)
Prescribed by ANSI Std. Z39-18

TABLE OF CONTENTS

Section **Page**

LIST OF FIGURES

Figures **Page**

FOREWORD

This report was prepared and the effort summarized herein was performed jointly by L. Rogers of the Structural Mechanics Branch, Structures Division, Air Vehicles Directorate, Wright-Patterson AFB and B. Fowler of CSA Engineering, Inc. The performance period was from July 1, 2003 to June 30, 2004. The development reported herein occurred and evolved during several programs over several years under sponsorship of the U.S. Air Force, which is gratefully acknowledged. The technical advice and assistance received from many associates of the vibration damping community are gratefully acknowledged.

ACKNOWLEDGEMENT

The development reported herein occurred during several programs over several years under sponsorship of the U.S. Air Force, which is gratefully acknowledged.

1 INTRODUCTION

There have been a growing number of successful, high-payoff service applications of viscoelastic damping materials for vibration and noise control. A crucial factor in the further advancement and application of damping technology is accurate and efficient smoothing, interpolation, modeling (SIM), presentation, retrieval, and dissemination of damping material design data[1]. The present document purports to improve the SIM state of the art. Most sets of data for dynamic mechanical properties of damping materials are generated for screening purposes or for engineering applications and, therefore, typically and justifiably, do not cover temperature and frequency ranges in a scientific manner. It is challenging to interpret the data in such a way as to be useful to the designer while providing a reliable indication of limitations.

The basic fractional calculus model for complex modulus (CM) is extremely valuable for a crucial step in the present effort. Fractional calculus has performed an important historical role and has been established as the basis for an accurate and efficient model for the CM of vibration damping materials[2,3,4]; it has also been related to molecular dynamics[5]. The slope of the temperature shift function (STSF) has been established as the property which causes CM data to be correctly shifted[6,7]. Bode diagrams from feedback control system methodology have been introduced for fractional powers[8], which are used here to lend insight into the CM model comprised of first-order powers. Historically, the wicket plot has been utilized in order to check for an obvious lack of quality/accuracy.

Viscoelastic material undergoing stress and strain of present interest is treated as a linear system; this may be sufficiently accurate or simply a first approximation. Consequently, a well-established body of mathematics from servomechanism feedback control systems applies. Specifically, the real and imaginary components (or any other pair) of CM (actually a frequency response function) must satisfy a certain mathematical interrelationship. The new model (the Ratio Model or just ratio) of the CM as a function of reduced frequency is used, namely, ratios of factored polynomials of integer order, and the individual factors are of first order, while the numerator and the denominator are of the same order. One pair of first order factors, one in the numerator and the other in the denominator, result in one step with respect to Bode diagram considerations. The Ratio Model intrinsically guarantees that the above interrelationship is satisfied. The wicket plot actually displays two components of the CM, namely the material loss factor and the magnitude (or real part) of the modulus. The present approach is based on evaluating parameters in the Ratio Model such that the interrelationship established by the wicket plot are maintained. The form of the Ratio Model has been selected for ease of fitting the wicket plot by initialization and iteration and for ease of interconversion between any one dynamic mechanical property and any other.

Once the values of the parameters of the Ratio Model are established, the set of CM data has been modeled as a function of reduced radian frequency with no knowledge of the temperature shift function (TSF) being required. Implicitly, each point on the arc length of the wicket plot is associated with a value of reduced radian frequency. To evaluate the temperature shift function for each experimental data point, the perpendicular distance from the point to the wicket plot determines an associated value of the reduced radian frequency. Knowing the associated value of the reduced radian frequency and the experimental frequency and temperature enables the calculation of the TSF for that point.

The present approach is interactive and highly automated and exploits modern computational power. This contrasts with the historical approach of defining the TSF visually, or perhaps by curve fitting techniques, for which at least three decades of experimental frequency coverage for each experimental temperature is highly desirable, which requires considerable experience, and is extremely time consuming.

2 CONSTITUTIVE EQUATIONS

The operator form of the constitutive equation for the linear, isothermal, isotropic, macroscopically homogenous, thermorheologically simple (TRS) (defined after Equation 19) viscoelastic material being deformed in shear is[2,9,10]

$$P(q_R)\tau(t) = Q(q_R)\gamma(t) \tag{1}$$

where $\tau(t)$ is the shear stress, $\gamma(t)$ is the strain, $P(q_R)$ and $Q(q_R)$ are polynomials in q_R, the operator, which is defined as

$$q_R = d/dt_R = \alpha_T d/dt = \alpha_T q\,, \tag{2}$$

where the reduced time and its differential are

$$t_R = t/\alpha_T(T); dt_R = dt/\alpha_T(T), \tag{3}$$

and the logarithmic form is

$$\log t_R = \log t - \log \alpha_T\,, \tag{4}$$

where t is time and $\alpha_T(T)$ is the TSF dependent on temperature, T [11]. The laplace transform (LT) of Equation 1 is

$$P(s_R)\tau(s_R) = Q(s_R)\gamma(s_R), \tag{5}$$

and the Fourier transform (FT) is

$$P(j\omega_R)\tau(j\omega_R) = Q(j\omega_R)\gamma(j\omega_R). \tag{6}$$

It is convenient to change between the time domain, the frequency domain and the laplace domain by simple algebraic substitution:

$$q_R = \alpha_T q \leftrightarrow s_R = \alpha_T s \leftrightarrow j\omega_R = \alpha_T j\omega\,. \tag{7}$$

The FT of Equation 1 leads to the definition of the complex shear modulus valid for steady state sinusoidal stress and strain

$$G(j\omega_R) = \tau^*(j\omega_R)/\gamma^*(j\omega_R) = Q(j\omega_R)/P(j\omega_R), \tag{8}$$

where $\tau^*(j\omega_R)$ denotes the FT of $\tau(t)$ and the reduced radian frequency is

$$\omega_R = \omega\alpha_T(T) = 2\pi f_R = 2\pi f\alpha_T(T), \tag{9}$$

which is a product of ω, the radian frequency in radians/s and the dimensionless temperature shift function, while f_R and f are in Hz, which is potentially confusing. The logarithmic form is

$$\log(\omega_R) = \log(\omega) + \log(\alpha_T); \log(f_R) = \log(f) + \log(\alpha_T). \tag{10}$$

Alternatively, let a viscoelastic material element undergo a sinusoidal shear strain[12]

$$\gamma = \gamma_A \sin\omega t\,, \tag{11}$$

which lags the sinusoidal shear stress

$$\tau = \tau_A \sin(\omega t + \delta_G) \tag{12}$$

by phase angle δ_G. The sinusoidal strain and stress may be represented in complex notation as

$$\gamma^* = \gamma_A e^{j\omega t} \tag{13}$$

$$\tau^* = \tau_A e^{j(\omega t + \delta_G)}, \tag{14}$$

and the complex shear modulus, *G*, equivalently defined and the imaginary component is

$$G = \tau^*/\gamma^* = \tau_A e^{j\delta_G}/\gamma_A = G_M e^{j\delta_G} = G_M \cos\delta_G \left(1 + j\tan\delta_G\right) \quad (15)$$

$$= G_R + jG_I = G' + jG'' = G_R\left(1 + j\eta_G\right), \quad (16)$$

where G_M is the magnitude of the shear modulus, $G_R = G'$ is the real (storage) modulus, the imaginary component is

$$G_I = G'' = G_R\eta_G\,, \quad (17)$$

and the material loss factor is

$$\eta_G = \tan\delta_G\,. \quad (18)$$

The CM is a mathematical convenience to represent the magnitude and phase relationship between stress and strain. The complex shear modulus is dependent on both temperature and frequency

$$G = G(\omega, T) = G\left(j\omega\ \alpha_T(T)\right) = G\left(j\omega_R\right) \quad (19)$$

in a very specific way, i.e., Equation 19 applies; a material obeying Equation 19 is called TRS.

A value for reference frequency which is reasonably close to that of many applications

$$f_{REF} = 100Hz; \omega_{REF} = 200\pi \sim rad/\sec \quad (20)$$

is used in the present effort.

3 THE BASIC FRACTIONAL MODEL

Many viscoelastic damping materials have a rubbery plateau, a transition region (where the modulus changes rapidly and the loss factor reaches a peak), and a glassy plateau. The basic fractional equation[2,13], which possesses these characteristics, is

$$G(j\omega_R)=\left[G_e+G_g(j\omega_R/\omega_{RO})^{\beta}\right]/\left[1+(j\omega_R/\omega_{RO})^{\beta}\right], \tag{21}$$

where the form of the parameters has been chosen to facilitate physical and mathematical interpretation. This expression is plotted in Figure 1. The expression for the maximum loss factor,

$$\eta_{\max}=(1-C)\tan(\pi\beta/2)/\left[1+C+2C^{1/2}/\cos(\pi\beta/2)\right];C=G_e/G_g\,, \tag{22}$$

$$\eta_{\max}\approx\tan(\pi\beta/2);Csmall \tag{23}$$

is of interest and the expression for the exponent

$$\beta=\left(\frac{2}{\pi}\right)\arctan\left\{\eta_{\max}\left[\frac{\left(1-C^2\right)+2(1-C)C^{1/2}\left(1+\eta_{\max}{}^2\right)^{1/2}}{(1-C)^2-4C\eta_{\max}{}^2}\right]\right\} \tag{24}$$

in terms of the other parameters in E21 is useful. Another useful relationship is that maximum loss factor occurs at a reduced radian frequency of

$$\omega_{R_{\eta\max}}=\omega_{RO}\left(G_e/G_g\right)^{1/2\beta}=\omega_{REF}\alpha_{\mathrm{T}}(\mathrm{T}_{REF}), \tag{25}$$

from which it may be determined

$$\omega_{R0}=\omega_{REF}\left(G_g/G_e\right)^{1/2\beta} \tag{26}$$

By combining Equation 26 and Equation 20 it follows that

$$\omega_{R0}=\omega_{REF}\left(G_g/G_e\right)^{1/2\beta}=200\pi\left(G_g/G_e\right)^{1/2\beta} \tag{27}$$

An alternative form of Equation 21 is useful for some purposes

$$G(j\omega_R)=G_g+\left[G_e-G_g\right]/\left[1+(j\omega_R/\omega_{RO})^{\beta}\right]. \tag{28}$$

The quantity

$$(\omega_R/\omega_{RO})^{\beta}=(\omega\alpha_T/\omega_{RO})^{\beta} \tag{29}$$

governs the transition and may cover a range of 10 decades or so. The phase is governed by

$$j^{\beta}=e^{j\pi\beta/2}=\cos(\pi\beta/2)+j\sin(\pi\beta/2). \tag{30}$$

Equation 28 $G(j\omega_R)$ may be written

$$G(j\omega_R)=G_g+\left[G_e-G_g\right]/P_B(j\omega_R);P_B(j\omega_R)=\left[1+(j\omega_R/\omega_{RO})^{\beta}\right],$$

where the subscript B is for the basic operator. B. Hartman, G. Lee, and J. Lee[14] have had success in fitting polyurethane CM data using the polynomial

$$P_{HN}(j\omega_R)=\left[1+(j\omega_R/\omega_{RO})^{\beta}\right]^{\gamma}$$

due to Havriliak and Negami (HN)[15] where

$$\gamma\approx 0.1;0.3\le\beta\le 0.7\,.$$

Salvia[16] had success in fitting sets of data using the polynomial

$$P_{SH}(j\omega_R) = 1 + \delta(j\omega_R)^{-h} + (j\omega_R)^{-k}$$

due to Huet[17] where

$$0 \le k \approx 0.6; 0 \le h \approx 0.3.$$

These models have the advantage of having a small number of parameters, which was especially desirable before the availability of modern computational power.

4 SOME PROPERTIES OF LINEAR SYSTEMS

Consider a single input, single output, causal, linear, constant-coefficient, stable, finite system and its associated frequency response function (FRF) in the form

$$H(f) = e^{-A}e^{j\delta}; \ln \mathrm{H} = -\mathrm{A} + j\delta \tag{31}$$

Properties of such a system are 1) a cause and effect relationship holds between input and output, 2) an applied input causes a unique output, 3) after a small perturbation, the output returns to an equilibrium state and the output dies out after a duration of the input, and 4) the value of all physical quantities are finite at all frequencies including zero and infinity.

It is well known that if one component (i.e., magnitude, phase, real or imaginary) of the FRF is specified over the entire frequency range, any other may be obtained from the one given. This relationship is believed due originally to Kramers and Kronig[11,18,19]. Gross published the following equations

$$G_R(\omega) = \frac{2}{\pi}\int_0^\infty G_I(\xi)\frac{\xi}{\omega^2 - \xi^2}d\xi \tag{32}$$

$$G_I(\omega) = \frac{2}{\pi}\int_0^\infty G_R(\xi)\frac{\omega}{\xi^2 - \omega^2}d\xi \quad . \tag{33}$$

The form of the CM model to be selected below will intrinsically guarantee that this property will be satisfied; this is a crucial point in the present work.

The property of systems will also be used to obtain relationships of the CM in general and also near the center of the transition region. It is well known that the loss factor is approximately proportional to the slope of both the magnitude and the real modulus. With reference to Equation 31, an equation useful for the present purpose is[20]

$$\begin{aligned} &\delta(\omega_d) = (\pi/2)\left|d\mathrm{A}/du\right|_0 + \\ &(1/\pi)\int_{-\infty}^{+\infty}\left[\left|d\mathrm{A}/du\right| - \left|d\mathrm{A}/du\right|_0\right]\ln\coth\left|u/2\right|du \end{aligned} \quad , \tag{34}$$

where

$$u = \ln(\omega/\omega_d). \tag{35}$$

An element of viscoelastic material may be considered to be a linear system with input of stress and output of strain or vise versa and the CM is a FRF. By comparing Equation 15 and Equation 31, it may be seen that

$$G_M = e^{-A}; \ln G_\mathrm{M} = -\mathrm{A}; dA/du = d\ln G_\mathrm{M}/d\ln\omega, \tag{36}$$

and, because the integral term is small (note that ω and ω_R are interchangeable in most of these relationships),

$$\delta \approx (\pi/2)d\log G_\mathrm{M}/d\log\omega, \tag{37}$$

or substituting Equation 18[21],

$$\eta \approx \tan[(\pi/2)d\log G_\mathrm{M}/d\log\omega]. \tag{38}$$

A numerical evaluation of this approximation is included in Figure 1. The inverse expression is sometimes useful

$$d\log G_\mathrm{M}/d\log\omega \approx (2/\pi)\arctan\eta \tag{39}$$

and shows that high values of loss factor and a large value of the derivative are associated. This relationship, Equation 38, is a first approximation over the entire frequency range and can be very good near the center of the transition region, or wherever $d\log G_{\mathrm{M}}/d\log\omega$ is nearly constant over a wide frequency range. For most materials of interest sufficiently near the center of the transition region

$$G_M \propto \omega^{\beta}; G_R \propto \omega^{\beta}; d\log G_{\mathrm{M}}/d\log\omega \approx \beta \tag{40}$$

or, combining Equation 38 and Equation 40, considering the particular properties of the CM,

$$\eta_{\max} = \tan(\pi\beta/2) = \tan\delta_{\max} \quad . \tag{41}$$

(Compare with Equation 23.)

5 BODE DIAGRAMS

The technique of Bode diagrams is a highly developed tool in servo feedback control systems analysis[21]. The logarithm of a complex number

$$z = Me^{j\phi} \tag{42}$$

is also a complex number:

$$\log z = \log \mathrm{M} + (0.434....)(j\phi). \tag{43}$$

Multiplication and division of complex numbers or complex-valued functions become addition and subtraction in the logarithmic domain.

$$H = N_1 N_2 / D_1 D_2; \log \mathrm{H} = \log \mathrm{N}_1 + \log \mathrm{N}_2 - \log D_1 - \log D_2 . \tag{44}$$

Separating Equation 44 into real and imaginary components leads to expressions for the magnitude and the phase:

$$\begin{aligned} &\log|H| = \log|H| + \log|H| - \log|H| - \log|H|; \\ &\phi_H = \phi_{N_1} + \phi_{N_2} - \phi_{D_1} - \phi_{D_2} \end{aligned} . \tag{45}$$

A complex valued frequency response function in feedback control systems may be written as ratios of factored polynomials. The asymptotes of individual factors play the dominant role in the Bode diagram technique. The CM is a frequency response function; only one type of factor is of interest here:

$$z = 1 + (jR)^{1/2}, \tag{46}$$

where R is a normalized frequency. The magnitude and the phase of Equation 46 are plotted in Figure 2 together with their asymptotes. The frequency where the magnitude asymptotes intersect (at R = 1) is called a “corner” or “break” frequency. When the factor appears in the denominator, its magnitude and phase are mirror images reflected about 1 and 0, respectively. Consider now a pair of factors, one in the numerator and another in the denominator:

$$\left[1 + (j\omega/z_1)^{1/2}\right] / \left[1 + (j\omega/p_1)^{1/2}\right]; z_1 < p_1 . \tag{47}$$

This ratio of a pair of factors results in a stair step in the magnitude asymptotes where the slope of the riser is 1/2. Two such steps are illustrated in Figure 3.

General fractional order factors are similar; while integer orders are standard in servo feedback systems methodology. It happens that an adequately large number of this type of step accurately, efficiently and conveniently represents a CM and that any other dynamic mechanical property of interest can be easily obtained. The asymptotes provide a basis of visualizing expressions for the CM. The basic fractional model Equation 21 can be considered to advantage in terms of Bode diagrams. It is valuable both for visualization and as a first approximation in modeling a set of experimental CM data.

6 THE MODEL FOR CM

A model which is a ratio of factored polynomials of fractional order[1,2,8,22],

$$G(j\omega_R) = G_e \prod_{l=1}^{N} \left[1 + (j\omega/z_1)^{\beta}\right] / \left[1 + (j\omega/p_1)^{\beta}\right], z_1 < p_l, \tag{48}$$

has been investigated, and it has been observed that using the fractional power, β;0<β<1, does not result in either accuracy or efficiency in fitting CM data; it does preclude ease of interconversion with other dynamic properties unless β=1/2. Its use does not enable a relatively small number of parameters to be used. After extensive experience in fitting sets of CM data, the model selected is a ratio of factored polynomials of integer order, where each factor is of the first order and the numerator and denominator are of equal order. It happens that this form is particularly convenient for interconversion to other dynamic mechanical properties, as will be shown. Furthermore, Bode diagram considerations lead to convenient iteration algorithms in determining values for the parameters. Modern computational power is used to great advantage:

$$G(j\omega_R) = G_e \prod_{i=1}^{N} (1 + j\omega_R/z_i)/(1 + j\omega_R/p_i); z_i < p_i. \tag{49}$$

See Figure 4. It is convenient to rewrite this equation in terms of r_i, which determines the location of the center of the riser, and a_i, which determines the vertical height of the riser (the asymptote of the riser is slope one), as follows:

$$G(j\omega_R) = G_e \prod_{i=1}^{N} (1 + j\omega_R a_i/r_i)/(1 + j\omega_R/a_i r_i); \tag{50}$$

the parameters are related by

$$p_i = a_i r_i; z_i = r_i / a_i; r_i^2 = p_i z_i; a_i^2 = p_i / z_i. \tag{51}$$

This equation is called the Ratio Model and inherently satisfies the real-imaginary component relationship, Equation 32 and Equation 33; this is vital to the present approach. Note the use of ω_R in lieu of f_R; this is a source of potential confusion in numerical work. Equation 49 is a frequency response function and the associated transfer function is

$$G(s_R) = G_e \prod_{i=1}^{N} (1 + s_R / z_i)/(1 + s_R / p_i). \tag{52}$$

If Equation 52 is divided by s_R, the method of partial fractions and the heaviside expansion formula (see any text covering laplace transforms) may be applied; the result is then multiplied by s_R to give a sum of fractions:

$$G(s_R) = G_e + \sum_{i=1}^{N} (G_i s_R / p_i)/(1 + s_R / p_i), \tag{53}$$

where

$$G_k = -G_e \prod_{l=1}^{N} (1 - p_k / z_l) / \prod_{\substack{l=1 \\ l \neq k}}^{N} (1 - p_k / p_l), \tag{54}$$

which may be placed in the form

$$G_k = G_e\left(a_k^2 - 1\right)\prod_{\substack{l=1 \\ l\neq k}}^{N} \frac{1 - a_k a_l r_k\,/(r_l)}{1 - a_k r_k\,/(a_l r_l)}.$$

Note that Equation 53 may be placed in GHM form[23,24]; consider two terms, without loss of generality, from Equation 53:

$$\frac{G_1 s_R}{p_1 + s_R} + \frac{G_2 s_R}{p_2 + s_R} = \frac{\left(G_1 + G_2\right)s_R^2 + \left(G_1 p_2 + G_2 p_1\right)s_R}{s_R^2 + \left(p_1 + p_2\right)s_R + p_1 p_2}. \tag{55}$$

The CM in a form corresponding to E53 is

$$G\left(j\omega_R\right) = G_e + \sum_{\iota=1}^{\mathrm{N}} \left(G_\iota\, j\omega_R/p_\iota\right)/\left(1 + j\omega_R/p_\iota\right), \tag{56}$$

which may be written such that real and imaginary components are apparent:

$$G\left(j\omega_R\right) = G_e + \sum_{\iota=1}^{\mathrm{N}} G_\iota\left[\left(\omega_R/p_\iota\right)^2 + j\left(\omega_R/p_\iota\right)\right]/\left[1 + \left(\omega_R/p_\iota\right)^2\right]. \tag{57}$$

The transfer function for the relaxation modulus is easily found from Equation 53[9]

$$G_{RLX}\left(s_R\right) = G\left(s_R\right)/\,s_R = G_e\,/\,s_R + \sum_{i=1}^{N} G_i\,/\left(p_i + s_R\right) \tag{58}$$

and, its inverse LT leads to the relaxation modulus

$$G_{RLX}\left(t_R\right) = G_e + \sum_{k=1}^{N} G_k e^{-p_k t_R}. \tag{59}$$

Shapery has had success in representing the relaxation modulus with this expression, which is a Prony series. The discrete relaxation spectra is[9]

$$H\left(\tau_{p_k}\right) = \mathrm{H}_k = G_k \tau_{p_k}/\Delta_k \tau_p, \tag{60}$$

where

$$\tau_{p_k} = \frac{1}{p_k}; \Delta_k \tau_p = \frac{\tau_{p_{k+1}} - \tau_{p_k}}{2} - \frac{\tau_{p_k} - \tau_{p_{k-1}}}{2}. \tag{61}$$

Substitution leads to

$$H_k = G_k \Big/ \left[\frac{p_k}{2}\left(\frac{1}{p_{k+1}} - \frac{1}{p_{k-1}}\right) - 1\right]. \tag{62}$$

Consider a specimen subjected to a positive step shear strain input at time = 0, as in the stress relaxation case, but then immediately followed by a negative step function at time =δt. The magnitude of the step is such that the area under the strain-time curve (i.e., the strain impulse) is unity. The time increment is then allowed to become a differential. In systems analysis, the resulting response quantity is called the impulsive admittance, and by analogy is here called the impulsive modulus. It is found by taking the derivative of Equation 59:

$$G_{IM}\left(t_R\right) = -\sum_{k=1}^{N} G_k p_k e^{-p_k t_R}. \tag{63}$$

The complex compliance is the reciprocal of Equation 49. A similar development yields analogous expressions for creep compliance and retardation spectra:

$$J(j\omega_R) = J_e - \sum_{\iota=1}^{N} J_\iota j\omega_R/(z_\iota + j\omega_R). \tag{64}$$

Knaus, following Schapery, represented the creep compliance as[9]

$$J_{CRP}(t_R) = J_g + \sum_{i=1}^{N} J_i\left(1-e^{-z_i t_R}\right), \tag{65}$$

where

$$J_k = -J_e \prod_{l=1}^{N} (1 - z_k / p_l) / \prod_{\substack{l=1 \\ l\neq k}}^{N} (1 - z_k / z_l) \tag{66}$$

which may be placed in the form

$$J_k = J_e\left(1/a_k^2 - 1\right)\prod_{\substack{l=1 \\ l\neq k}}^{N} \frac{1 - r_k/(a_k a_l r_l)}{1 - a_l r_k/(a_k r_l)}.$$

The discrete retardation spectra is[9]:

$$L_k = J_k \Big/ \left[\frac{z_k}{2}\left(\frac{1}{z_{k+1}} - \frac{1}{z_{k-1}}\right) - 1\right]. \tag{67}$$

When the specimen is subjected to a stress impulse, the impulsive compliance is found from Equation 65:

$$J_{IM}(t_R) = \sum_{i=1}^{N} J_i z_i e^{-z_i t_R}. \tag{68}$$

When the input function is a force, then the area is actually a mechanical impulse. The impulsive modulus and impulsive compliance would be useful in studies of response to impulsive types of loading, e.g., shock, or for use in convolution integrals.

At this juncture, the ratio of polynomials of first-order factors has been covered as the preferred model. Expressions have been developed for relaxation modulus, relaxation spectrum, creep compliance, and retardation spectrum. Some interconversion of the dynamic mechanical properties is accomplished in closed form as indicated above; others may be performed numerically but are greatly facilitated by the above expressions.

7 MOLECULAR WEIGHT DISTRIBUTION

Some investigators may be interested in an indication of the relative molecular weight distribution. The following is extracted from the literature in only a formal manner and presented without comment regarding applicability or appropriateness. One investigator has developed an expression for the cumulative molecular weight distribution[25]:

$$C_{MWD_W} = G_R(j\omega_R)/G_g, \tag{69}$$

while an expression developed by another investigator[26] is

$$C_{MWD_T} = \left[G_R(j\omega_R)/G_g\right]^{1/2}. \tag{70}$$

In both of these expressions, the plateau modulus, which is the maximum real modulus in the terminal zone, has been taken as the glassy asymptote. The molecular weight distribution is proportional to the derivative,

$$M_{WD} \propto \frac{d}{d(\ln \omega_R)} C_{MWD}, \tag{71}$$

and the relative molecular weight distribution may be expressed

$$R_{MWD} = \frac{d}{d(\ln \omega_R)} C_{MWD} = \omega_R \frac{d}{d\omega_R} C_{MWD} \tag{72}$$

when Equation 69 is substituted into Equation 72:

$$R_{MWD_W} = \frac{1}{G_g} \frac{\omega_R dG_R(j\omega_R)}{d\omega_R}, \tag{73}$$

or when Equation 70 is substituted into Equation 72:

$$R_{MWD_T} = \frac{1}{2\left[G_g G_R(j\omega_R)\right]^{1/2}} \frac{\omega_R dG_R(j\omega_R)}{d\omega_R}. \tag{74}$$

The proportionality relationship between frequency and molecular weight is[26]

$$1/\omega_R \propto (\mathrm{M}_W)^{3.4}, \tag{75}$$

or the normalized molecular weight is given by

$$N_{MW} = \omega_R^{-0.294}. \tag{76}$$

The range of ω_R should be confined to the experimental range. The real part of Equation 57 is

$$G_R(j\omega_R) = G_g + \sum_{\iota=1}^{\mathrm{N}} G_\iota \omega_R^2/\left(\omega_R^2 + p_\iota^2\right), \tag{77}$$

and its derivative is

$$\frac{dG_R(j\omega_R)}{d\omega_R} = \sum_{\iota=1}^{\mathrm{N}} 2G_\iota \omega_R p_\iota^2/\left(\omega_R^2 + p_\iota^2\right)^2. \tag{78}$$

Substituting Equation 78 into Equation 73 results in one estimate of relative molecular weight distribution:

$$R_{MWD_W} = \frac{2}{G_g} \sum_{i=1}^{N} G_i \omega_R^2 p_\iota^2/\left(\omega_R^2 + p_\iota^2\right)^2; \tag{79}$$

substituting Equation 78 into Equation 74 results in another:

$$R_{MWD_T} = \frac{1}{\left[G_g G_R\left(j\omega_R\right)\right]^{1/2}} \sum_{i=1}^{N} G_i \omega_R^2 p_i^2 / \left(\omega_R^2 + p_i^2\right)^2 . \tag{80}$$

It may be seen that the form of the expressions facilitates these calculations.

8 A SPECULATED POISSON'S RATIO

Some investigators may be interested in a complex valued Poisson's ratio. The generalized Hooke's law for elastic materials may be written:

$$\sigma_{kl} = \lambda \delta_{kl} \Phi + 2Ge_{kl} . \tag{81}$$

By analogy with Equation 1, operators may be placed in front of each term[2,9]

$$P(q_R)\sigma_{kl} = R(q_R)\delta_{kl}\Phi + 2Q(q_R)e_{kl} , \tag{82}$$

which is consistent with the previous complex shear modulus (see Equation 8), where the operators are taken to be

$$P(j\omega_R) = 1 + (j\omega_R/\omega_{RO})^{\beta} \tag{83}$$

and

$$Q(j\omega_R) = G_{RBR} + G_{GLS}(j\omega_R/\omega_{RO})^{\beta} . \tag{84}$$

The other operator (obviously correct in the rubbery and also the glassy regions, which only leaves the transition open to discussion) by analogy, assumption, conjecture, and/or speculation is taken to be

$$R(j\omega_R) = \lambda_{RBR} + \lambda_{GLS}(j\omega_R/\omega_{RO})^{\beta} , \tag{85}$$

and, therefore, the complex valued lamme expression is obtained as

$$\lambda(j\omega_R) = \frac{\lambda_{RBR} + \lambda_{GLS}(j\omega_R/\omega_{RO})^{\beta}}{1 + (j\omega_R/\omega_{RO})^{\beta}} . \tag{86}$$

It might be interesting to investigate

$$Q(j\omega_R) = G_{RBR} + G_{GLS}[P(j\omega_R) - 1]$$

in order to accommodate a more general operator such as P_{HN} or P_{SH} above. It is further conjectured that

$$R(j\omega_R) = \lambda_{RBR} + \lambda_{GLS}[P(j\omega_R) - 1],$$

which leads to

$$\lambda(j\omega_R) = \{\ \lambda_{RBR} + \lambda_{GLS}[P(j\omega_R) - 1]\ \} / P(j\omega_R).$$

At the present writing, these quantities have not been investigated.

Due to the correspondence principle of viscoelasticity, the relationships,

$$\lambda = G/(1/2\upsilon - 1) \tag{87}$$

$$E = G(3\lambda + 2G)/(\lambda + G) \tag{88}$$

$$\upsilon = \lambda/2(\lambda + G) \tag{89}$$

$$\mathrm{K} = \lambda + 2G/3 \tag{90}$$

$$\mathrm{W} = \lambda + 2G \tag{91}$$

are valid for the rubbery region, the glassy region, the Fourier transform, the laplace transform, the operator form, and complex valued quantities. The quantities are lamme, Youngs, Poissons, bulk, and plane wave (or longitudinal), respectively. For certain types of materials, there is a tendency for Poisson's ratio to be considered as a basic quantity along with another such as shear

modulus. As the rubbery value of Poisson's ratio approaches 0.5, it has a dramatic effect on the rubbery value of W, K, and λ, and also on the max loss factor of these quantities. By contrast, the glassy value of Poisson's ratio does not have a large effect on the other quantities. To illustrate this, a table has been constructed with a glassy shear modulus of 200.0 and a rubbery shear modulus of 0.0004; the glassy values for Poisson's ratio are 0.35 and 0.3, while the rubbery values are 0.495 and 0.49995. Rubbery and glassy values for the other quantities are tabulated. Figure 5 shows a typical transition for Poisson's ratio for the hypothesized relations. Figure 6 and Figure 7 show a comparison of loss factor for the quantities and the dramatic effect of the value for Poisson's ratio as it approaches 0.5. As a consequence, the modal frequencies and damping for structures and modes where a significant amount of strain energy is in bulk type of stress and strain will be sensitive to the rubbery value of Poisson's ratio. In this event, Modal Strain Energy (MSE) calculations should distinguish between bulk and shear strain energy due to the effect on modal damping (or modal loss factor) and on material loss factor.

9 THE WICKET PLOT

The first step in processing any set of CM data is to examine the collection of the experimental data points in the wicket plot format, which is $log\eta_G$ versus $logG_R$. Although $logG_R$ is often displayed because it is of interest during design applications, $\log G_M$ is used for Bode plot visualization and in the software calculations. For conventional viscoelastic damping materials ($\eta_{\max} \approx 1$), consideration of $log\eta_G = logtan\delta$ is satisfactory. It does distort the scale for high loss factor and for low loss factors, where a scale in linear phase angle, δ, would be more appropriate. Perhaps in the future, the damping industry will adopt the linear scale in phase angle. The wicket plot is related to the Nichols chart and the attendant body of mathematics developed by electrical engineers during the 1940s for analysis and design of feedback servo systems. If the set of data represents a TRS material, does not require a vertical shift of modulus for temperature and/or density, and has no scatter, the collection of data points will plot as a curve of vanishing width. Each location along the arc length, s, of the curve corresponds to a unique value of reduced radian frequency (see Equation 19); however, this consideration is postponed until after the mapping step below. The material loss factor and the real modulus are cross-plotted in the wicket plot, and the reduced radian frequency, temperature, and frequency parameters do not appear. No part of any scatter in the wicket plot can be attributed to an imperfect temperature shift or modeling. The wicket plot may possibly reveal valuable information regarding scatter in the experimental data. The width of the band of data, as well as the departure of individual points from the band, are indicative of scatter. Acceptable scatter depends on the application. Nothing is revealed about the accuracy of measurements or about any systematic error. Low scatter in a wicket plot is a necessary but not a sufficient condition of data quality. Consistency does not indicate accuracy.

Ideally, the wicket plot would be maintained current as the set of data is being gathered to ensure adequate range of temperature and frequency as well as a real time indication of data quality or any problems. The wicket plot is an ideal way to remove individual outlying data points.

At one time, the approach to smooth, interpolate, and model a set of CM data began with using the wicket plot interactively to estimate values for G_e, G_g, and η_{max} (respectively the equilibrium or rubbery asymptote, the glassy asymptote, and the maximum material loss factor). These quantities were used to calculate the exponent, β, using E 24. A value for η_{cutoff} was also determined to select that subset of data points within the transition region (see Figure 8). This approach results in a reasonable approximation to the VEM properties in the transition region, and was necessary in the previous SIM approach.

After the set of data is examined and edited in the wicket plot, an Analytical Wicket is developed as the next step of the latest approach to the SIM process. The vertical axis is taken as $y=\log\eta$; the horizontal axis $x = logG_M$. The range of experimental data on the wicket plot is represented by a series (approximately 15) of cubic splines. The set of data is divided into regions along the arc length of the wicket with approximately the same number of points in each region. The points in each region are used to determine a best fit quadratic from which an xyy' are determined and used as a common knot for the two splines on each side of the knot. The knots are represented by

open circles in Figure 8 through Figure 12. Each experimental data point has a perpendicular distance, d, to the set of splines (shown in Figure 8 through Figure 12) and is associated with a unique arc length, s. The xyy'/sdd' knots may be adjusted to minimize the sum of squares of the d's. After the data region is characterized, the model Equation 50 cannot be terminated because of considerations of Equation 34. A graceful/reasonable extrapolation of the skirts of the wicket plot beyond the range of experimental data is essential. At present, a set of splines is used in the rubbery skirt region from the last data knot to a knot with loss factor two decades less and the slope gradually changing. A similar set is used in the glassy skirt region. (Alternatively, skirts from the basic CM equation could be used.) The combined set of splines (i.e., rubbery skirt, data region, and glassy skirt) serve to define uniquely and precisely the loss factor as a function of modulus magnitude as well as to smooth and interpolate the data and is called the Analytical Wicket. It is intended to be a good representation of the center and of the slope for the band of data and an appropriate extrapolation into the skirts. The maximum value of the Analytical Wicket defines the η_{max} and the associated $G_{M\eta max}$. Furthermore, consistent with Equation 20, the numerical value for the reduced radian frequency associated with this point will be assigned later is this process to be identical to that of the reference-reduced radian frequency, 200π rad/s (see Figure 8 through Figure 12).

If the skirts of the basic fractional model were to be used to extrapolate, cutting the curve at the points where the slopes of the curve and of the slope, y', of the end knots of the range of experimental data are identical, and shifting the skirt left and right (adjusting x), and also up and down (adjusting y) until the slope and the xy points are superimposed would be required. Final values of the G_e and the G_g must be obtained by adjusting the old values by the amount of the horizontal shift and a final value for $\beta\left(G_e, G_g, \eta_{\max}\right)$ representative of this set of data can be calculated. This grafting of the skirts onto the set of splines has the effect of extending the definition of loss factor as a function of modulus magnitude for this set of data.

The Analytical Wicket is taken as the definition of the data in so far as the relationship between material loss factor and the modulus magnitude is concerned. The experimental points will be used further in determining the TSF. The constraint of the Analytical Wicket must be followed in the determining of values for the parameters in the Ratio Model.

10 MAPPING

The x-y trajectory of a thrown ball is used as an example of mapping and is illustrated by Figure 13. Imagine that a set of tabulated x-y displacement data from a multiple stroboscopic photographic exposure through a window is available. The set of data may be cross plotted in the x-y domain without regard to time. Analytic geometry may be used to describe the trajectory in the x-y domain, and also if desired, to describe x and y as functions of the arc length of the trajectory. From physics, the equations of x and y as functions of time are known in terms of parameters whose values may be determined from experimental data. The arc length of the trajectory may be mapped into time and is justified by consideration of physics.

Very intricate x-y curves (e.g., handwriting) can be represented by using the Bezier or other parametric approach. The present application is not so challenging.

Similar to the trajectory, the arc length of the wicket plot may be mapped into reduced radian frequency and is justified by the mathematical properties of systems. The basis of the mapping is the real-imaginary (or any other two components) relationship of linear systems. The form of the Ratio Model is particularly amenable to the mapping and rapid convergence.

The mapping consists of first initiation and then iteration until convergence. Equation 53 using the r_i's and a_i's has been found to be most convenient; the r_i's are equally spaced on the log reduced radian frequency, ω_R, and do not change for the iteration. Nr = Ndec * Nspd; where Nr is the total number of points, Ndec is the number of decades of reduced radian frequency and Nspd is the number of steps per decade. The *r's* become

$$r_{i+1} = r_i \delta r; \delta r = 10^{1/\mathrm{N}spd}. \tag{92}$$

The set of initial estimates of parameter values for the Ratio Model is determined by evaluating Equation 21 at each Bode diagram step (i.e., at the center of each ratio of an associated pair of factors) in the model. The effective G_e for the initialization is taken to be (gadjust*G_e) from the last rubbery knot, while the effective G_g is taken to be G_g/gadjust. These adjustments are necessary to ensure that the Analytical Wicket defines a loss factor for the entire range of modulus magnitude from the ratio. The value for $\eta_{\max}$ is from the Analytical Wicket; an effective beta is calculated. The Ratio Model with initial values of parameters is shown in Figure 14 through Figure 16 where the initial location of the r_i's are indicated by the circles and compared to the Analytical Wicket.

Iteration is based on Equation 34 approximated by Equation 37 or, equivalently, Equation 38; the loss factor is strongly dependent on the local slope of the magnitude. With reference to Figure 17, r_i indicates the beginning location of the center of a vertical strip/slice with associated values for the magnitude and loss factor from the Ratio Model. The horizontal and vertical axes do not change and the curves are on a stretchable/compressible transparent layer portions of which also possibly slides right and left and/or up and down as a rigid body. If the width of the strip is increased or stretched (by increasing the value for a_i), the slope of the magnitude curve is decreased and consequently the ratio loss factor would be decreased. When the strip is stretched,

the curves for either the higher or lower reduced radian frequency will slide left or right, and some accommodation must be made.

In present practice, iteration consists of calculating the modulus magnitude and loss factor given by the Ratio Model at each value of r_i, calculating the loss factor from the Analytical Wicket associated with the value of the Ratio Model modulus, comparing the Ratio Model loss factor to the wicket loss factor, and adjusting the value of the a_i's to make the ratio loss factor value more closely agree with that of the Analytical Wicket. The new a_i is approximated by Equation 38 in terms of the old a_i, the loss from the ratio, and the loss from the wicket, but only a fraction of the indicated change is made during each iteration pass. Bode diagram visualization provides guidance on this adjustment algorithm.

Convergence has been achieved when the values for the parameters in the Ratio Model do not change significantly with successive iterations; hopefully the Ratio Model matches the Analytical Wicket very closely (see Figure 18 through Figure 20). The location of the r_i's are again indicated on the plots. Very often, the ratio does not closely match the Analytical Wicket at the extremes; this is due to a numerical artifact not yet understood. Most often it occurs beyond the range of experimental data.

After convergence, all of the r_i's are changed by a constant multiplier in order to cause $G_{M\eta\max}$ to occur at the reference reduced radian frequency, $\omega_{REF} = 200\pi$. This causes the temperature for which the value of the temperature shift function (which is yet TBD) is one to be the temperature for which the loss factor is the maximum for the reference 100 Hz cyclic frequency.

At this juncture, the SIM of the complex valued modulus as a function of reduced radian frequency is complete and the frequency and temperature of the data points have not yet been considered. Also, the arc length of the Analytical Wicket has been implicitly mapped into reduced radian frequency; i.e., a unique value of reduced radian frequency is associated with every value of arc length and therefore with the intersection of the perpendicular distance to each experimental point. This will be used to calculate the TSF. The operators in Equation 1 have been synthesized and are available for all other possible uses.

11 THE TEMPERATURE SHIFT FUNCTION

The value of reduced radian frequency associated with each experimental data point may be found by considering the perpendicular distance to the wicket plot as illustrated in Figure 21. Given the experimental temperature, the experimental frequency, and the associated reduced radian frequency for each CM data point, the individual values for the TSF may be calculated:

$$\alpha_T\left(T_{E_t}\right) = \omega_{R_t}/2\pi f_{E_t} . \tag{94}$$

This is a totally new method of determining the TSF. See TSF points in Figure 22 through Figure 26; TSF versus 1000/T in Figure 27 through Figure 29. It may be desirable to fit a local quadratic or the Arrhenius equation (see Equation 95) to only the transition points to obtain an initial estimate of the reference temperature and of the corresponding value of the slope.

The set of CM data itself implicitly defines the TSF, and one purpose of any method to smooth, interpolate and model a set of CM data is to facilitate this. The present method is well founded on mathematical rigor and is believed to be insensitive to limited frequency and temperature ranges, data scatter, etc.

It is assumed that a single TSF is applicable.

12 TSF EQUATIONS

It remains to smooth, interpolate, and model the temperature shift as a function of temperature. This is done by a best fit of equations to the TSF points. The Arrhenius expression is one TSF (designated "A" TSF) commonly used; in the present notation it is

$$\log \alpha_T(T) = s_{AZ} T_Z^2 (1/T - 1/T_Z) \tag{95}$$

it follows that the slope (STSF) of the Arrhenius expression is a one-term quadratic in (1/T):

$$d \log \alpha_T / dT = s_{AZ} T_Z^2 / T^2 . \tag{96}$$

Some investigators are interested in the apparent activation energy (AAE) and the general expression is

$$\Delta H_A = 2.303 R T^2 d \log \alpha_T / dT , \tag{97}$$

where the gas constant is

$$R = 0.00828 newton^* km/gram^* mole^* degK . \tag{98}$$

If the Arrhenius expression for TSF and its associated STSF are substituted, the corresponding expression for the Arrhenius AAE is

$$\Delta H_A = 2.303 R s_{AZ} T_Z^2 , \tag{99}$$

which is a constant. This expression shows that the apparent activation energy is proportional to s_{AZ} and indicates that if the TSF is insensitive to temperature (i.e., if the properties of a VEM do not change much as a function of temperature), then the AAE is small.

Because of the relevance of the Arrhenius expression, an expression has been developed in which the slope is a more general quadratic in $1/T$ [27] than the STSF of the Arrhenius:

$$- d \log \alpha_T(T)/dT = a(1/T - 1/T_Z)^2 + b(1/T - 1/T_Z) + s_{AZ} . \tag{100}$$

(Perhaps a different quadratic more closely related to the slope of the Arrhenius

$$s_{AZ} T_Z^2 / T^2 + b'(1/T - 1/T_Z) + c'$$

would have been more appropriate; compare with Equations 96 and 100.) Integrating the slope and choosing the constant of integration for convenience gives the following expression for the "Q" TSF yields

$$\log \alpha_T(T) = a(1/T - 1/T_Z) + 2.303(2a/T_Z - b)\log(T/T_Z) + (b/T_Z - a/T_Z^2 - s_{AZ})(T - T_Z) . \tag{101}$$

This equation may be fit through three points.

The WLF is also a widely used expression for the "W" TSF and, in the present notation is

$$\log a_T(T) = -s_{AZ}(T - T_Z)/(1 + (T - T_Z)/C_2) \; ; T > T_Z - C_2 , \tag{102}$$

where the commonly used parameters are related by $s_{AZ} = C_1/C_2$ and the STSF is

$$- d \log \alpha_T(T)/dT = s_{AZ}(1 + (T - T_Z)/C_2)^2 . \tag{103}$$

Another TSF expression used is the exponential which in the present general (EG TSF) notation is

$$\log \alpha_T(T) = -2.303 C_e s_{AZ} \log(1 + (T - T_Z)/C_e) \; ; T > T_Z - C_e , \tag{104}$$

and its STSF is

$$-d\log\alpha_{\mathrm{T}}(\mathrm{T})/d\mathrm{T} = s_{\mathrm{AZ}}\left(1+(\mathrm{T}-\mathrm{T}_{\mathrm{Z}})/C_e\right)\ . \tag{105}$$

Two sets of values of parameters used in the past are (EA TSF & ED TSF):

$$ADN: s_{AZ} = 0.0490, C_e = 97.6K; DIGJ: s_{AZ} = 0.0394, C_e = 154.4K\ . \tag{106}$$

Figure 22 through Figure 26 present the TSF points as a function of temperature as well as three equations (the WLF, the slope as a quadratic in (1/T), and a fourth-order polynomial) which have been regression fitted to the data. Figure 27 through Figure 29 are plots of the TSF plotted versus 1000/T for the three VEMs processed in the present effort; because none of these three appear to be a straight line, the Arrhenius equation is not used further in the present effort. Using the fourth-order polynomial, slopes are plotted in Figure 30 through Figure 32 and the AAE in Figure 33 through Figure 35. The usual International Plot Nomograms[28] with solid lines/curves indicating the experimental range are presented as Figure 36 through Figure 40. Only the nomogram is of direct interest to designers, while the TSF, the slope, the AAE, and other quantities are of more detailed or specialized interest.

13 REDUCED TEMPERATURE

From the concept of reduced frequency, it follows that (within practical limits) there are equivalent combinations (T_1,f_1) and (T_2,f_2) for which

$$f_{R1} = f_1\alpha_T(T_1) = f_{R2} = f_2\alpha_T(T_2); T_1 \neq T_2,\ f_1 \neq f_2. \quad (107)$$

For reduced frequency, a reference temperature is selected and the experimental frequency and temperature are used

$$f_{Ri} = f_{REDi}\alpha_T(T_{REF}) = f_{Et}\alpha_T(T_{Et}) \quad (108)$$

or

$$f_{Ri} = f_{REDi} = f_{Ei}\alpha_T(T_{Et}); \alpha_T(T_{REF}) = 1. \quad (109)$$

For the reduced temperature concept, it follows that

$$f_{REF}\alpha_T(T_{REDt}) = f_{Et}\alpha_T(T_{Et}) \quad (110)$$

or

$$\alpha_T(T_{REDt}) = \alpha_T(T_{Et})f_{Et}/f_{REF}. \quad (111)$$

Given $\alpha_T(T)$,T_{Ei},f_{Ei} and f_{REF}, it is a simple matter to find a numerical value for T_{REDi} such that Equation 111 is satisfied. If the Arrhenius Equation 95 TSF is used, the reduced temperature may be expressed directly:

$$T_{REDi} = T_{Ei}/[1 + (T_{Ei}/s_{AZ}T_Z^2)\log\omega_{Et}/\omega_{REF}]. \quad (112)$$

A nomogram[28,29] to reduced temperature using Equation 111 can be included in plots of data based on reduced temperature. The CM as a function of reduced temperature could be plotted and would include a temperature-frequency nomogram.

14 OTHER QUANTITIES

The form of the Ratio Model makes interconversion to other dynamic mechanical properties such as molecular weight distribution (Figure 41 through Figure 43), relaxation modulus (Figure 44 through Figure 46), creep compliance (Figure 47 through Figure 49), and relaxation and retardation spectra (Figure 50 through Figure 52) convenient.

15 SENSITIVITY

There are regions in which the loss factor is insensitive to variations in temperature and/or frequency. Partial derivatives with respect to temperature and to log frequency are useful in considering the dependence and sensitivity of viscoelastic damping material dynamic mechanical properties. The partial of log modulus magnitude with respect to log radian frequency is

$$\partial \log G_{\mathrm{M}} / \partial \log \omega = \left(d \log G_{\mathrm{M}} / d \log \omega_R \right) \left(\partial \log \omega_R / \partial \log \omega \right). \tag{113}$$

Using the relationship Equation 10 for reduced frequency to simplify leads to

$$\partial \log G_{\mathrm{M}} / \partial \log \omega = \left(d \log G_{\mathrm{M}} / d \log \omega_R \right). \tag{114}$$

If the approximate relationship Equation 39 is substituted, the following is obtained

$$\partial \log G_{\mathrm{M}} / \partial \log \omega \approx (2/\pi) \arctan \eta \,. \tag{115}$$

This equation shows that, if the loss factor is significant, the modulus magnitude will always change substantially with respect to frequency. It indicates that vibration modes of different frequencies will operate at different values for the modulus. This is one of the practicalities of design and application which must be accommodated. The partial of modulus magnitude with respect to temperature is

$$\partial \log G_{\mathrm{M}} / \partial T = \left(d \log G_{\mathrm{M}} / d \log \omega_R \right) \left(\partial \log \omega_R / \partial T \right). \tag{116}$$

Using the relationship Equation 10 for reduced frequency to simplify leads to

$$\partial \log G_{\mathrm{M}} / \partial T = \left(d \log G_{\mathrm{M}} / d \log \omega_R \right) \left(\partial \log \alpha_T / \partial T \right). \tag{117}$$

Substituting the expression for the slope (STSF) of the Arrhenius TSF E 96 results in

$$\partial \log G_{\mathrm{M}} / \partial T = \left(d \log G_{\mathrm{M}} / d \log \omega_R \right) \left(s_{\mathrm{AZ}} \mathrm{T}_Z^2 / \mathrm{T}^2 \right). \tag{118}$$

If the expression for the AAE for the Arrhenius TSF Equation 99 is used, the following relationship is useful:

$$\partial \log G_{\mathrm{M}} / \partial T = \left(d \log G_{\mathrm{M}} / d \log \omega_R \right) \left(\Delta \mathrm{H}_{\mathrm{A}} / 2.303 R \mathrm{T}^2 \right). \tag{119}$$

Substituting the approximation Equation 39 leads to a relationship between the partial derivative and the product of two factors:

$$\partial \log G_{\mathrm{M}} / \partial T = \left(\Delta \mathrm{H}_{\mathrm{A}} / 2.303 R \mathrm{T}^2 \right) (2/\pi) \arctan \eta \,. \tag{120}$$

From this expression, it is obvious that, for the sensitivity of the modulus to temperature to be small (which is not important in itself), and for the loss factor to be large, the AAE must be small.

From observations, it is well known that there is an inverse relationship between the level of maximum loss factor and the breadth of the transition peak with respect to temperature, i.e., the higher the maximum loss factor, the narrower is the loss factor peak as a function of temperature. The present development offers some qualitative insight. With reference to Equation 25, the magnitude of the complex valued term varies from very small in the rubbery region to very large in the glassy region. In effect, it defines the transition and shows in what way the frequency and temperature variations are equivalent. The log of the quantity Equation 29 may be written and expanded

$$\log \left(\omega \alpha_{\mathrm{T}} / \omega_{R\mathrm{O}} \right)^{\beta} = \beta \left[\log \omega + \log \alpha_{\mathrm{T}} - \log \omega_{R\mathrm{O}} \right]. \tag{121}$$

If only polymers that have approximately the same value for the ratio G_g/G_e are considered, then a substitution using the approximation Equation 41 is appropriate. If also the Arrhenius TSF Equation 95 is used, then

$$\log\left(\omega\alpha_{\mathrm{T}}/\omega_{RO}\right)^{\beta} \approx \left[\log\omega + s_{\mathrm{AZ}}\mathrm{T}_{\mathrm{Z}}^{2}\left(1/\mathrm{T}-1/\mathrm{T}_{\mathrm{Z}}\right)-\log\omega_{RO}\right](2/\pi)\arctan\eta_{\max}. \tag{122}$$

The bracketed quantity is multiplied by a function of η_{max}, which controls the rapidity of variation of the quantity from small to large. This indicates that the width of the transition is indeed governed by the height of the peak.

Equation 96 indicates that, at the reference temperature, an increment of 1 decade in the TSF is caused by an increment in temperature of

$$\Delta\mathrm{T}_{1decade} \approx 1/s_{\mathrm{AZ}}. \tag{123}$$

For a value of s_{AZ}=0.05, the increment in temperature equivalent to 1 decade of frequency would be 20 degrees Kelvin.

16 DISCUSSION

The present method of SIMming a set of CM data and its TSF is a network of mutually complementary elements. It appears that a quantum leap of maturity and efficiency has been achieved. The wicket plot is at the core of the system. Initially, it is used to display the set of data under consideration. It can be used to edit individual points and reveal conspicuously bad data. On the other hand, a nice wicket plot does not guarantee accurate data. Once it is decided to proceed, the Analytical Wicket is constructed. In the data region, a series of splines is fitted to the center and slope of the band of data, thereby smoothing and interpolating the experimental region. Nothing beats accurate data. The analytic geometry fitting of experimental data is challenging. The middle half of the experimental range is usually easy, but the two ends can be especially difficult. High-order polynomials will generally go close to the points, but oscillate wildly. Note the glassy end of the Analytical Wicket in Figure 8 in which the fit has been forced to lower values of loss factor; the effect shows up in both the TSF in Figure 22 and the nomogram in Figure 36. Typically, all three of these plots should be examined for a subjective judgment on goodness of fit. The isotherms (the subset of data points at the same temperature) suggest either inaccurate data or a non-TRS material. Likewise, the glassy end shown in Figure 9, Figure 23, and Figure 37 are open to subjective consideration; the present approach is shown to interpolate the experimental gaps in modulus. Figure 38 reveals that the Analytical Wicket in Figure 10 did not capture the center of the band of data everywhere. Slopes from a previous investigation [29] have been included in Figure 32.

Figure 11, Figure 25, and Figure 39 show the Analytical Wicket, the TSF, and the nomogram for a set of data covering VAMAC[30]. This set has modulus and loss factor for only one frequency at each temperature. It extends into the rubbery and the glassy regions and appears to be fairly smooth. The present method of determining the TSF works well with this set, whereas historical methods do not determine a unique TSF. Consequently, the capability of the new approach is illuminated. Figure 12, Figure 26, and Figure 26 cover the rubber modified epoxy set of data [1] which has one of the tighter wicket plots.

Once the data region is fitted, extrapolations must be made toward the rubbery and glassy skirts. The fitting and extrapolations are automated and goodness of fit is somewhat subjective. The perpendicular distance, d, to the wicket and the arc length, s, along the wicket plot may be used to improve the fit (see Figure 8 through Figure 12.) The Analytical Wicket is treated as the definition of the material loss factor as a function of the modulus magnitude for the purposes of iteration.

The mathematical concept of mapping is then used. The Analytical Wicket may be considered to be two functions, namely material loss factor and modulus magnitude, of the independent variable, arc length, s. From systems theory, it is known that these two functions are also two components of a complex valued function of the independent variable, reduced radian frequency. Developing an expression (here the Ratio Model after the values of the parameters have been determined) for that complex valued function is called mapping.

Another key to the present approach is the form of the Ratio Model, which is a ratio of factored polynomials with first-order factors, with the numerator and denominator of equal order. This form guarantees that the interrelationship of any two components of the complex valued function

remains satisfied. The mapping consists of first initiation and then iteration until convergence. Both of these are facilitated by the form of the ratio.

The initialization is achieved by use of the simplest fractional model as described above (see Figure 14 through Figure 16). The iteration consists of stepwise fitting of the CM as a function of reduced radian frequency and is easily visualized by use of Bode diagrams. The iteration algorithm (see Figure 17) is based on Bode diagram visualization and converges rapidly (see Figure 18 through Figure 20). The ratio closely matches the Analytical Wicket for the most part; on occasion, there is a lack of match at a glassy tail (see Figure 18 and Figure 19) for reasons not understood at present. For every material, care should be taken that there are no unintentional extrapolations in any quantity.

The mapping process implicitly associates values of Analytical Wicket arc length with reduced radian frequency, thereby associating a unique value of reduced radian frequency with each experimental data point by means of its perpendicular distance to the wicket. This approach for TSF is believed to be new. The TSF for every experimental data point may be calculated and plotted and fitted with three equations for the TSF, i.e., the WLF, the quadratic slope in (1/T), and a fourth-order polynomial (see Figure 22 through Figure 26).

There is obvious scatter in the TSF at the glassy end in Figure 22 and Figure 23, and scatter throughout Figure 24. The purpose of the data should be brought to bear on whether or not the scatter is acceptable.

The corresponding slope of the TSF (see Figure 30 through Figure 32) and the apparent activation energy (see Figure 33 through Figure 35) may also be plotted. After the TSF is established, the standard nomogram (see Figure 36 through Figure 40) can be plotted.

The present approach is very highly automated, but maintains options for computer operator interaction.

The form of the Ratio Model makes interconversion to other dynamic mechanical properties such as molecular weight distribution (Figure 41 through Figure 43), relaxation modulus (Figure 44 through Figure 46), creep compliance (Figure 47 through Figure 49), and relaxation and retardation spectra (Figure 50 through Figure 52) convenient.

The present method is well founded on mathematical rigor and is believed to be insensitive to limited frequency and temperature ranges, data scatter, etc.

Once a database of information on several polymeric damping materials is established, it can become somewhat cumbersome to search the database. One method would be to develop a table wherein each material was described by one line. The materials would be sorted by the temperature (in degrees K, C, and F) of maximum loss factor for a frequency of 100 Hz. Then the maximum loss factor, the corresponding real modulus in metric and English units, the slope of the TSF, the data source, etc., would follow. Such a system would be convenient for manual sorting of materials and might possibly be adequate for some design applications. A computerized system for sorting or sifting would be most efficient.

Low values of loss factor and low slopes of modulus (real and magnitude) always occur together. When this happens, the SIM becomes challenging because of data scatter and numerical sensitivity. The present method performs satisfactorily in this situation.

The approach facilitates communication, is useful to the polymer engineer and to the designer, is fair to the material supplier and tester, and puts pressure on the damping industry to make further improvements and advancements within the limits of economic practicality.

17 SUMMARY

Typically, when a set of CM is taken, there will be scatter in the measurements. Therefore, some smoothing is required. Also, the measurement temperatures and frequencies are not covered in continuous fashion. Consequently, interpolation is required in the process of design or analysis of a vibration damping configuration. Computerized modeling greatly facilitates storage, retrieval, and dissemination of the dynamic mechanical properties of a damping polymer. These are crucial factors in the further advancement and application of damping technology. Historically, the Wicket Plot has been used to edit a set of data and to look for indications of poor quality or accuracy. The approach reported herein further used the wicket plot. A series of splines is used to represent the set of data, namely, loss factor as a function of modulus magnitude. These splines closely approximate the center of the band of data and its slope. Additional splines are used to gracefully extrapolate the data toward both the rubbery and glassy region. Collectively, these splines are called the Analytical Wicket. It treats the loss factor as a function of the modulus magnitude. The loss factor and modulus magnitude may also be treated as two functions of a parameter, in this case, arc length along the wicket. The loss factor and modulus magnitude may also be treated as two components of a complex valued function (actually a frequency response function) of a single independent variable, in this case, reduced radian frequency.

The complex valued function (i.e., the CM) is represented by the Ratio Model, which is a ratio of polynomials of first-order factors with the numerator and the denominator being the same order. One pair of first-order factors, one in the numerator and the other in the denominator, result in one step with respect to Bode diagram considerations. The Ratio Model intrinsically guarantees that the interrelationships of linear systems are satisfied. An initialization and iteration technique is used to determine values for the parameters in the Ratio Model. The basic fractional derivative equation for CM is critical to the initialization process. One characteristic of CM is that the loss factor is strongly dependent on the slope of the modulus magnitude as a function of reduced radian frequency. The iteration process is based on this characteristic. The Ratio Model is used to calculate modulus magnitude and loss factor at each step; and the Analytical Wicket is used to calculate the loss factor corresponding to the modulus from the ratio. If the two values for loss factor are not identical, the slope of the modulus is changed appropriately. Once the Ratio Model closely matches the Analytical Wicket, the perpendicular distance from individual data points to the wicket defines a unique value for arc length and for reduced radian frequency of the Ratio Model from which the value of the temperature shift function is calculated.

The form of the Ratio Model greatly facilitates fitting the wicket plot by initialization and iteration. It also is straightforward to calculate other dynamic mechanical properties based on the CM.

The present approach is interactive and highly automated and exploits modern computational power. It facilitates communication, is useful to the designer, is fair to the material supplier and tester, and puts pressure on the damping industry to make further improvements and advancements within the limits of economic practicality.

18 FIGURES

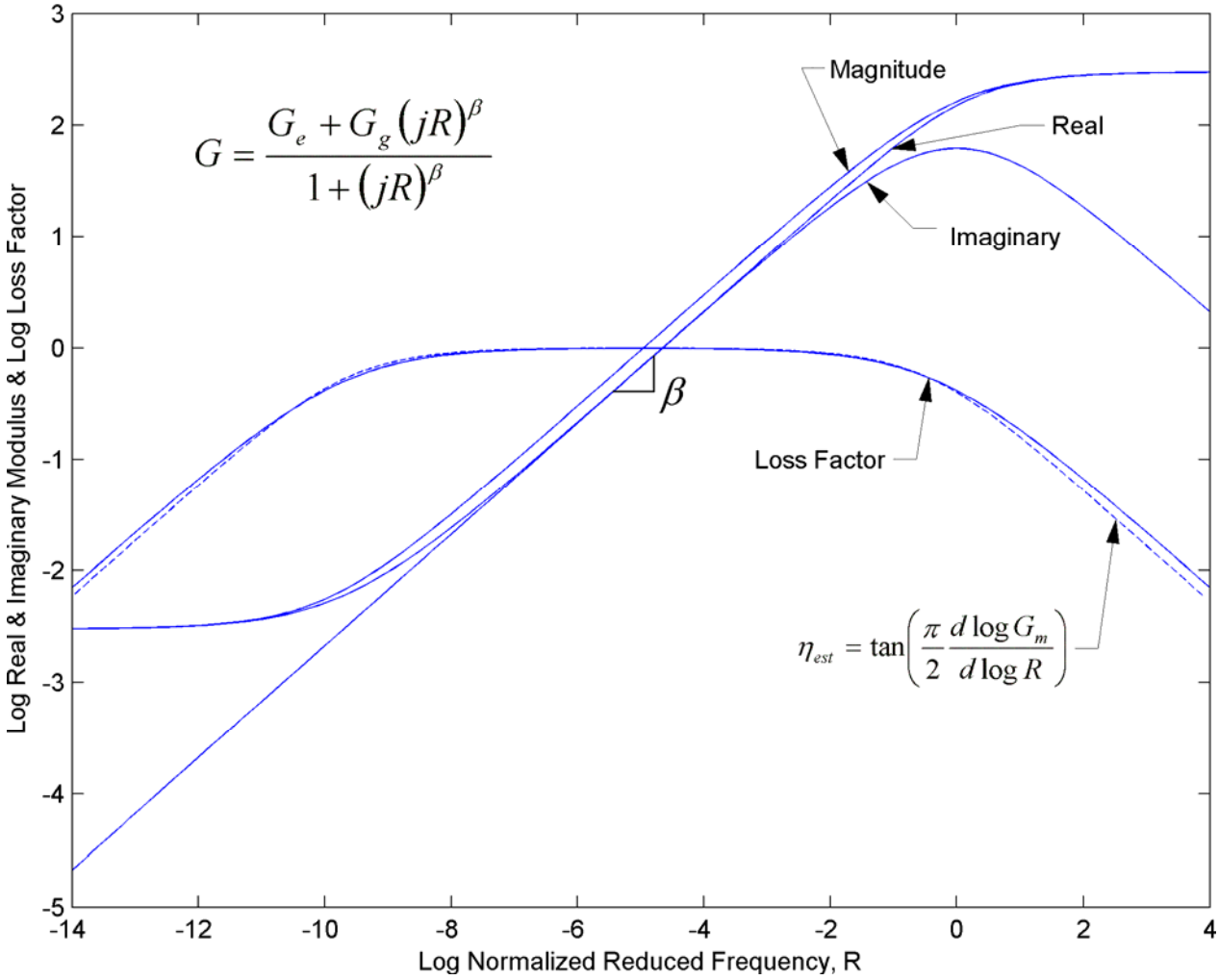

Figure 1: Basic CM Model

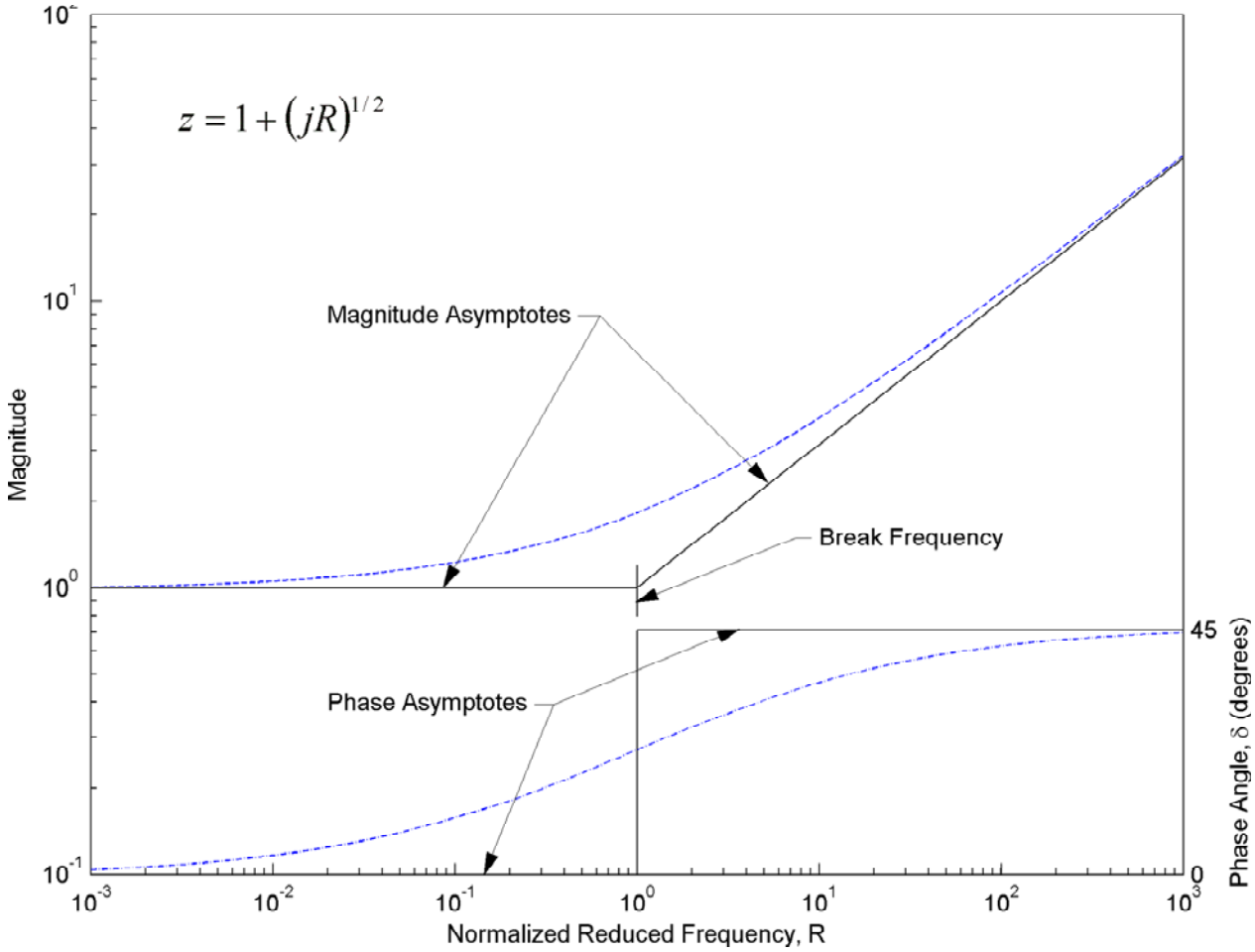

Figure 2: Bode Diagram for a Half Power Factor

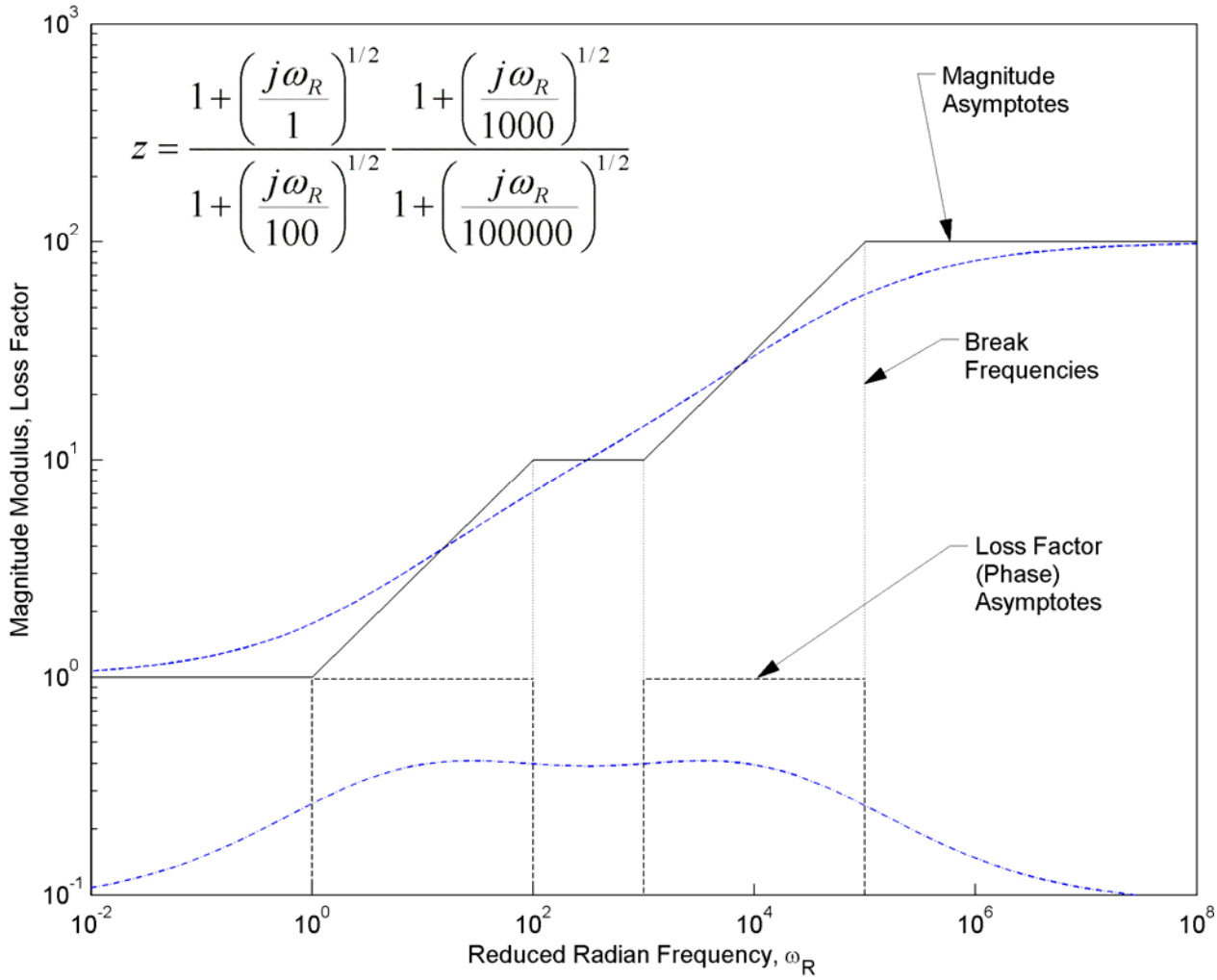

Figure 3: Diagram for a Two-Step Model

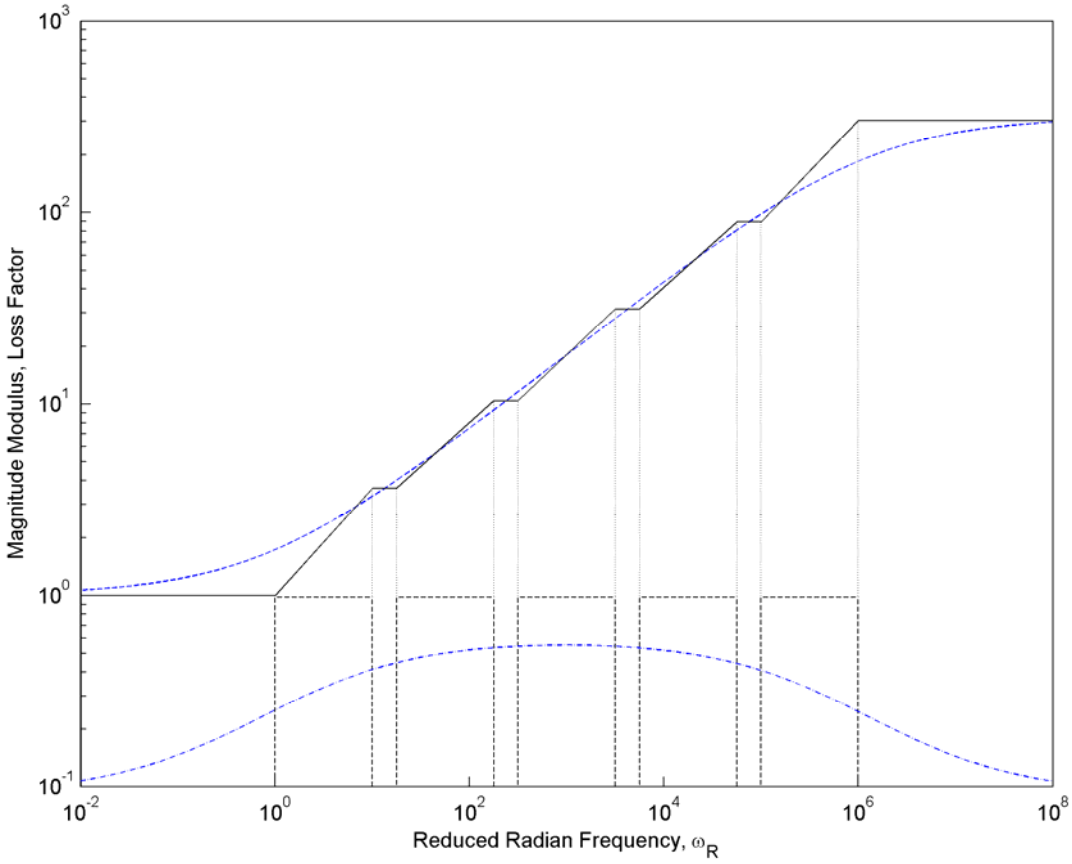

Figure 4: Conceptual Bode Diagram for the Ratio Model

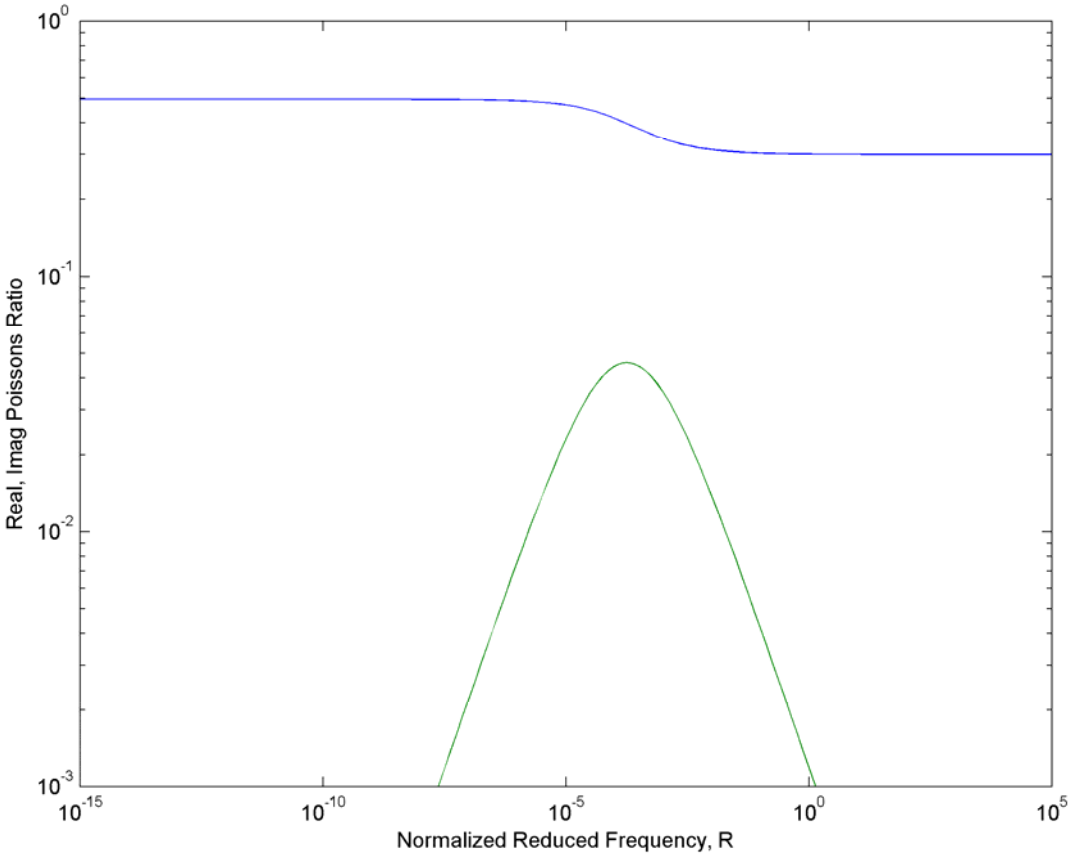

Figure 5: Speculated Transition of Poisson's Ratio

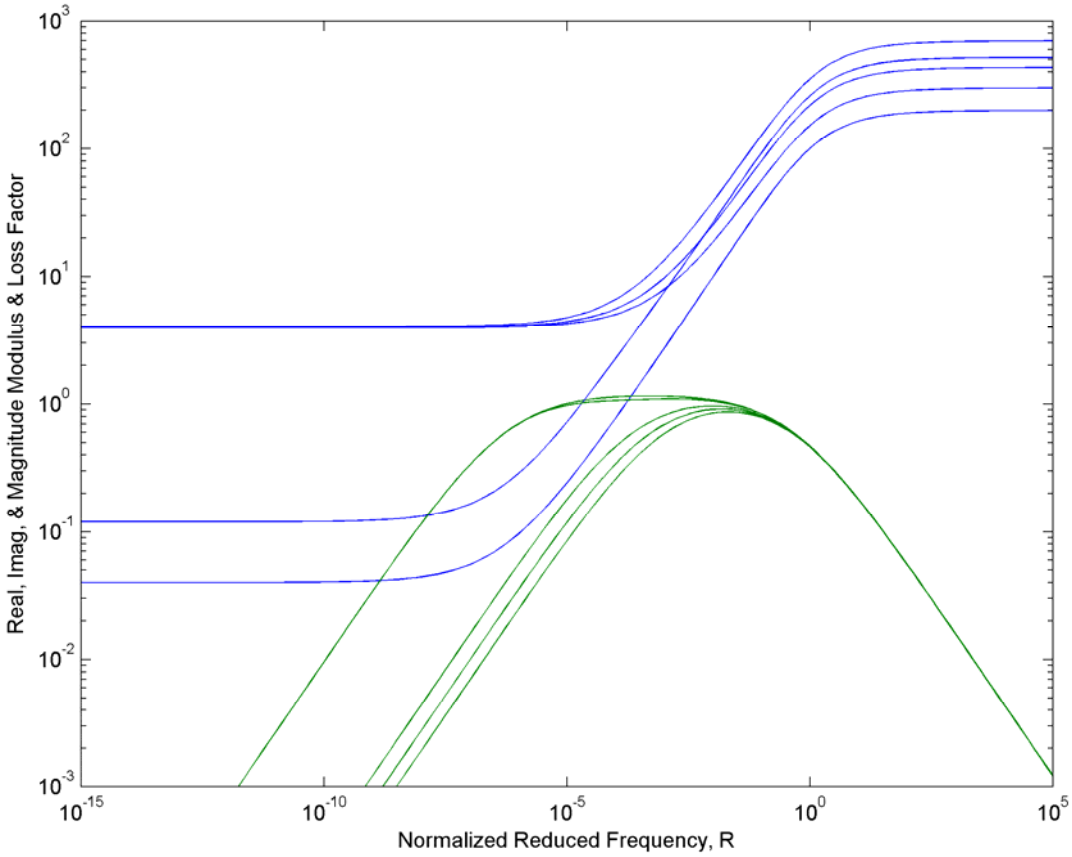

Figure 6: Modulus Transitions for a 0.495 Rubbery Poisson's Ratio

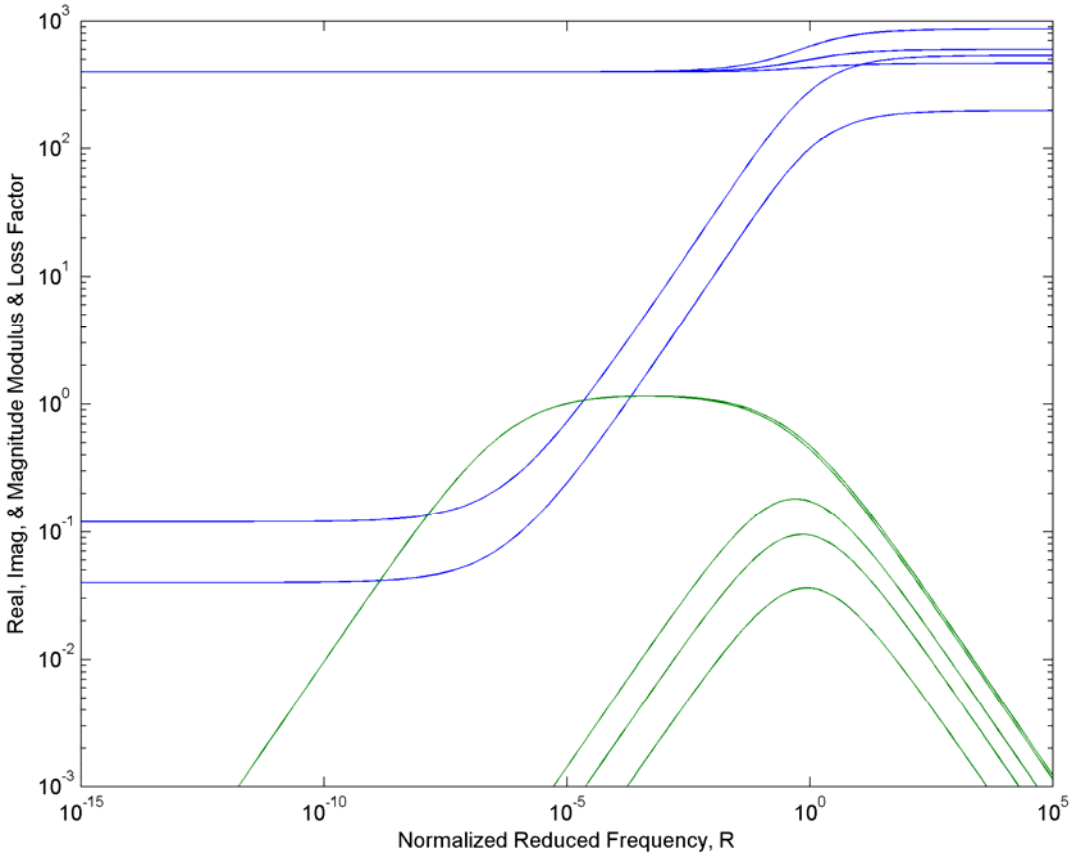

Figure 7: Modulus Transitions for a 0.49995 Rubbery Poisson's Ratio

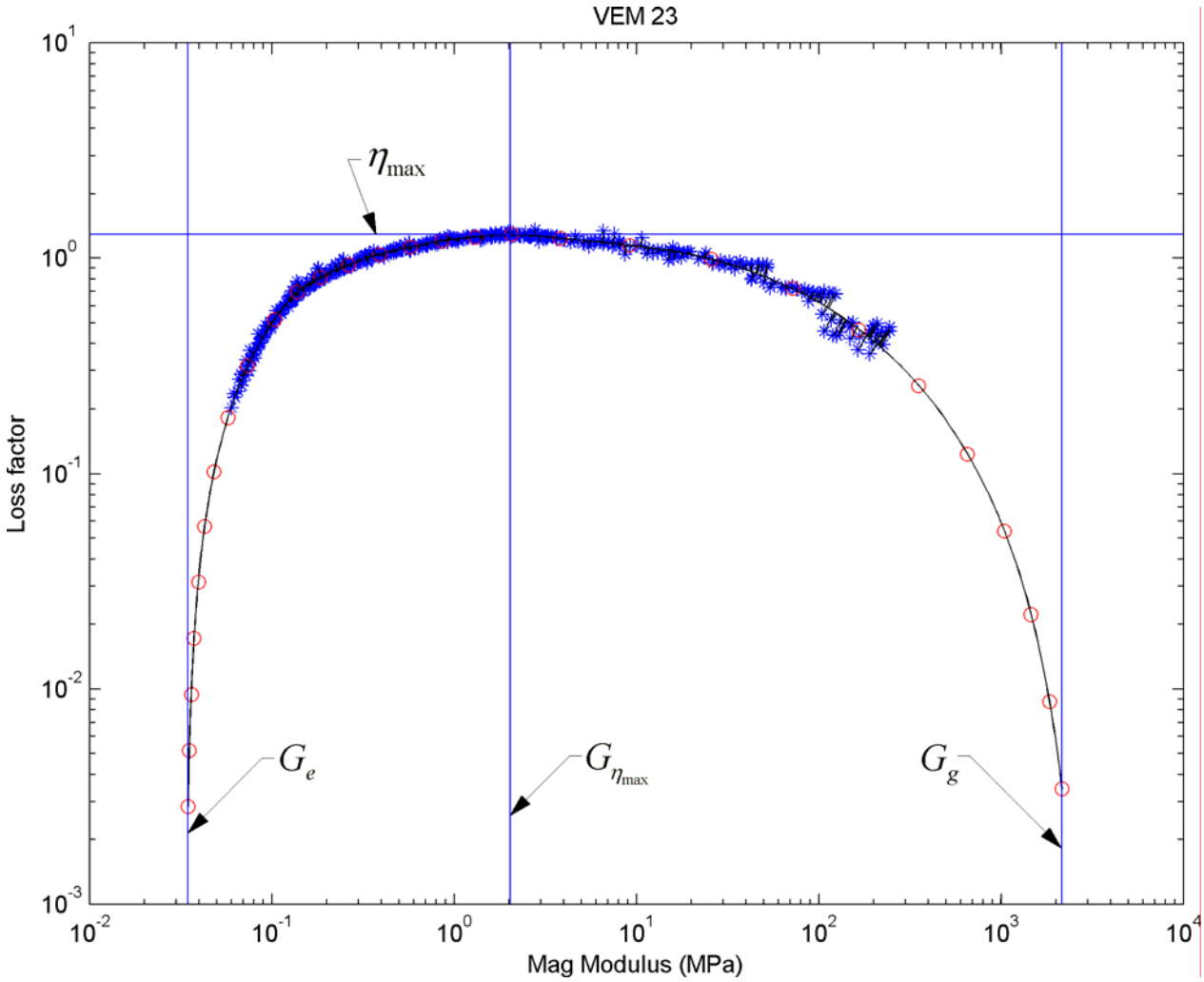

Figure 8: Analytical Wicket for VEM 23 with Key Features

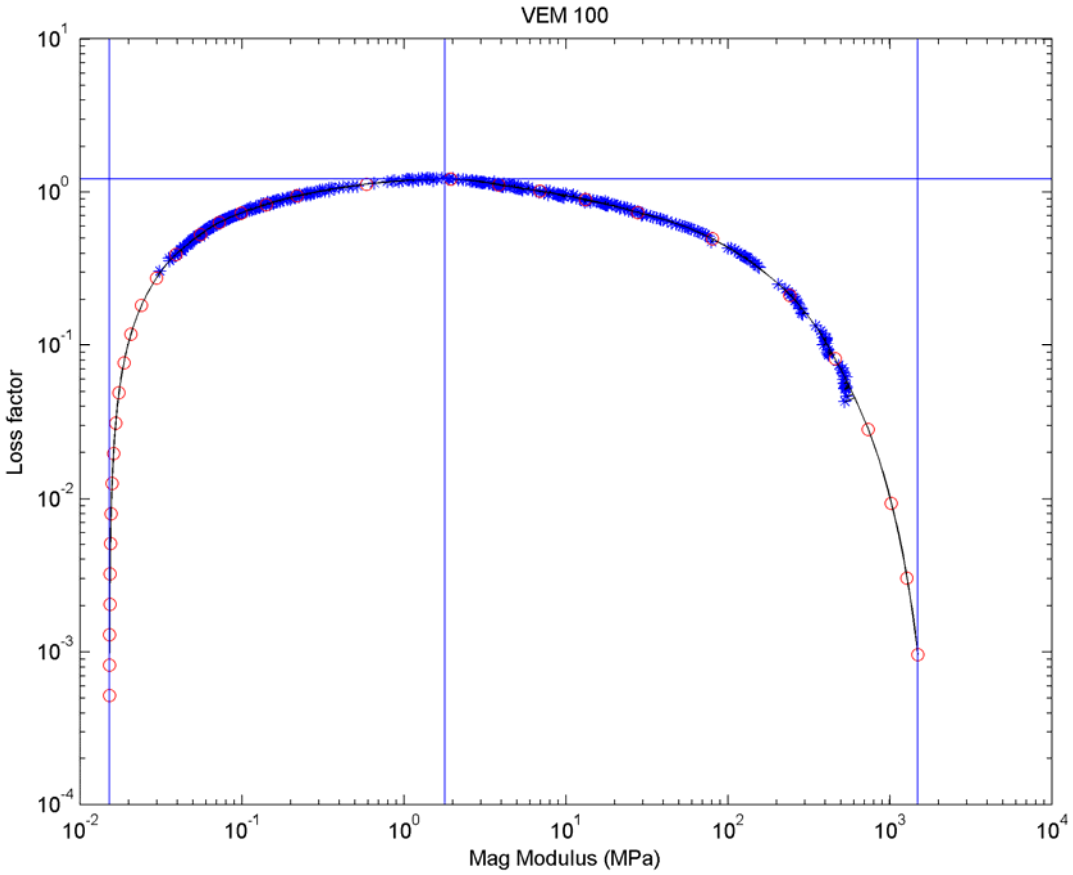

Figure 9: Analytical Wicket for VEM 100

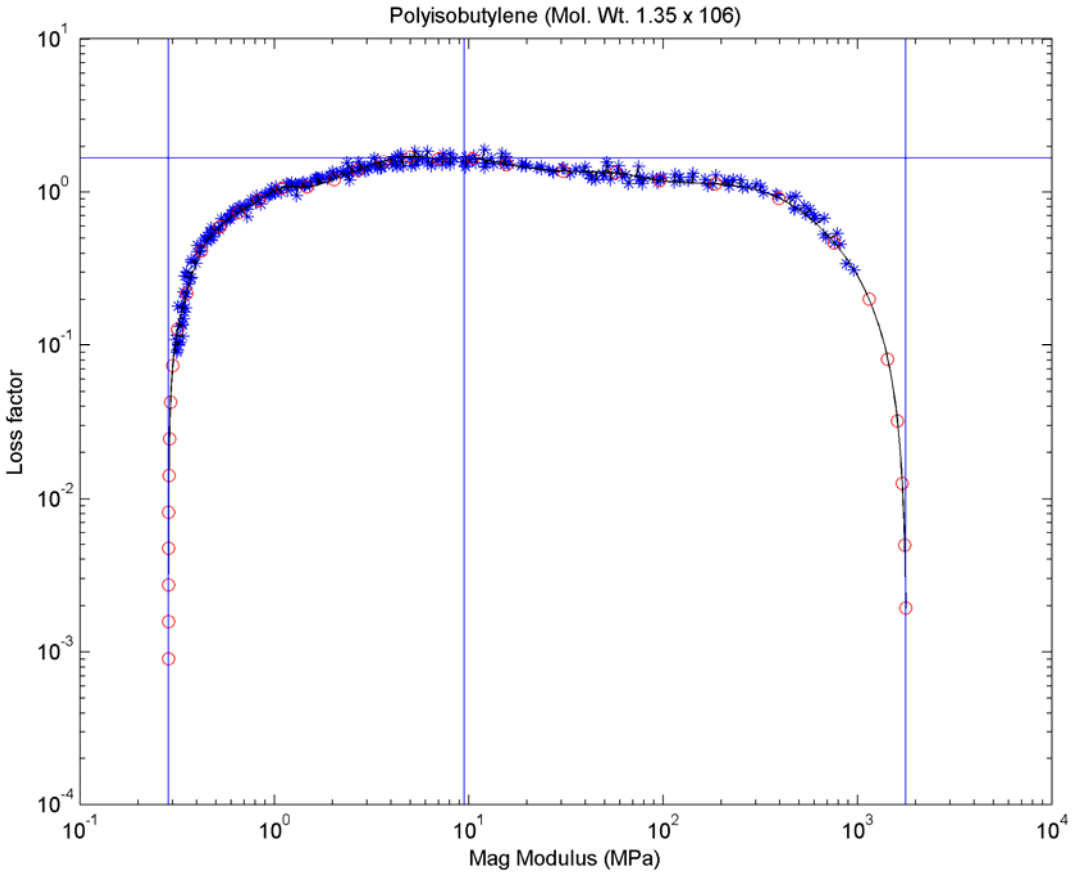

Figure 10: Analytical Wicket for VEM Polyisobutylene

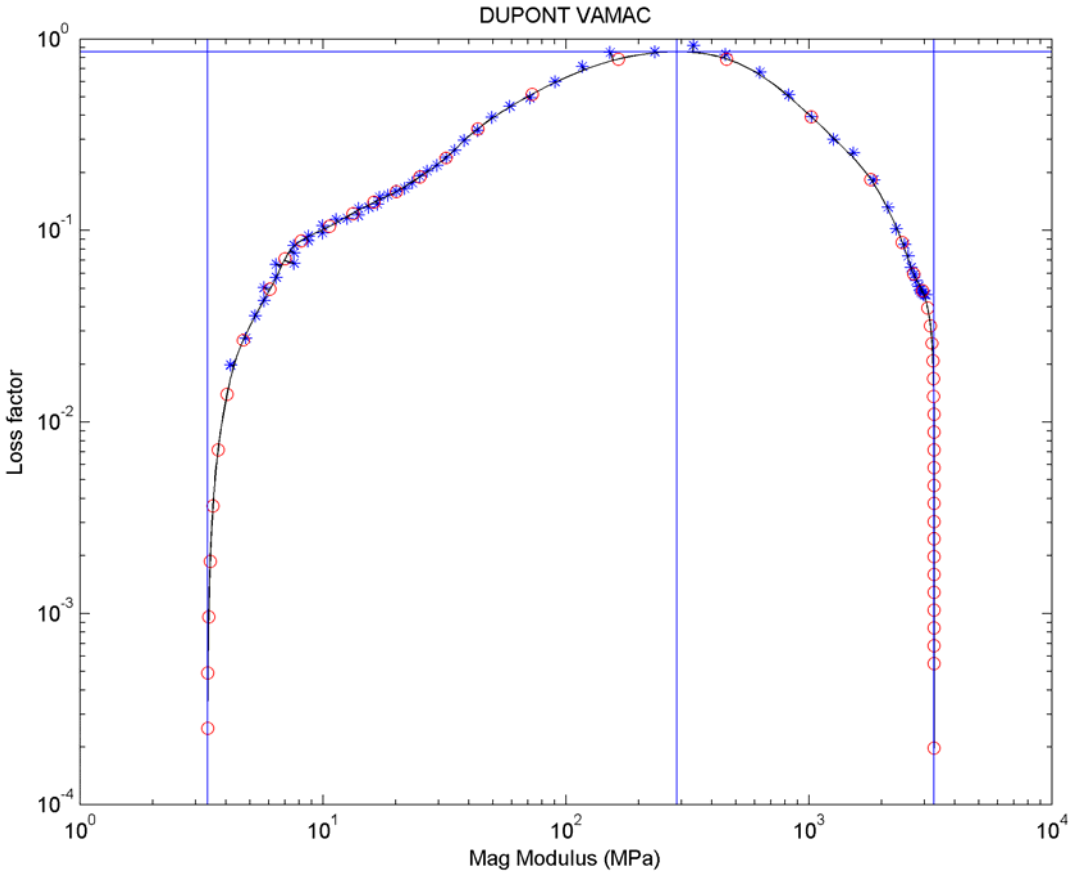

Figure 11: Analytical Wicket for VEM VAMAC

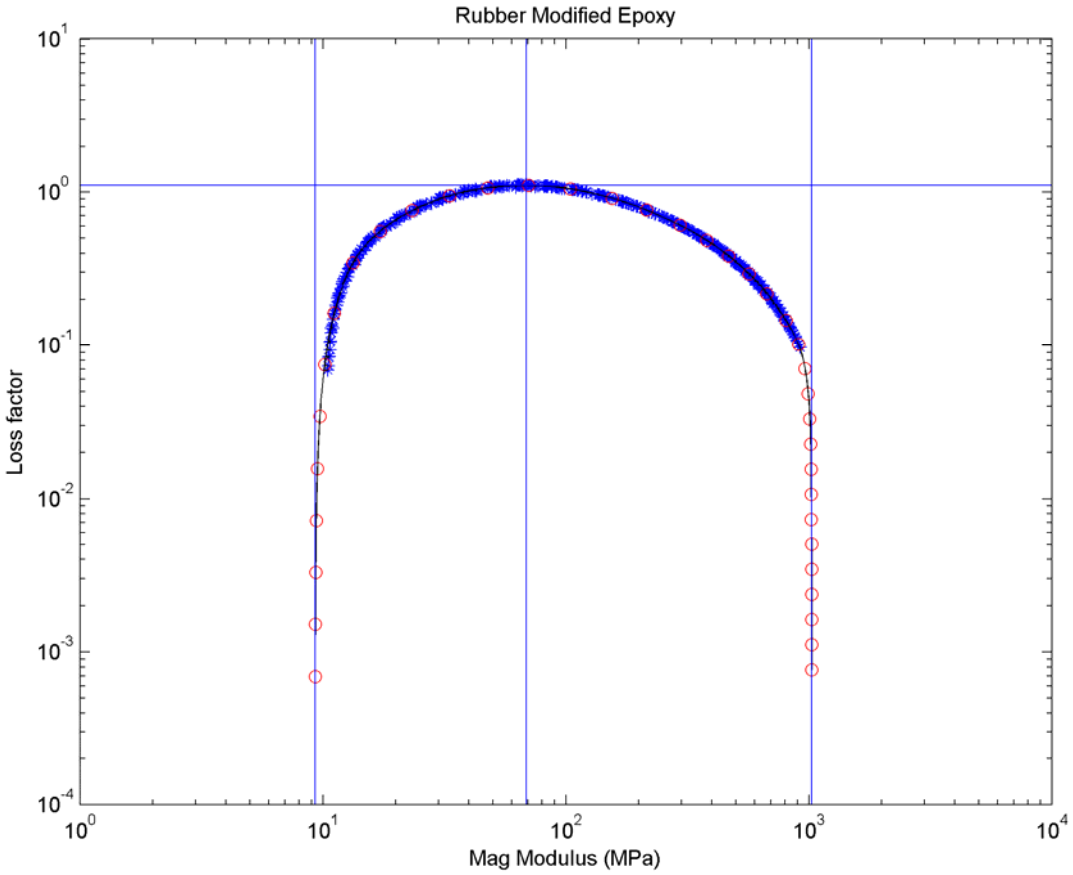

Figure 12: Analytical Wicket for VEM Rubber Modified Epoxy

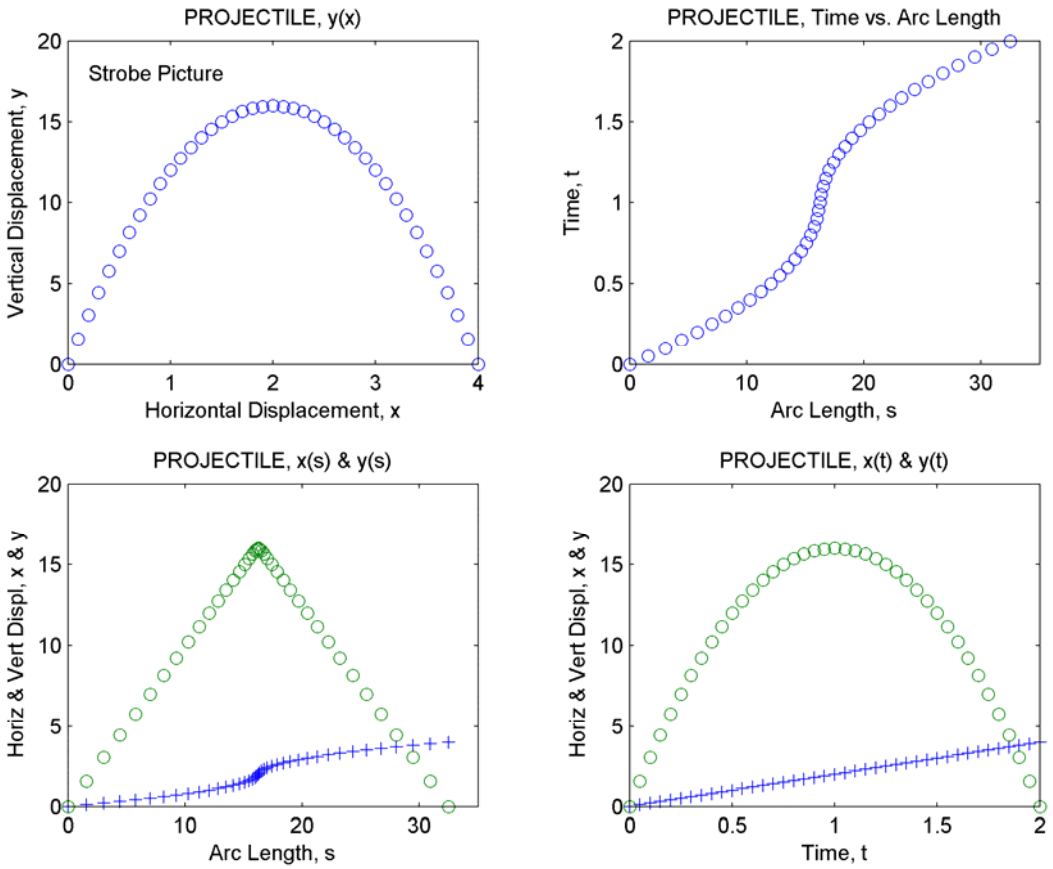

Figure 13: Projectile Parametric Illustration

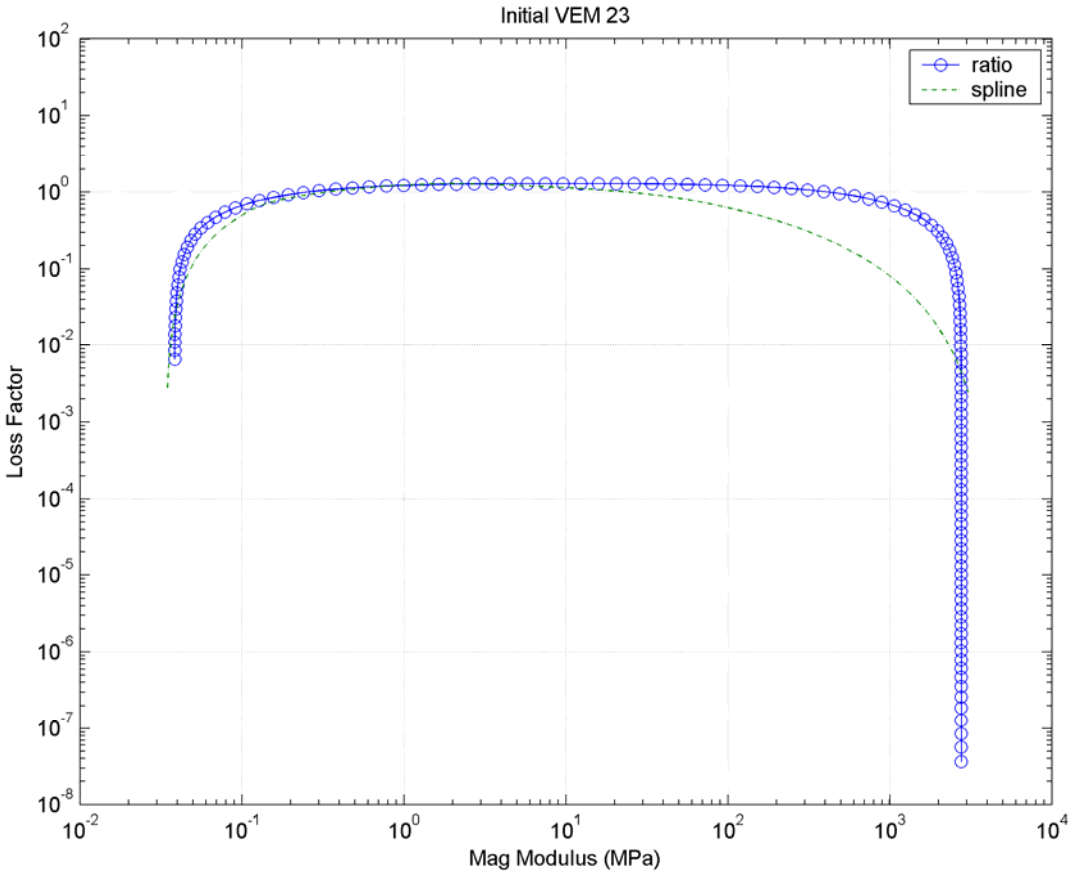

Figure 14: Ratio Initialization Wicket Plot for VEM 23

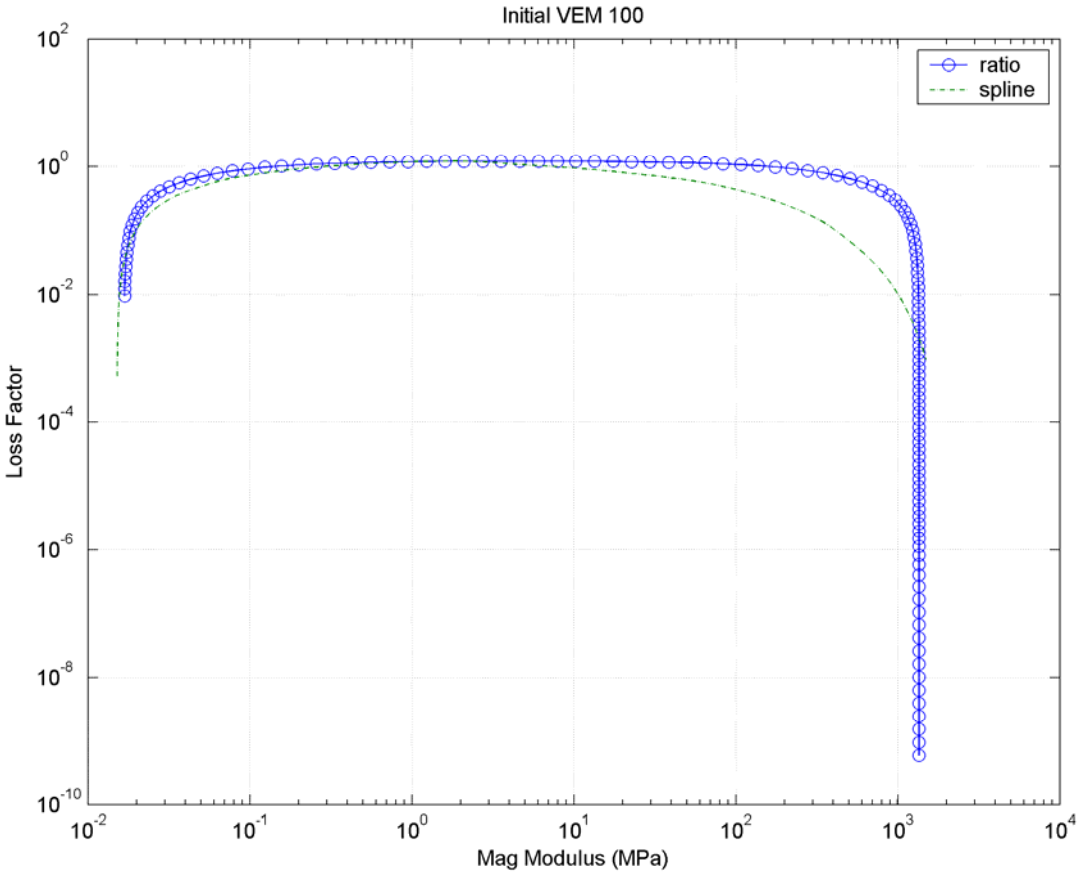

Figure 15: Ratio Initialization Wicket Plot for VEM 100

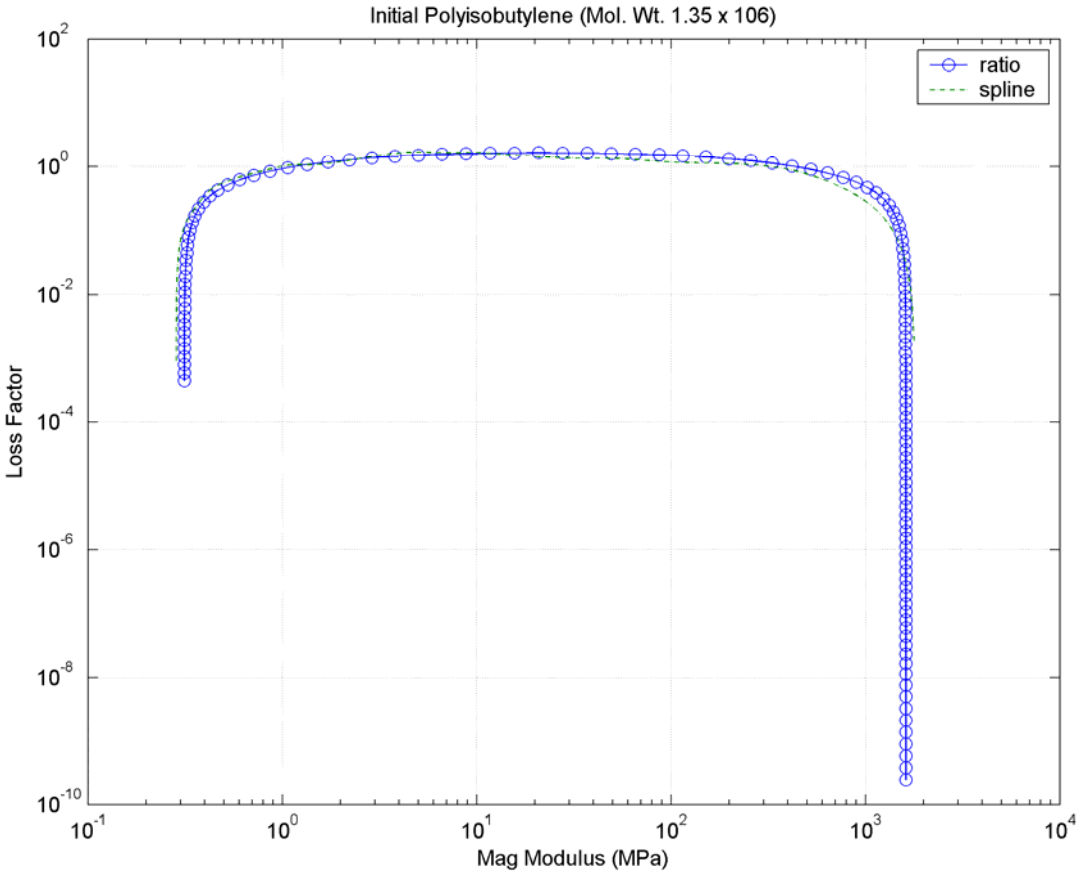

Figure 16: Ratio Initialization Wicket Plot for VEM Polyisobutylene

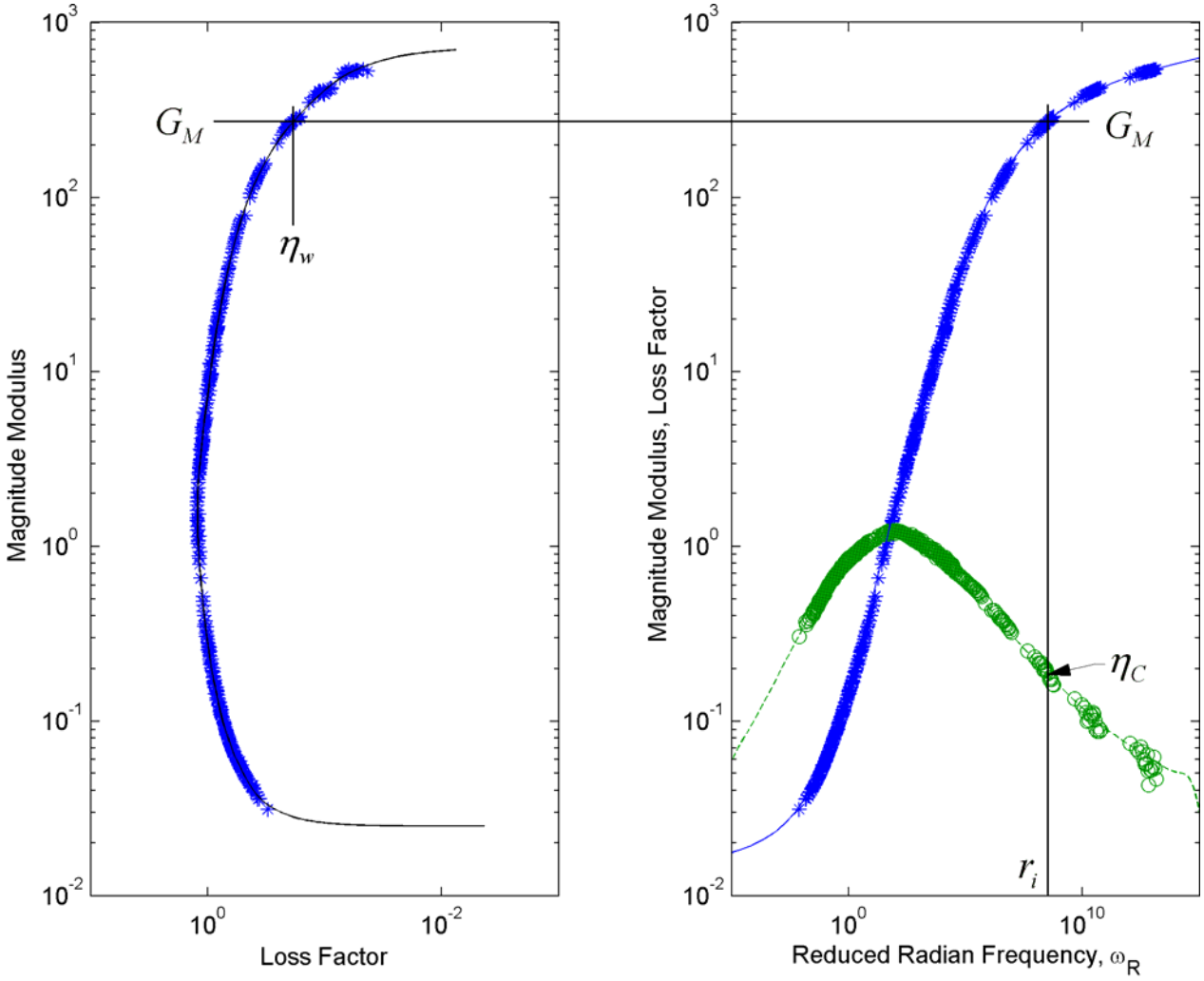

Figure 17: Illustration of the Iteration Algorithm

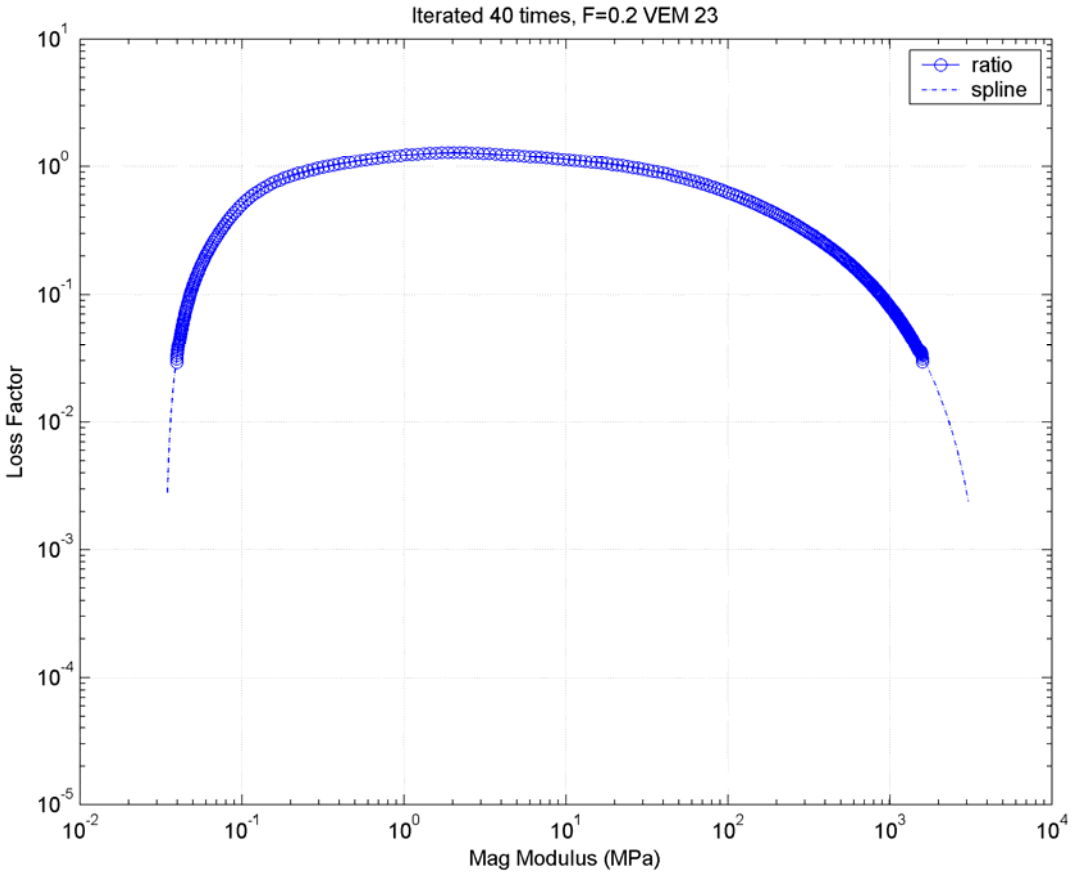

Figure 18: Ratio-Converged Wicket Plot for VEM 23

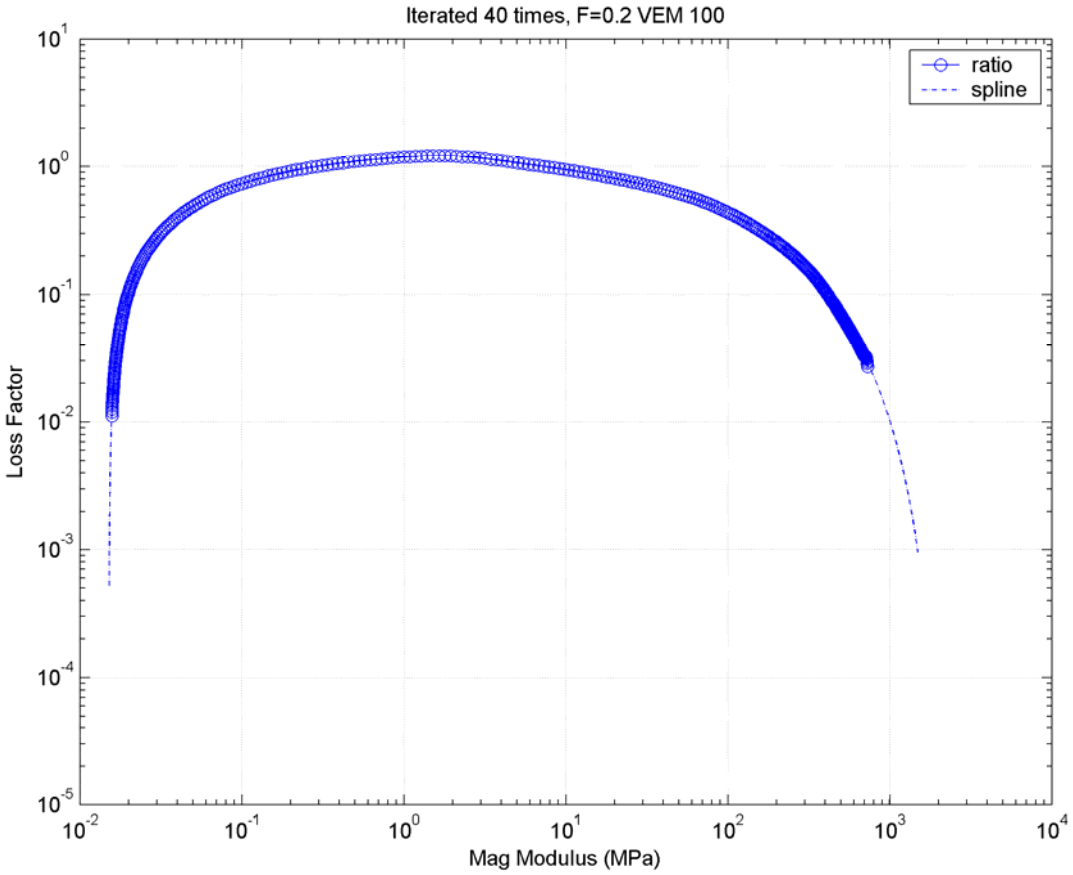

Figure 19: Ratio-Converged Wicket Plot for VEM 100

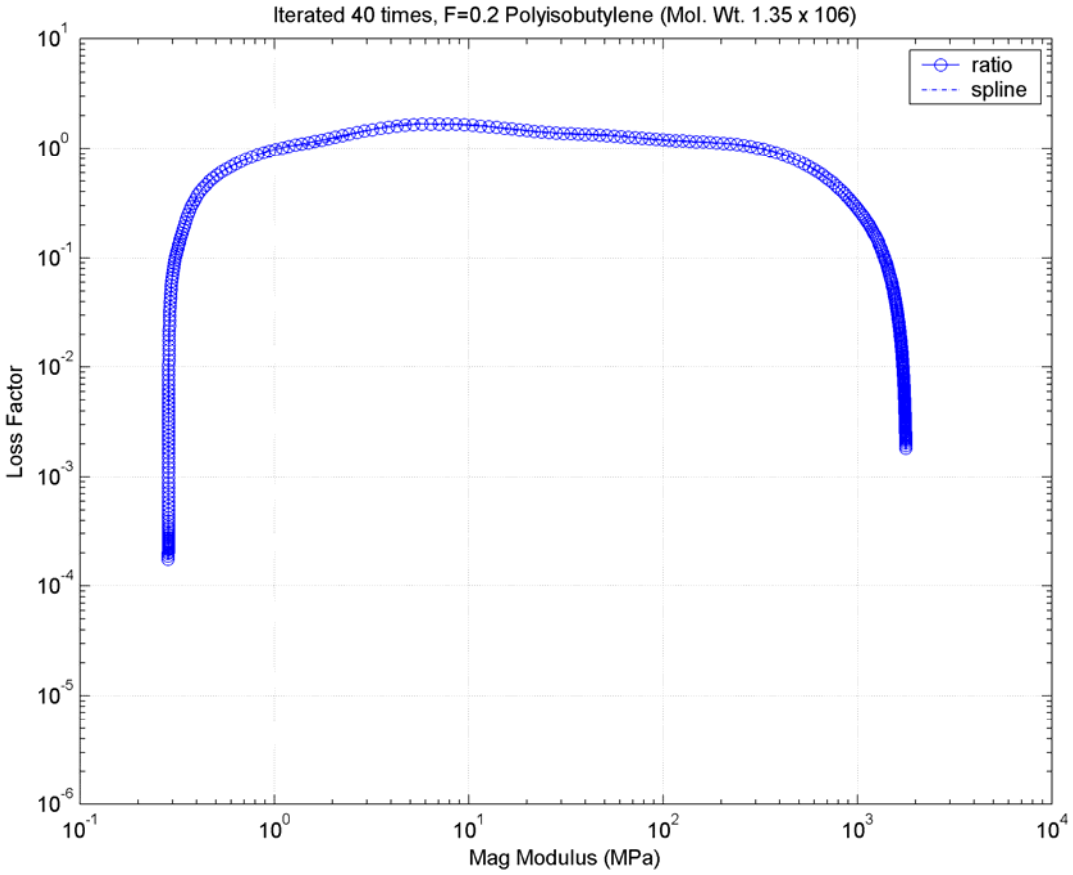

Figure 20: Ratio-Converged Wicket Plot for VEM Polyisobutylene

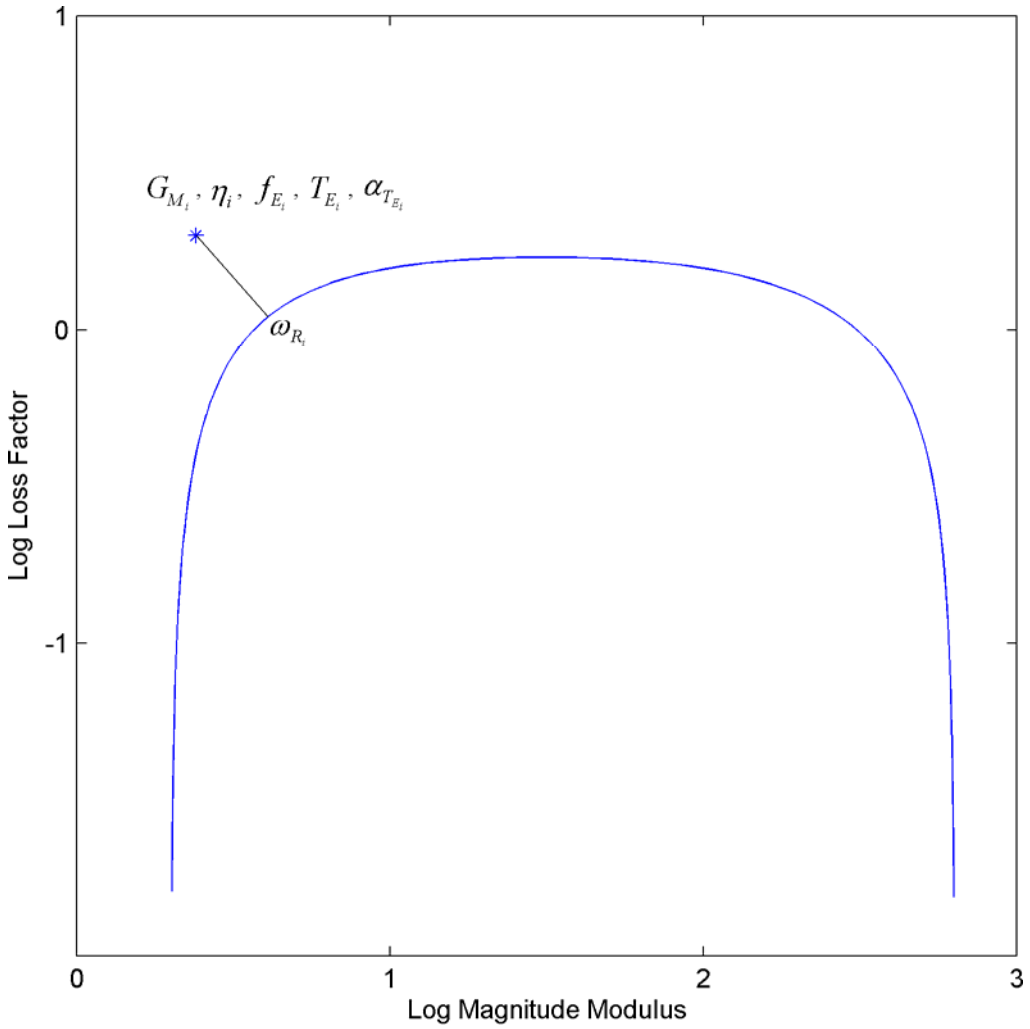

Figure 21: New Method to Determine TSF

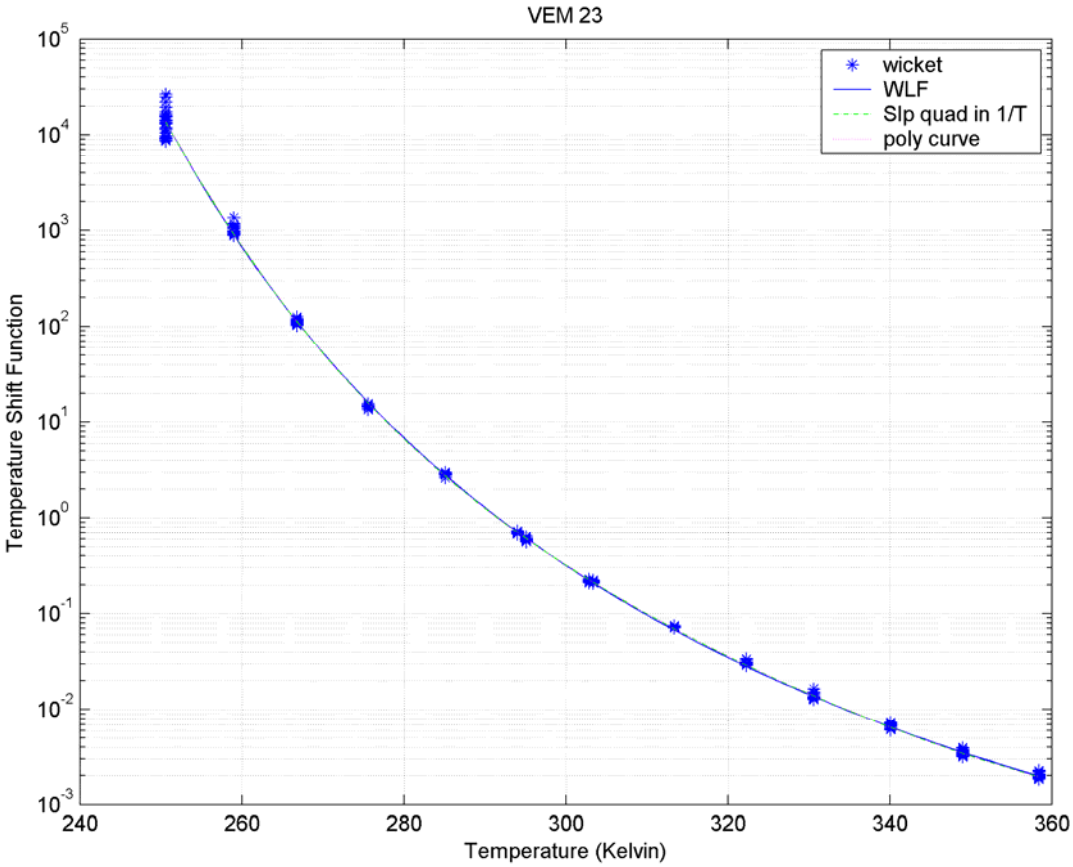

Figure 22: TSF for VEM 23

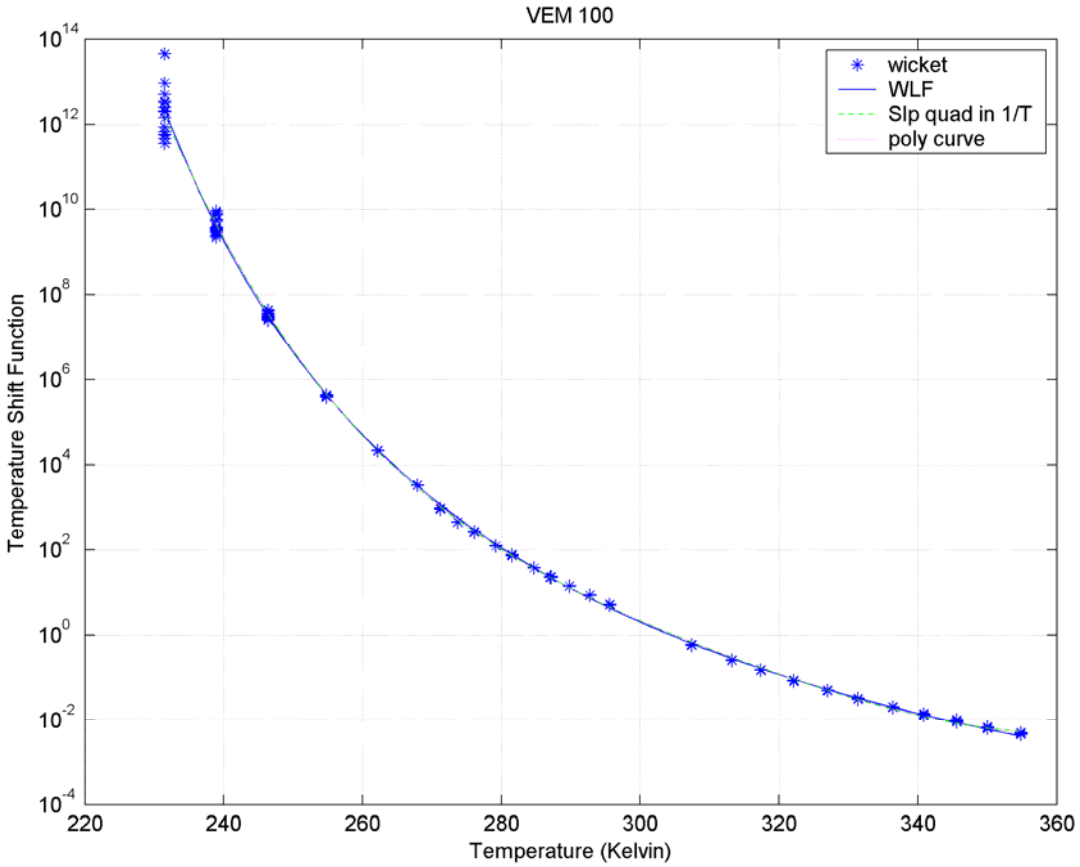

Figure 23: TSF for VEM 100

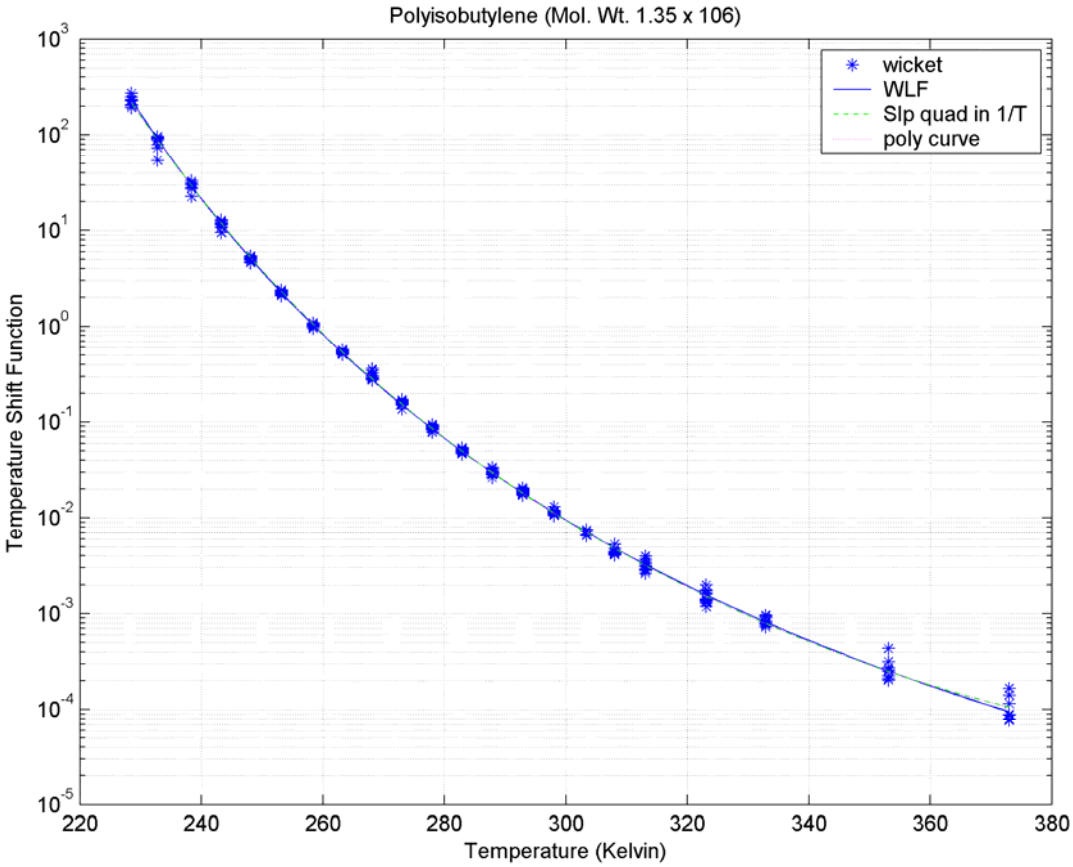

Figure 24: TSF for VEM Polyisobutylene

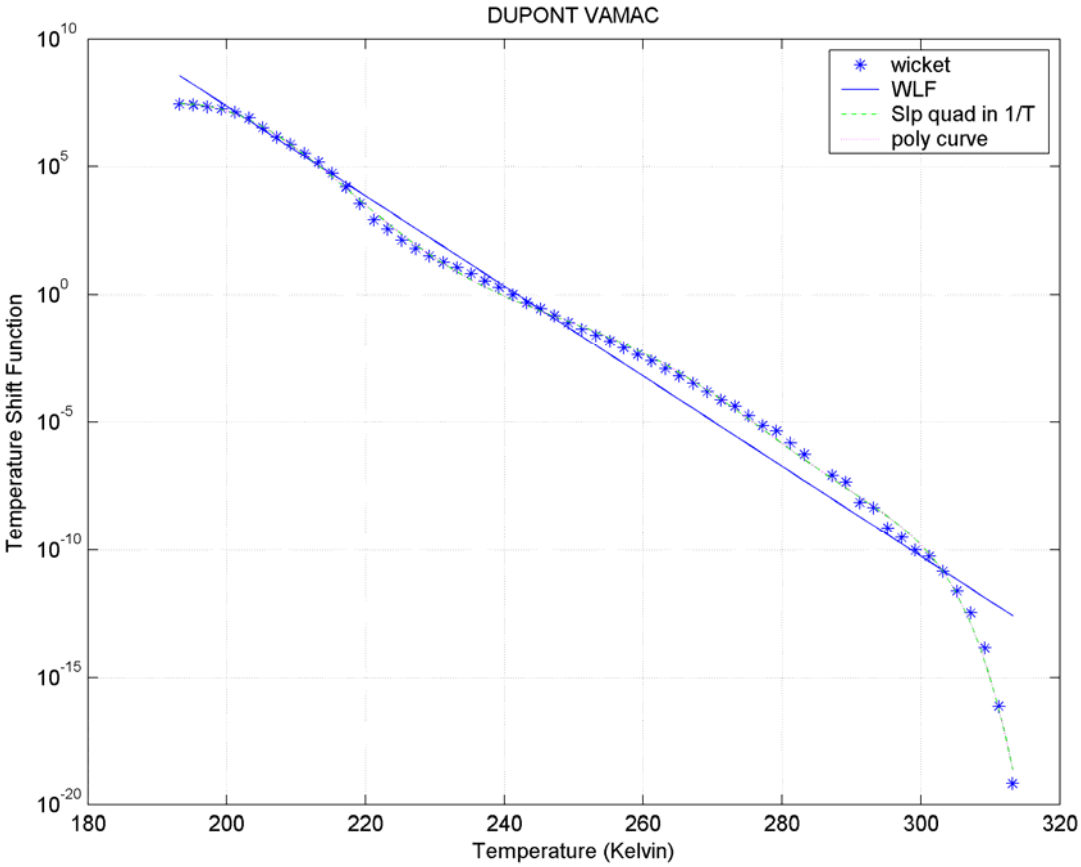

Figure 25: TSF for VEM VAMAC

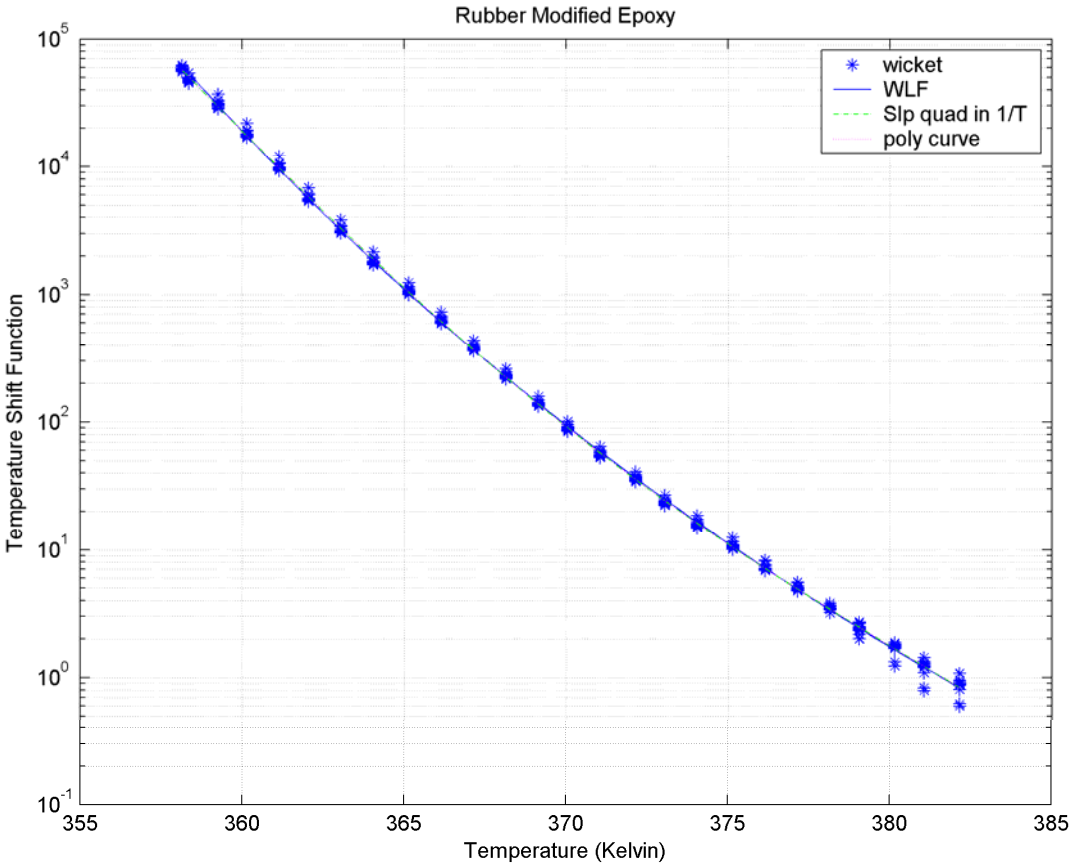

Figure 26: TSF for VEM Rubber Modified Epoxy

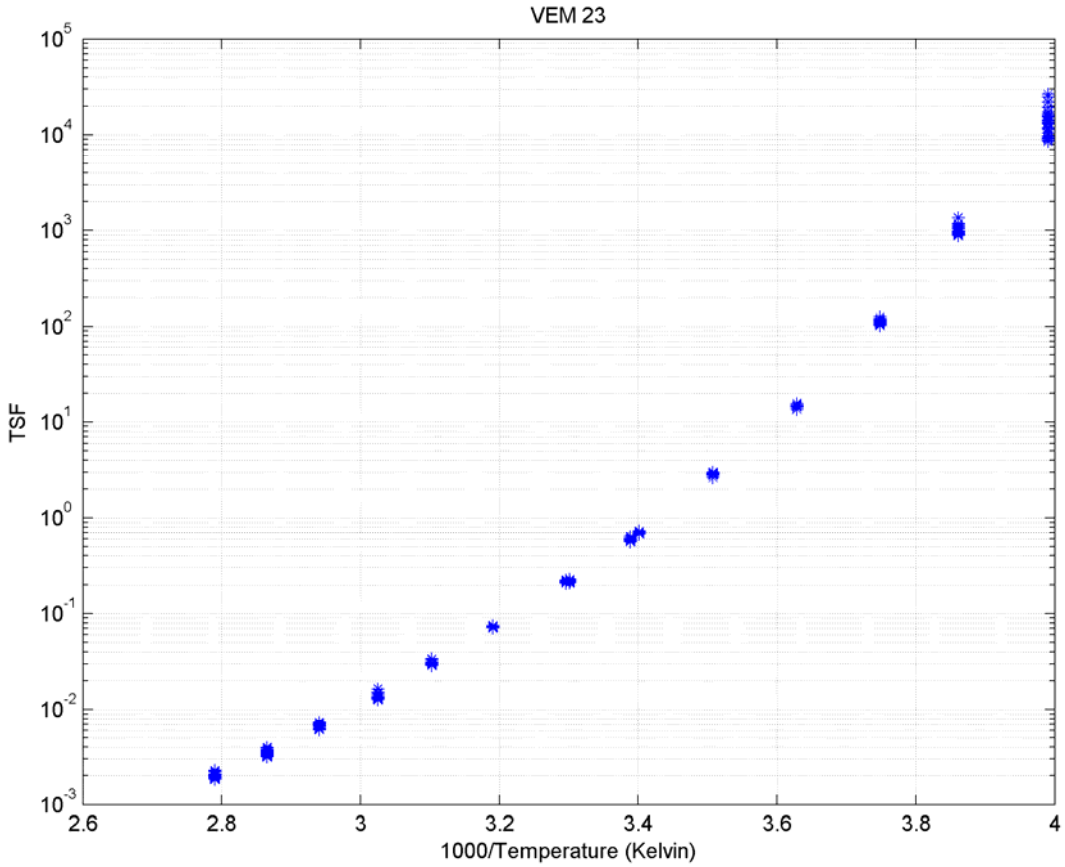

Figure 27: TSF versus 1/T for VEM 23

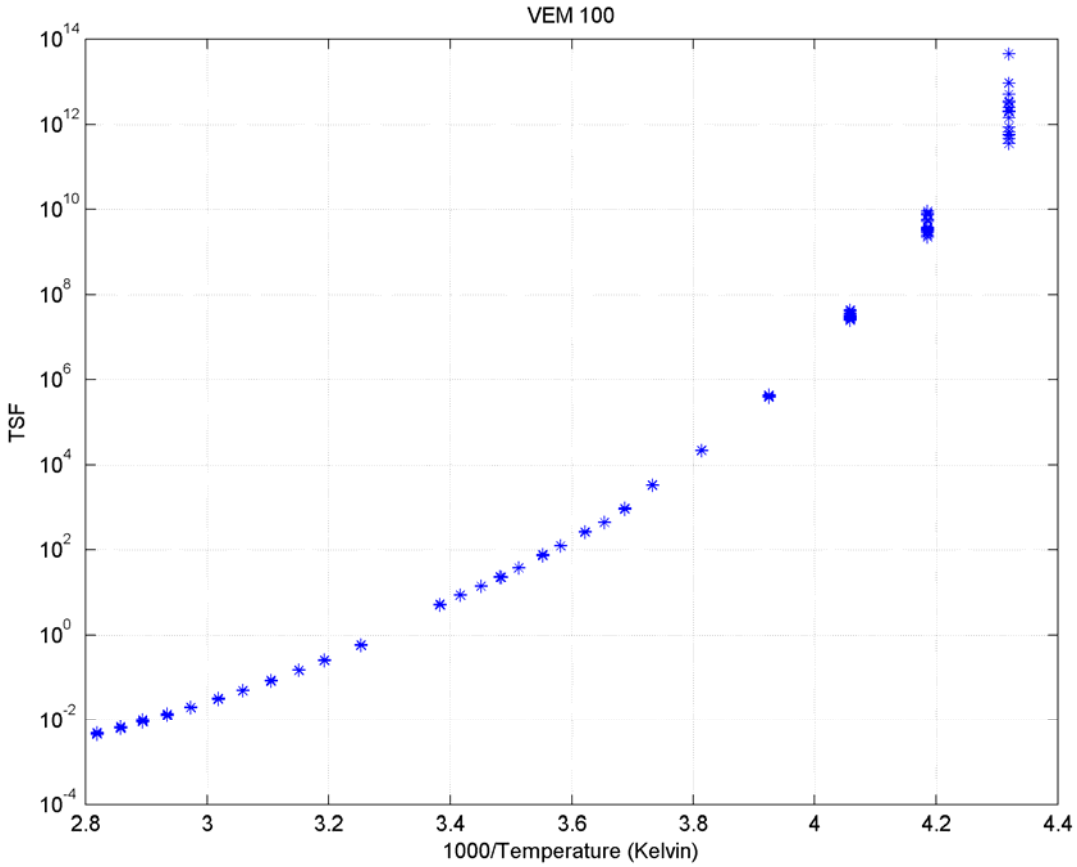

Figure 28: TSF versus 1/T for VEM 100

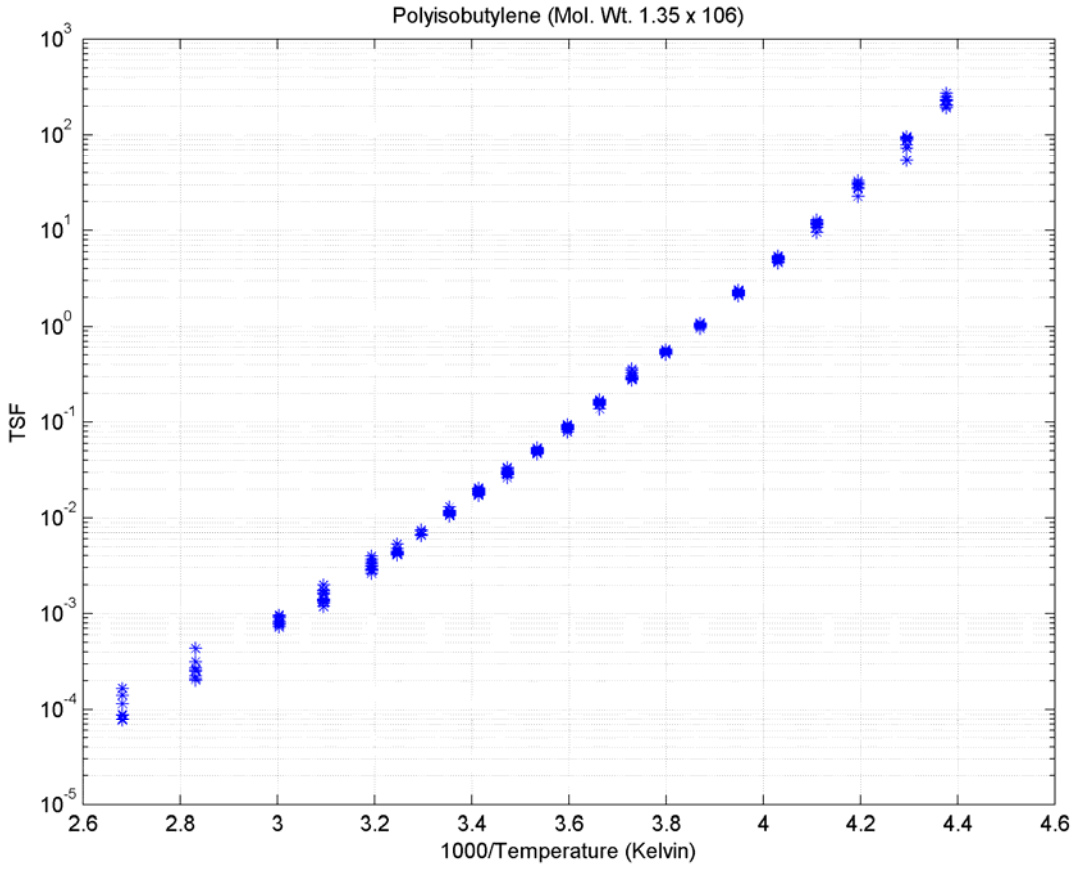

Figure 29: TSF versus 1/T for VEM Polyisobutylene

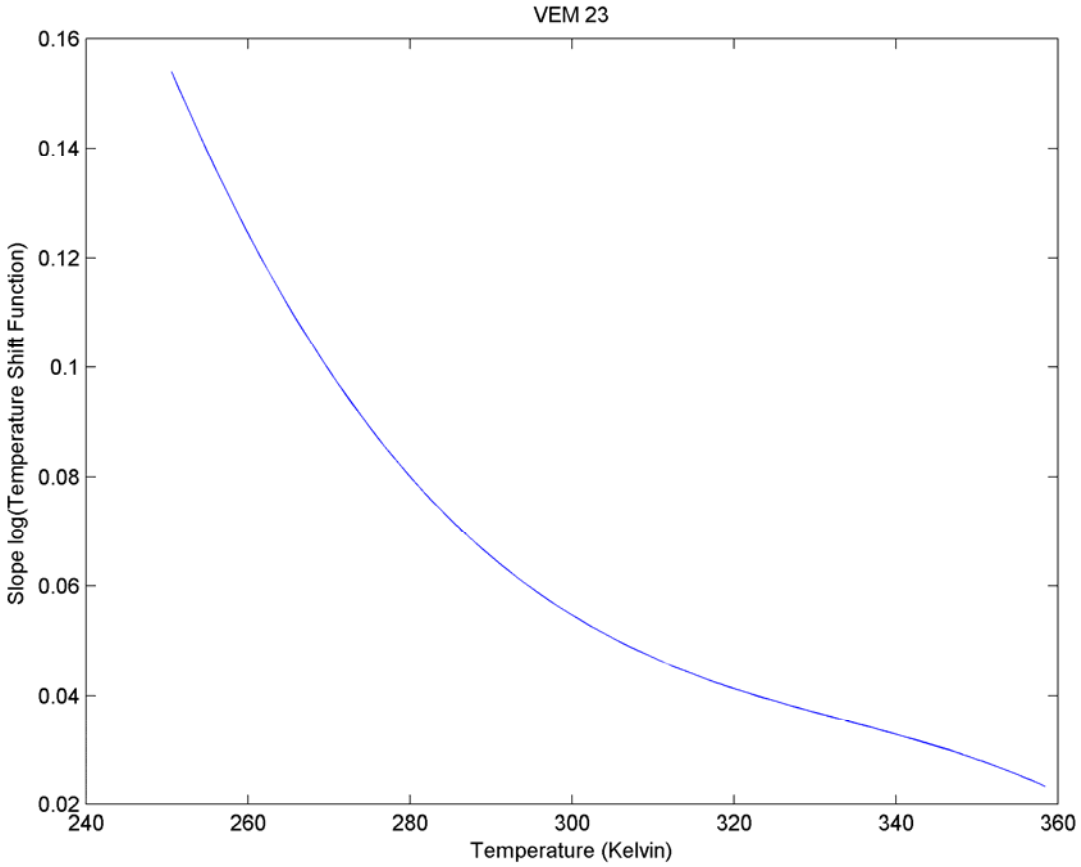

Figure 30: Slope of the TSF for VEM 23

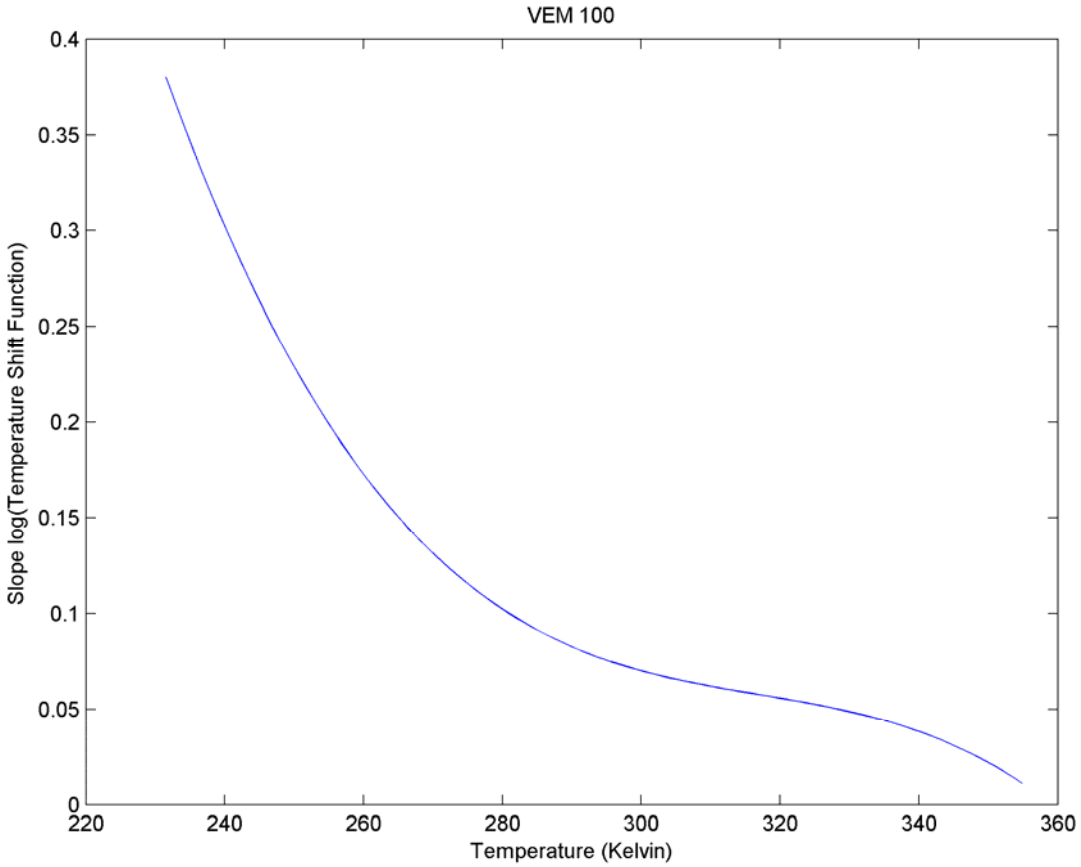

Figure 31: Slope of the TSF for VEM 100

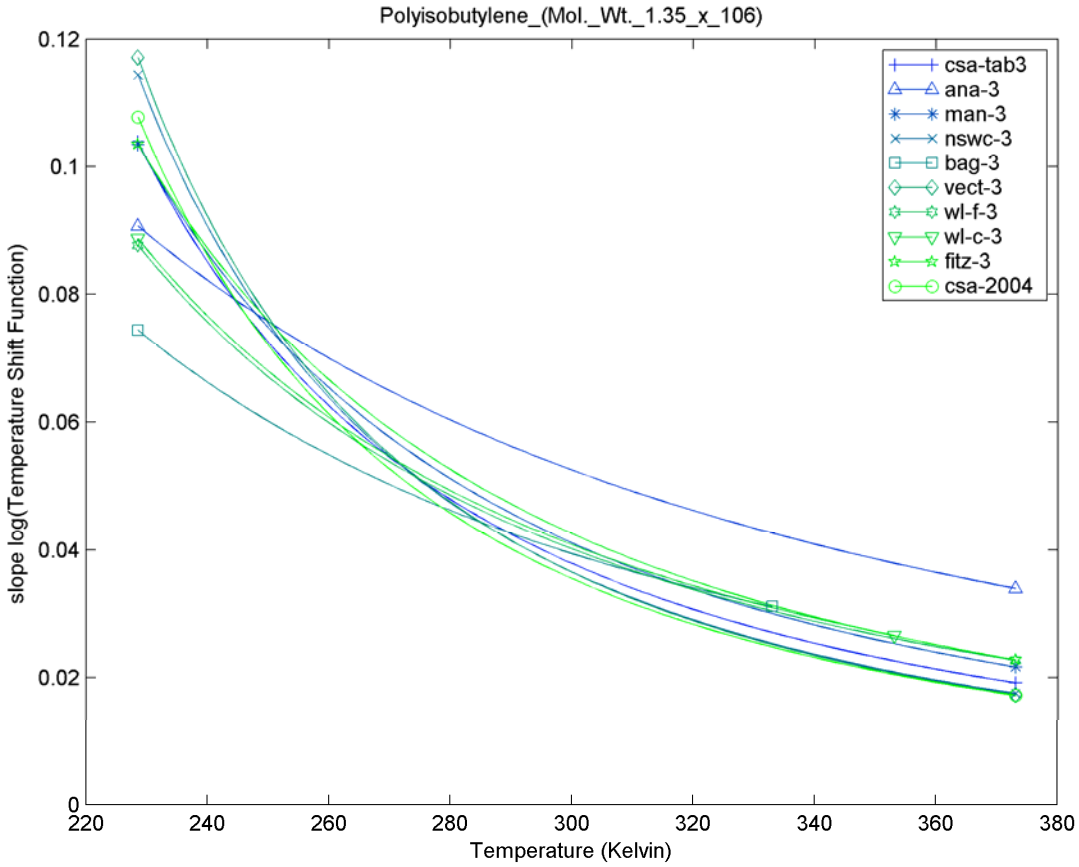

Figure 32: Slope of the TSF for VEM Polyisobutylene

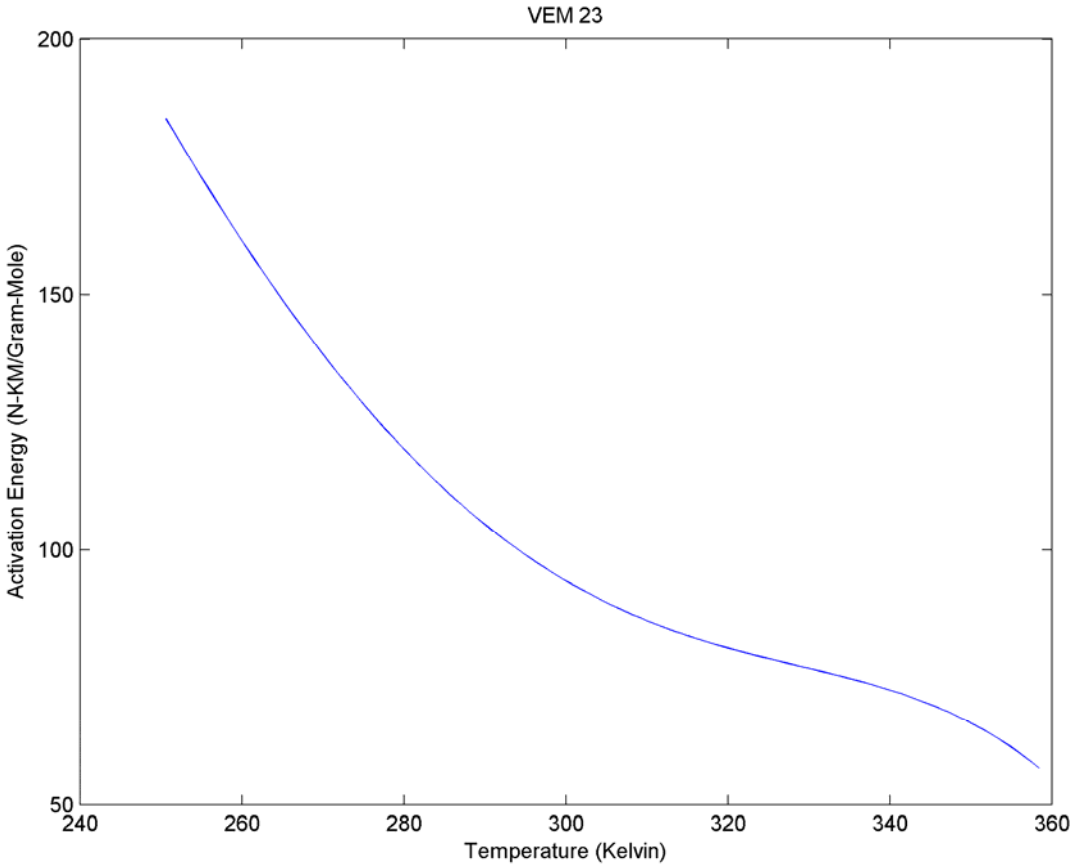

Figure 33: AAE for VEM 23

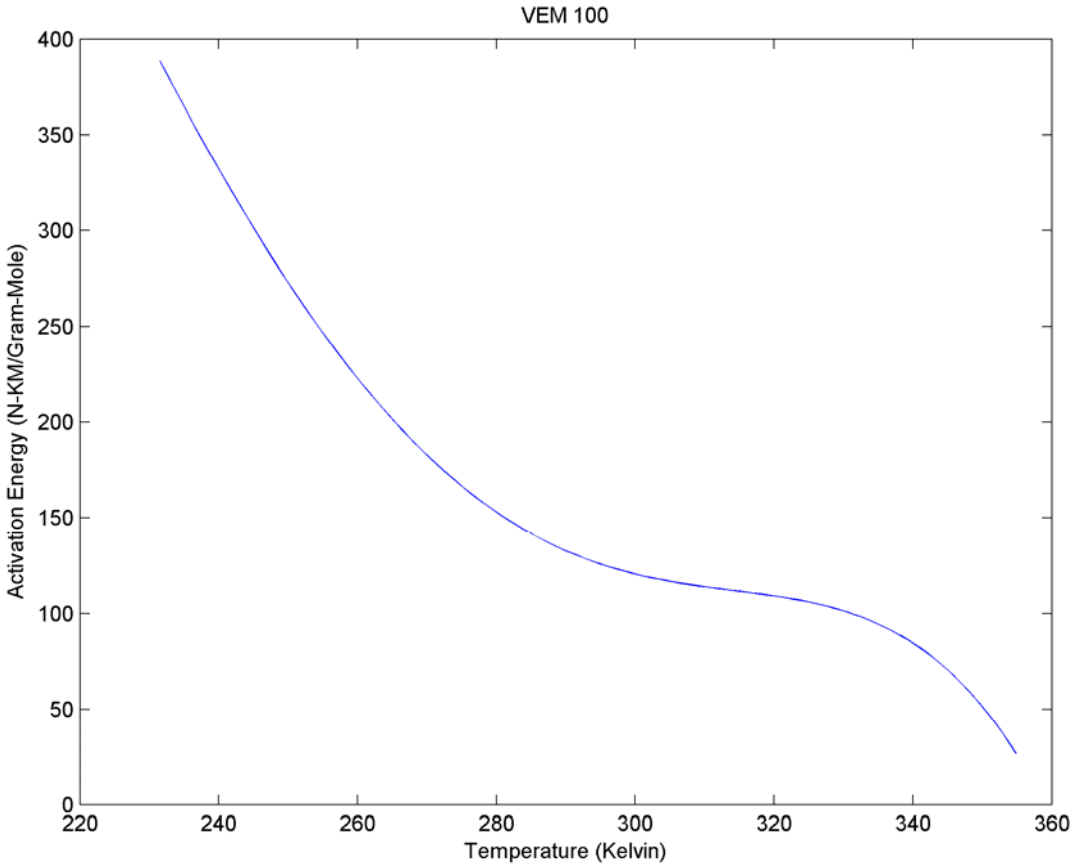

Figure 34: AAE for VEM 100

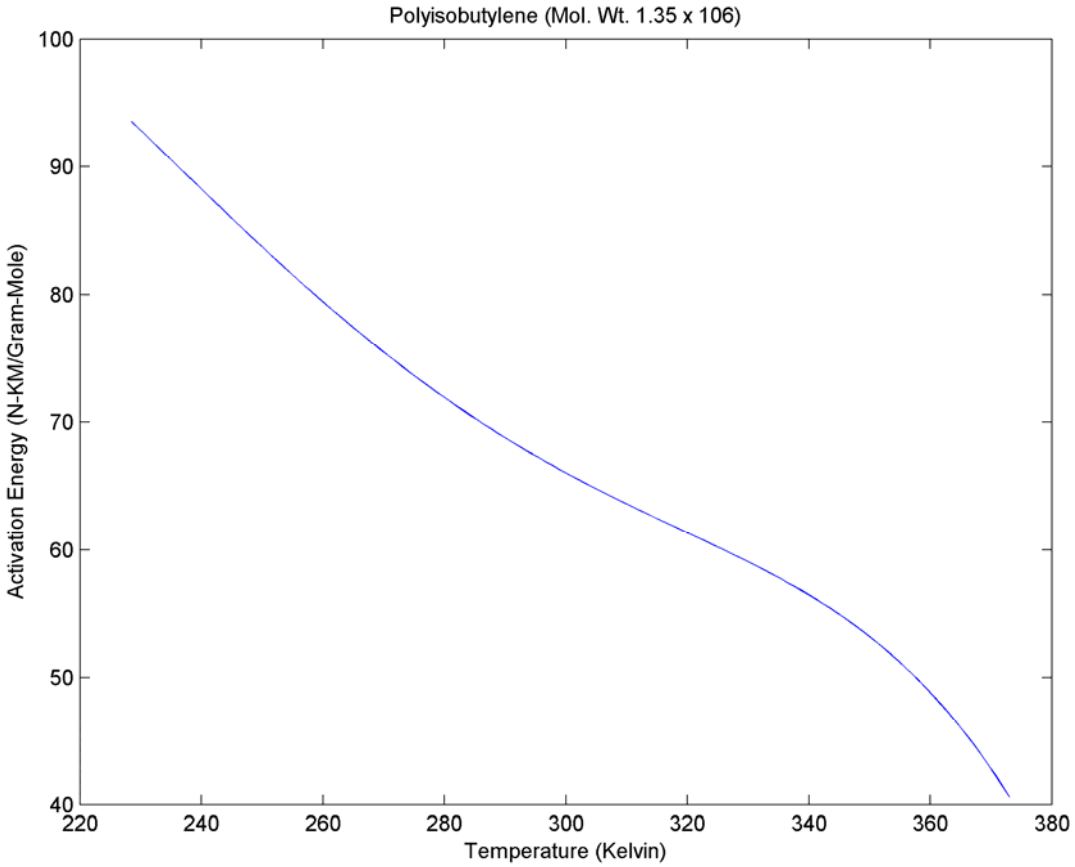

Figure 35: AAE for VEM Polyisobutylene

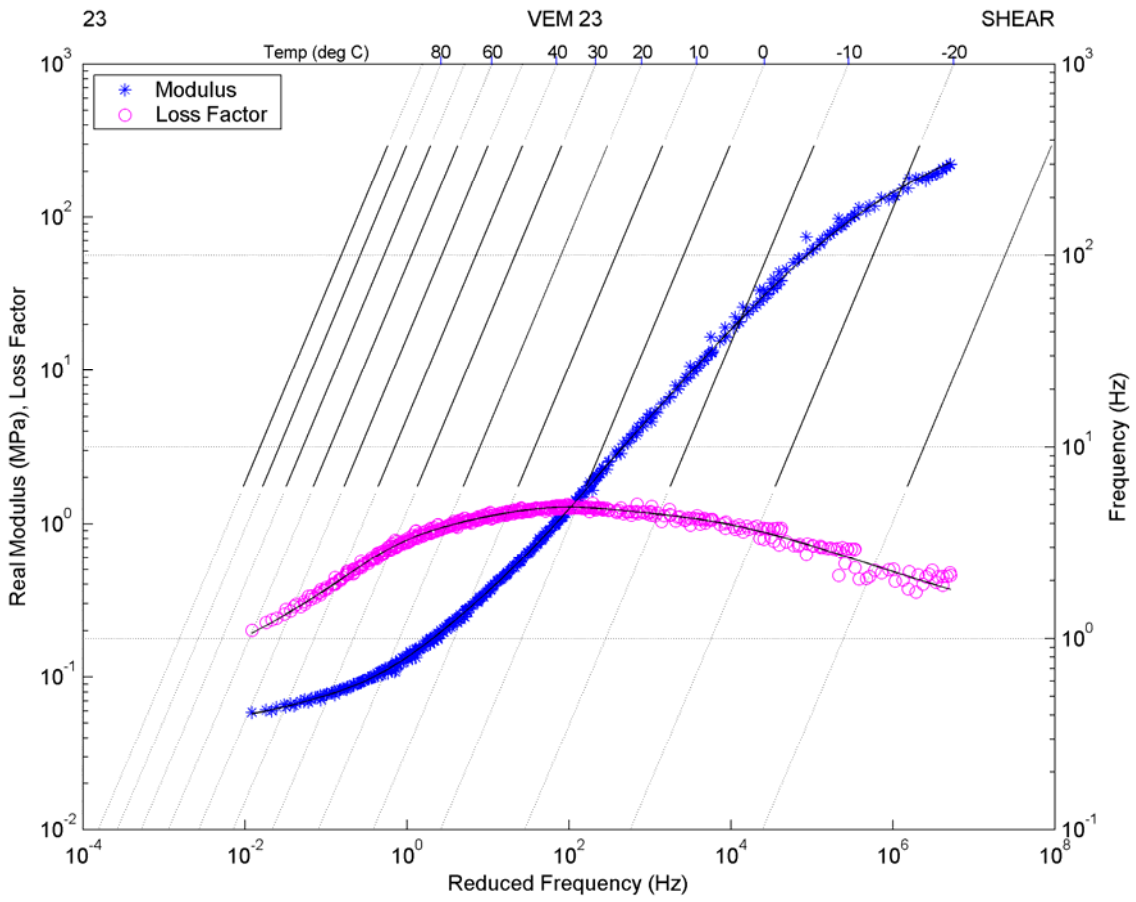

Figure 36: Nomogram for VEM 23

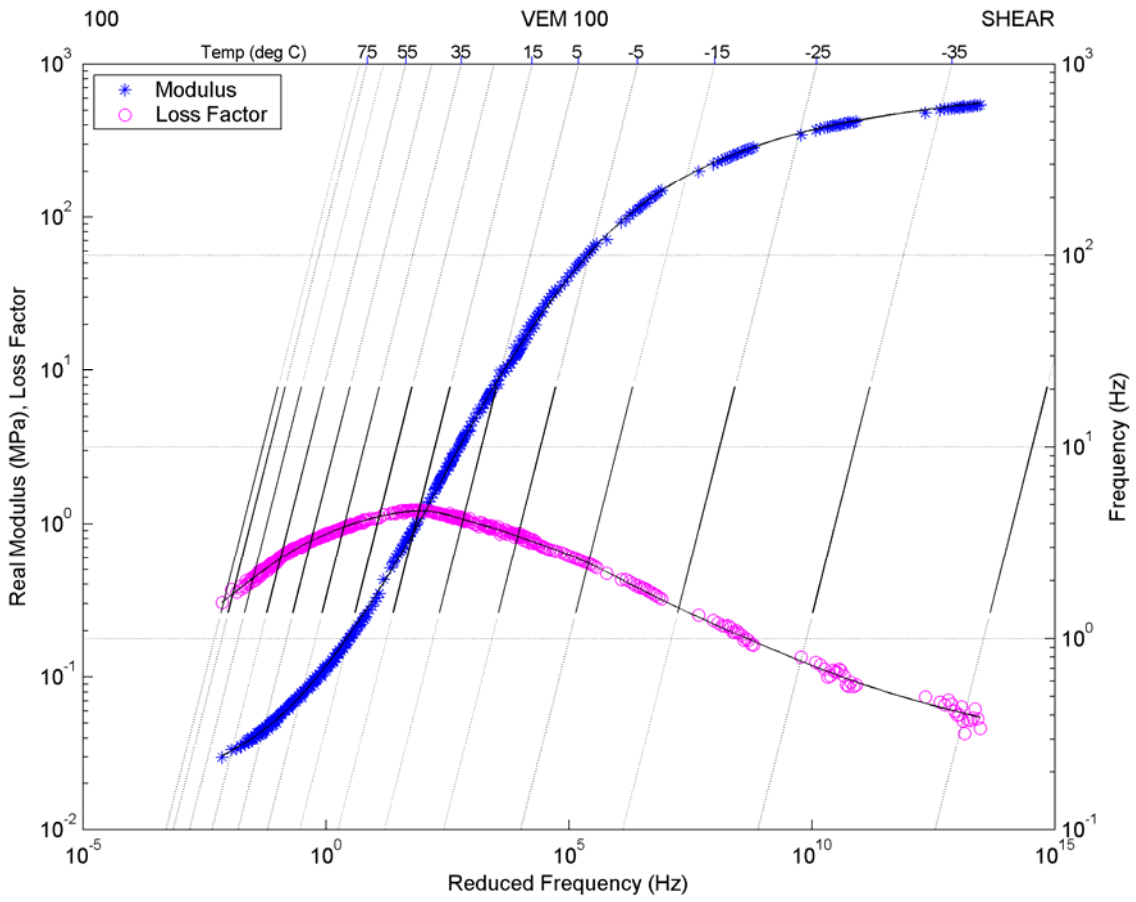

Figure 37: Nomogram for VEM 100

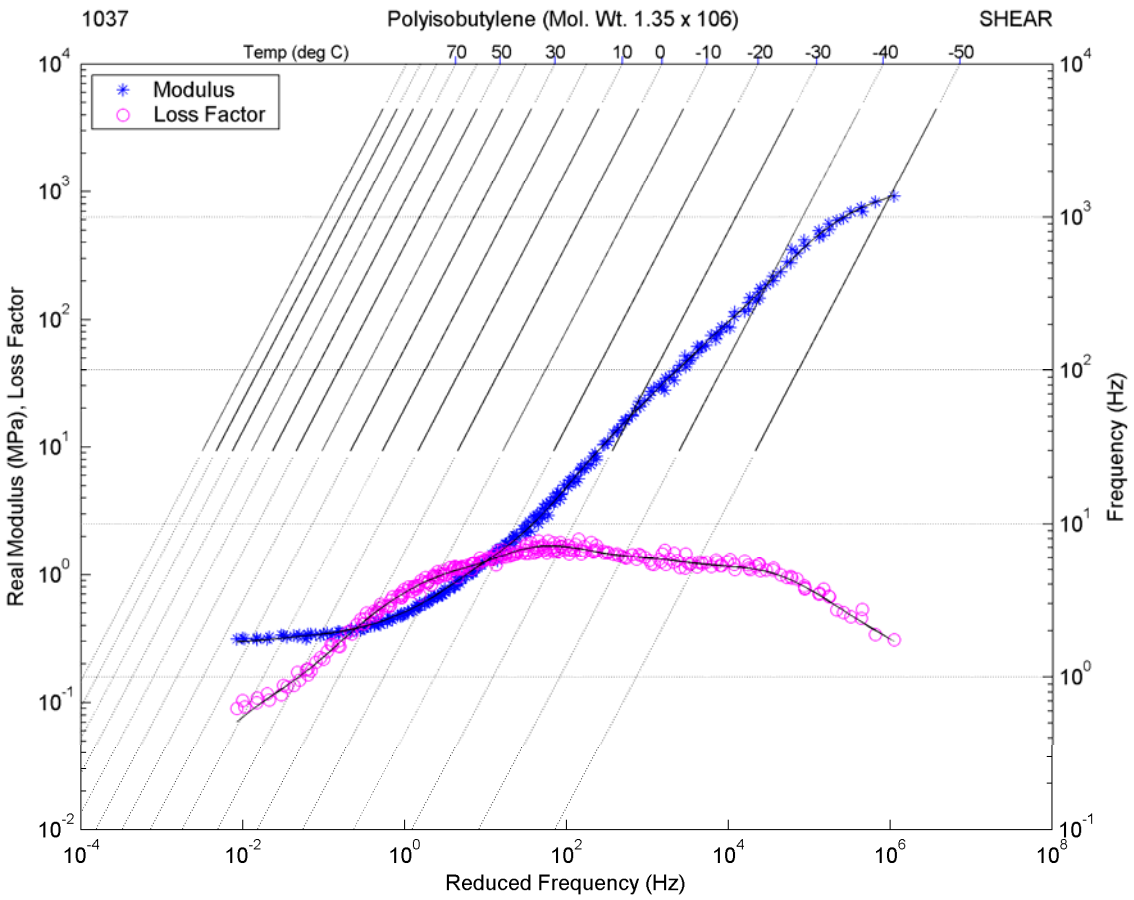

Figure 38: Nomogram for VEM Polyisobutylene

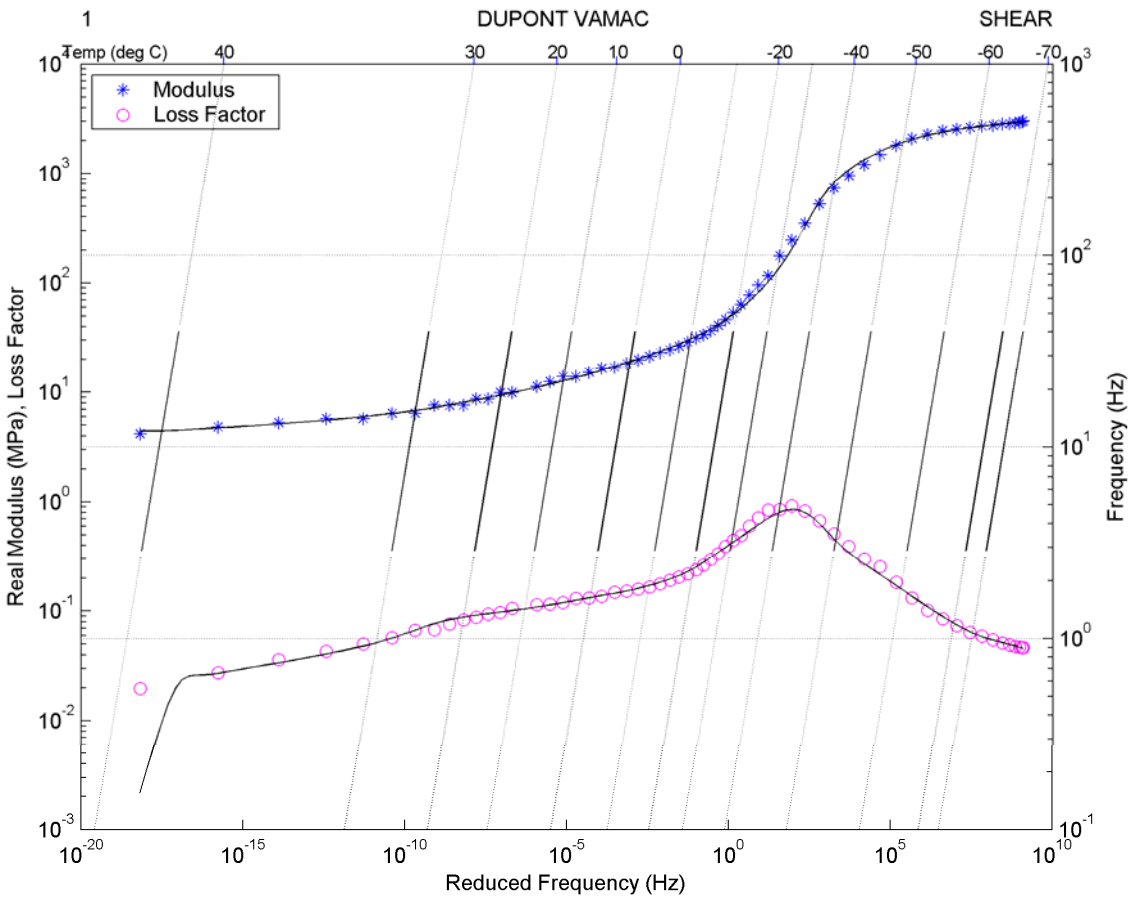

Figure 39: Nomogram for VEM VAMAC

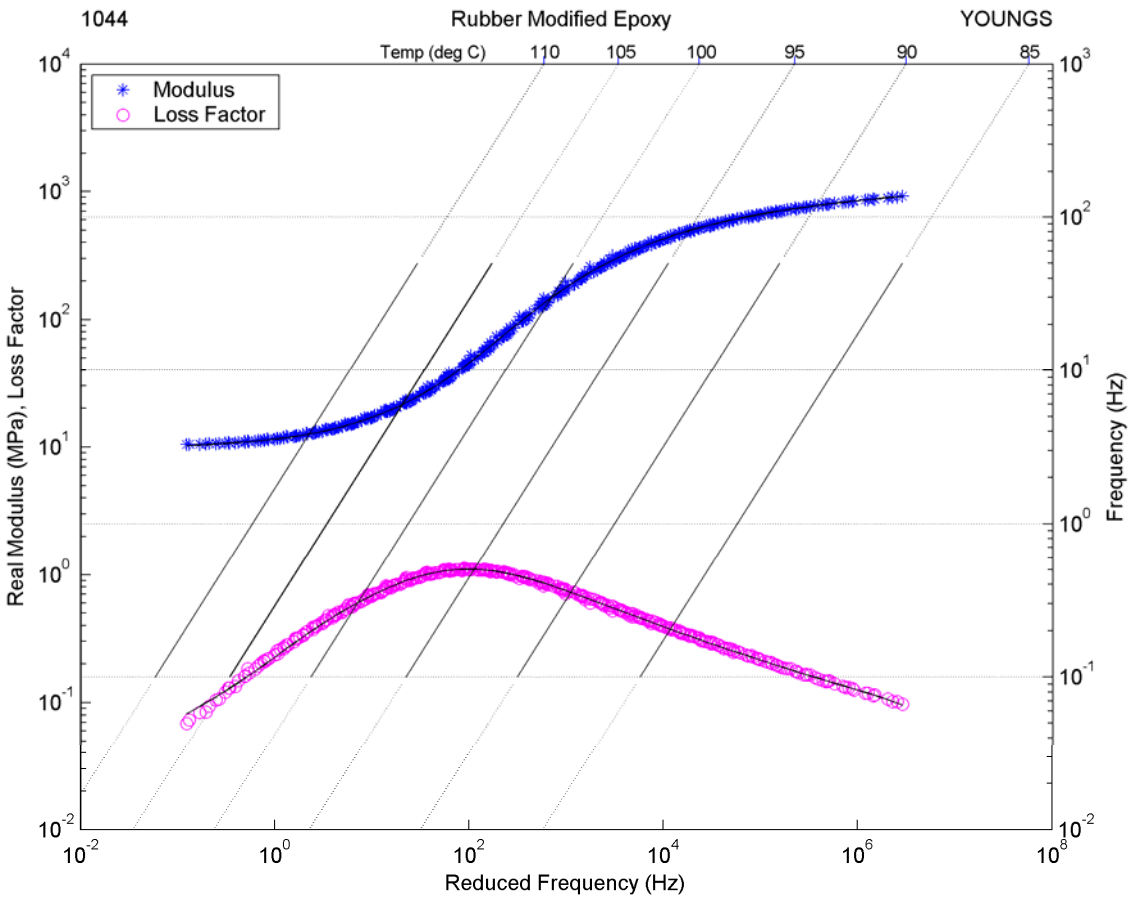

Figure 40: Nomogram for VEM Rubber Modified Epoxy

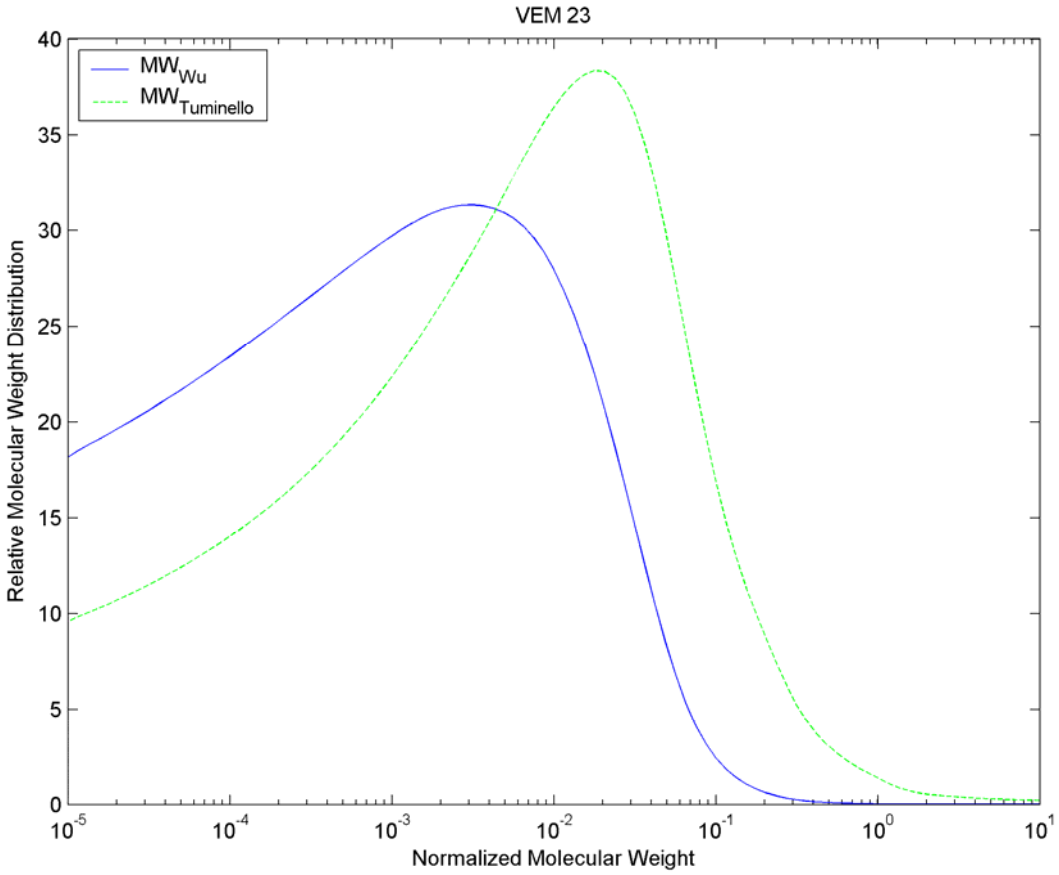

Figure 41: Molecular Weight Distribution for VEM 23

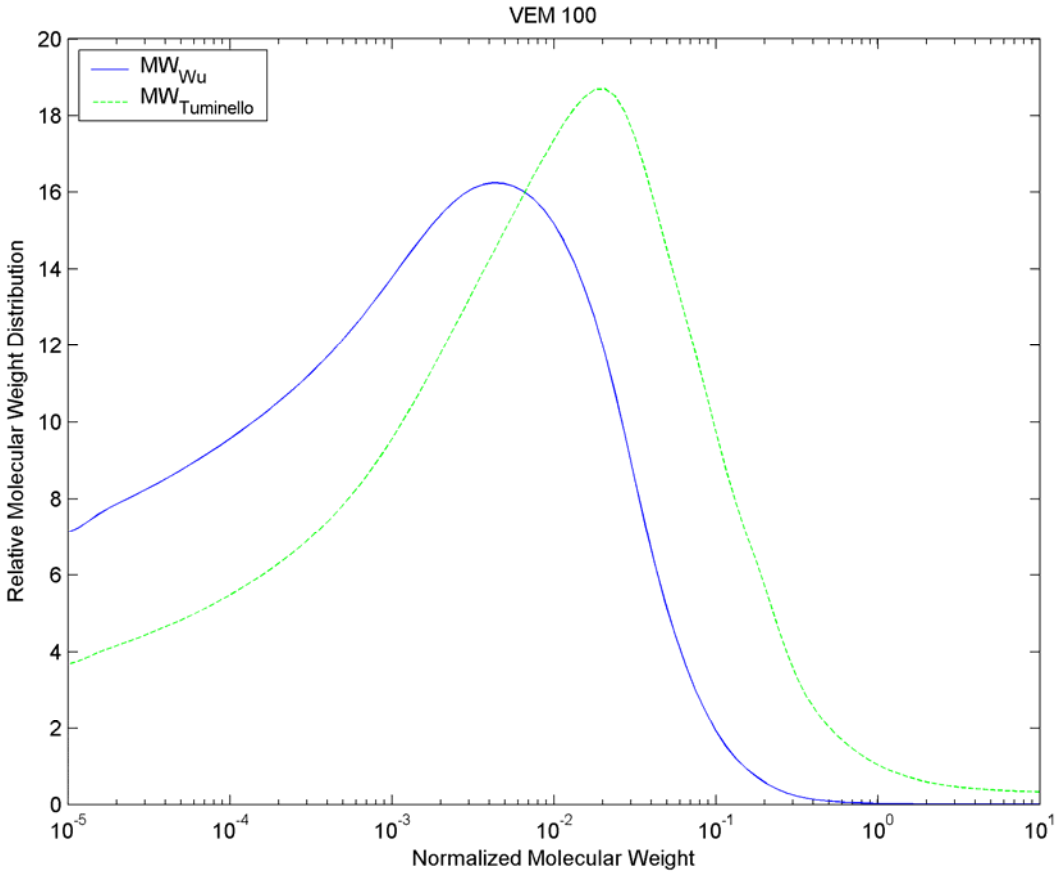

Figure 42: Molecular Weight Distribution for VEM 100

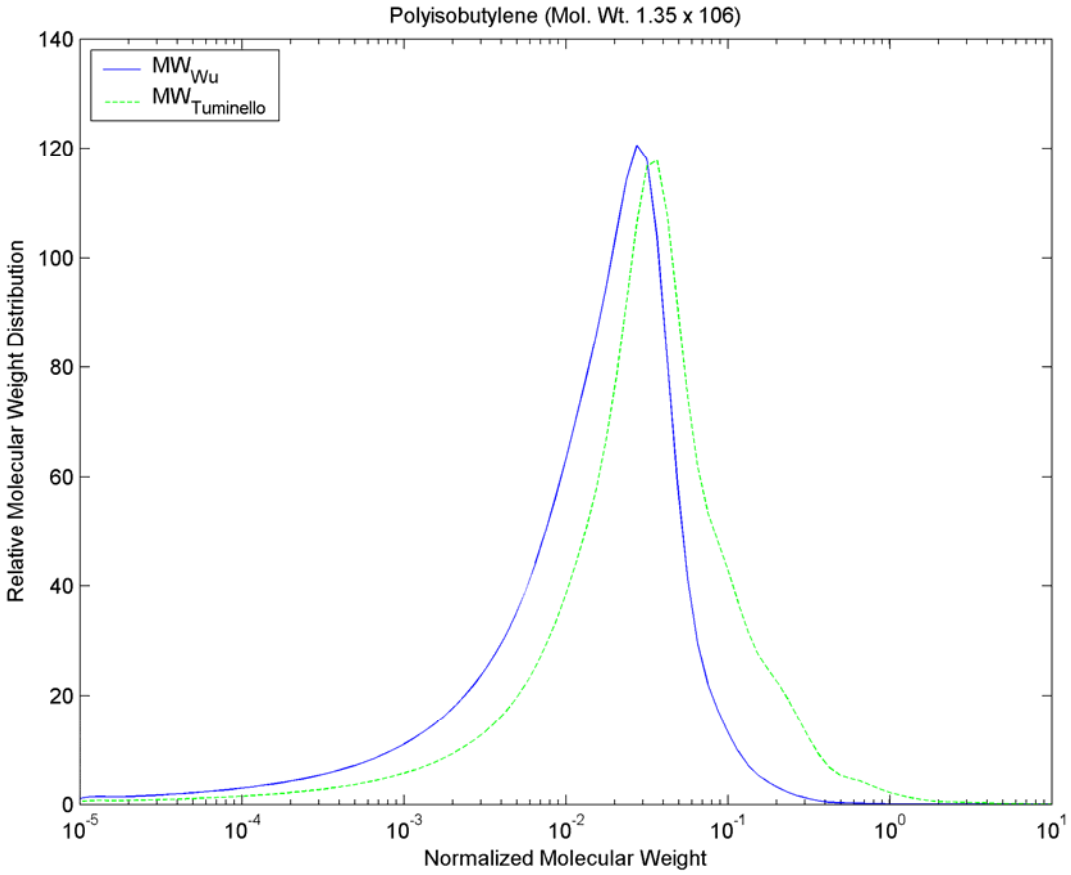

Figure 43: Molecular Weight Distribution for VEM Polyisobutylene

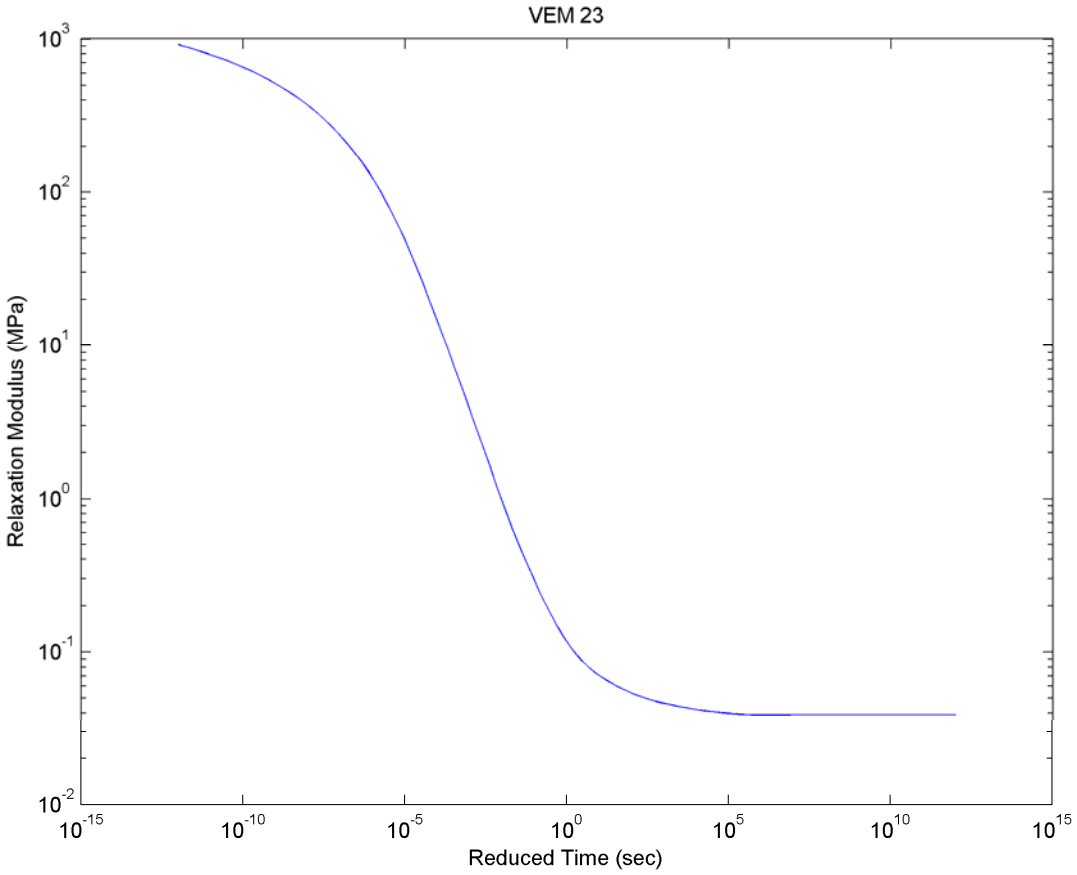

Figure 44: Relaxation Modulus for VEM 23

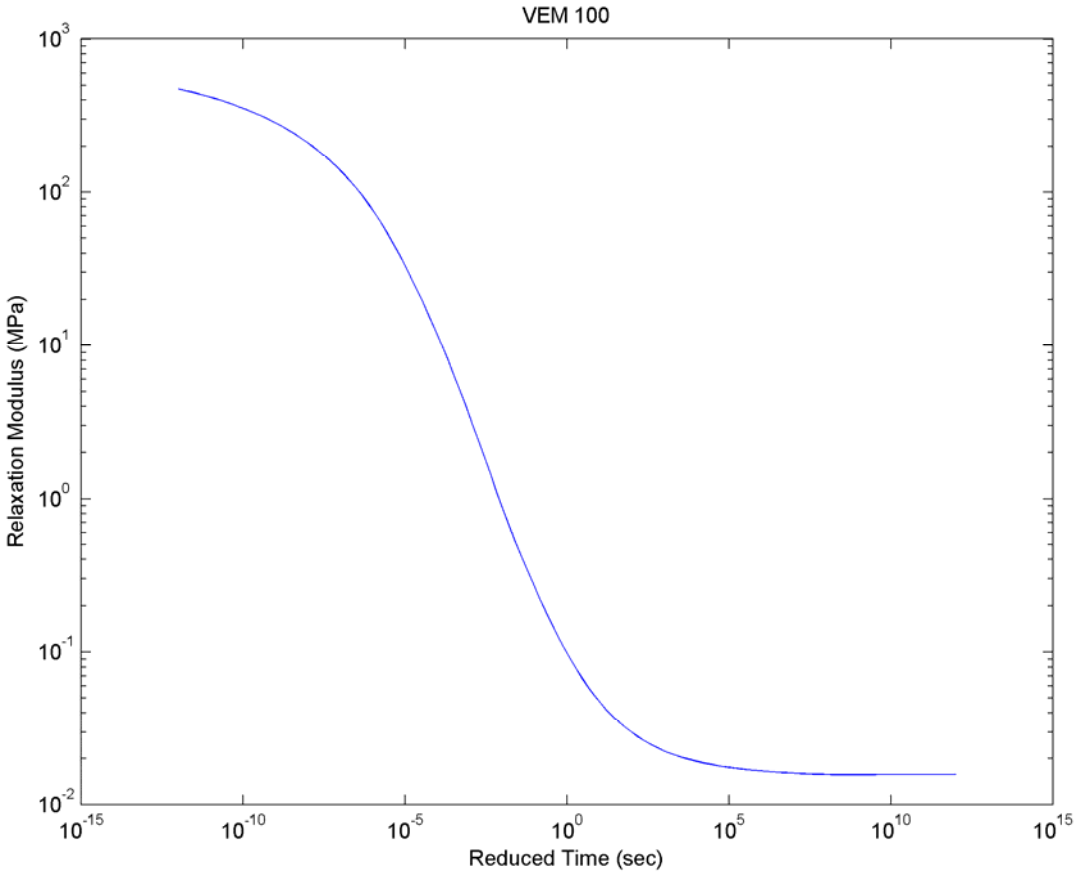

Figure 45: Relaxation Modulus for VEM 100

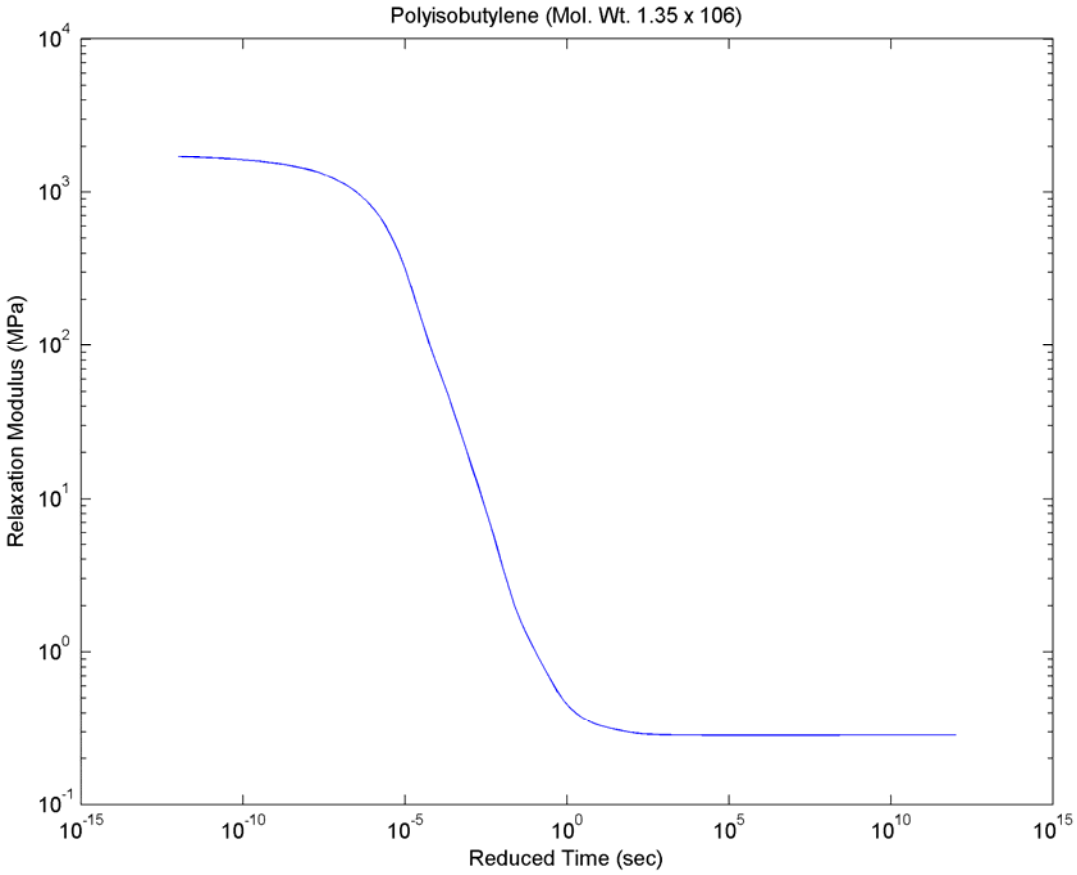

Figure 46: Relaxation Modulus for VEM Polyisobutylene

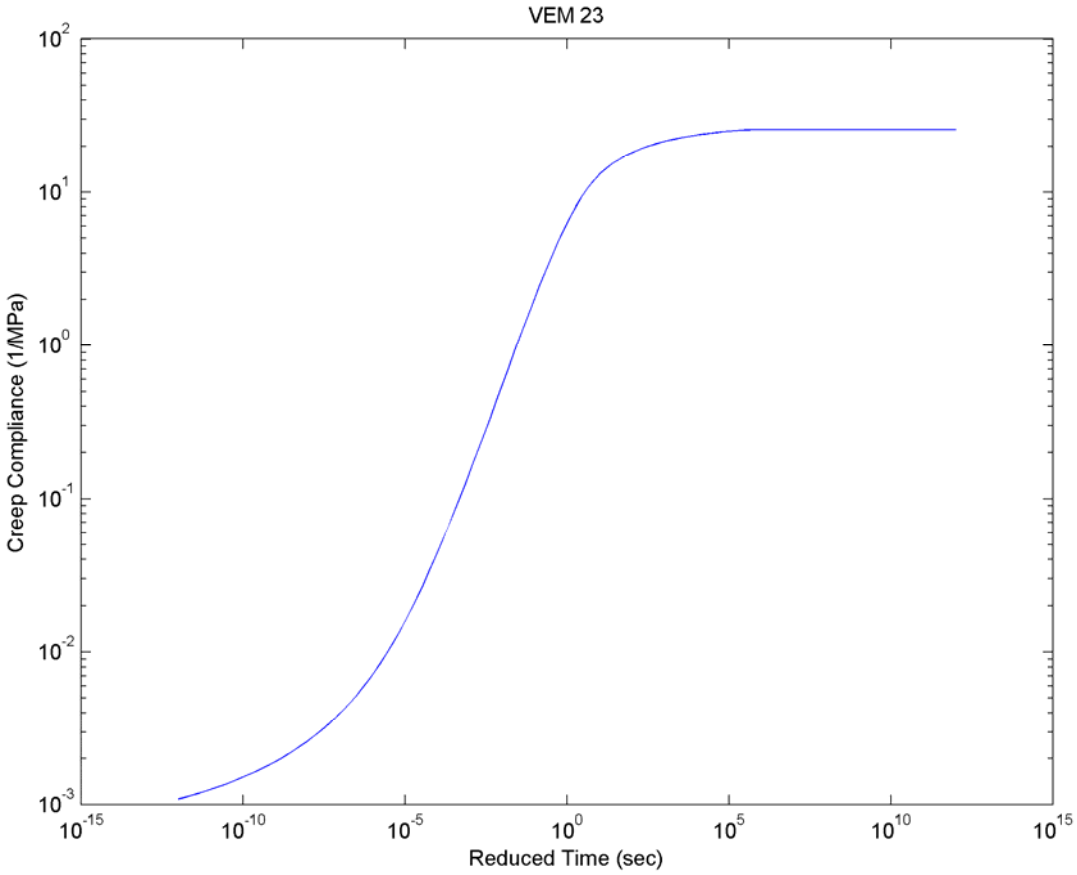

Figure 47: Creep Compliance for VEM 23

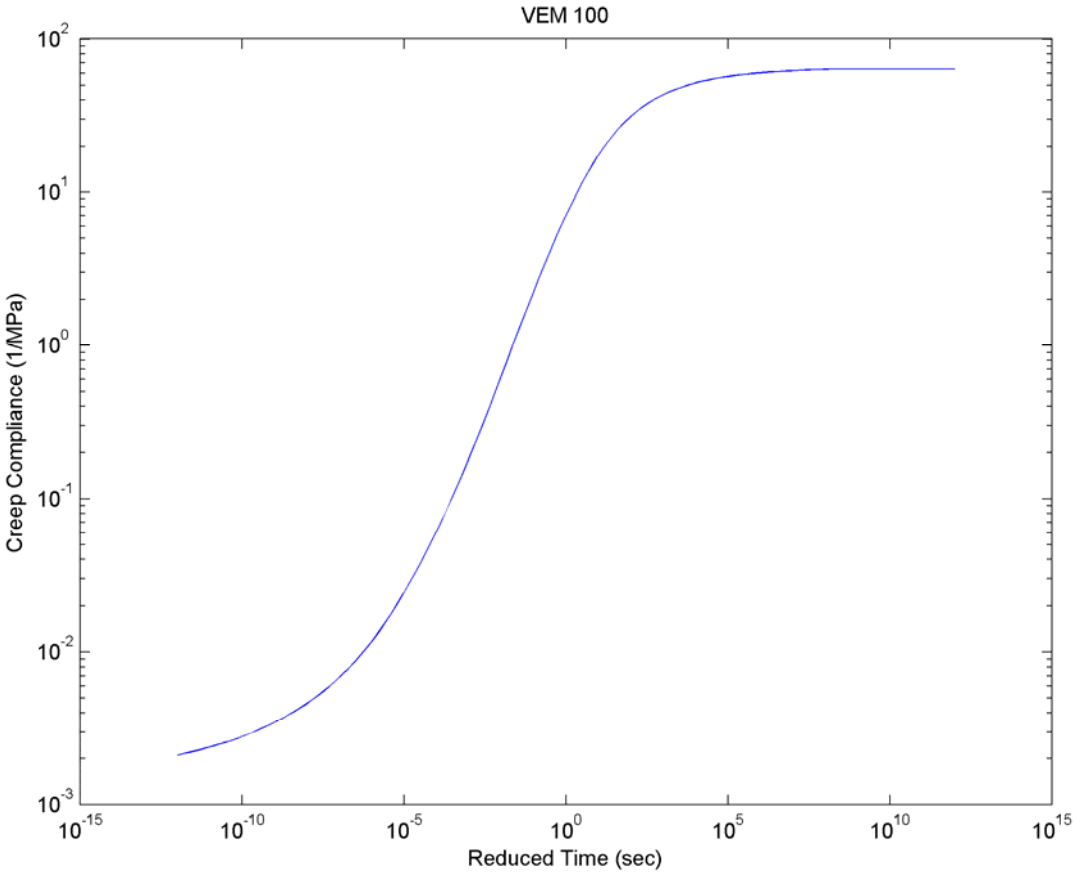

Figure 48: Creep Compliance for VEM 100

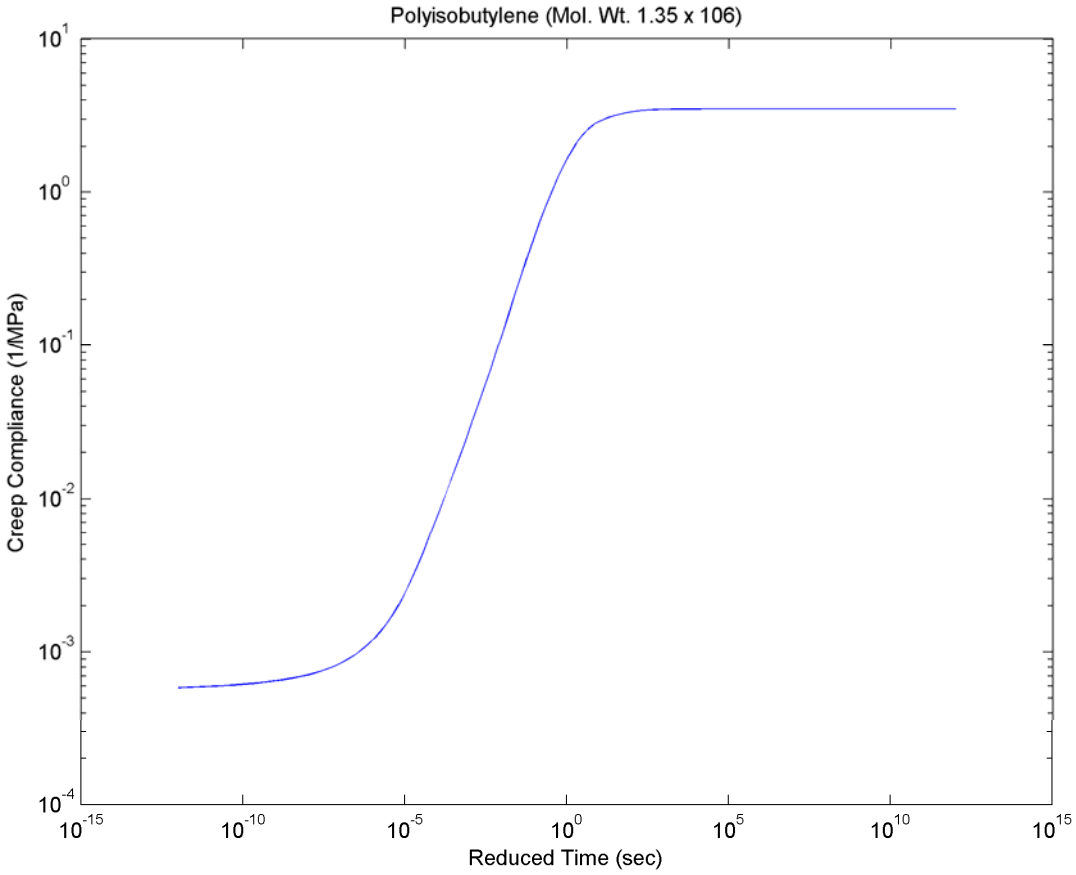

Figure 49: Creep Compliance for VEM Polyisobutylene

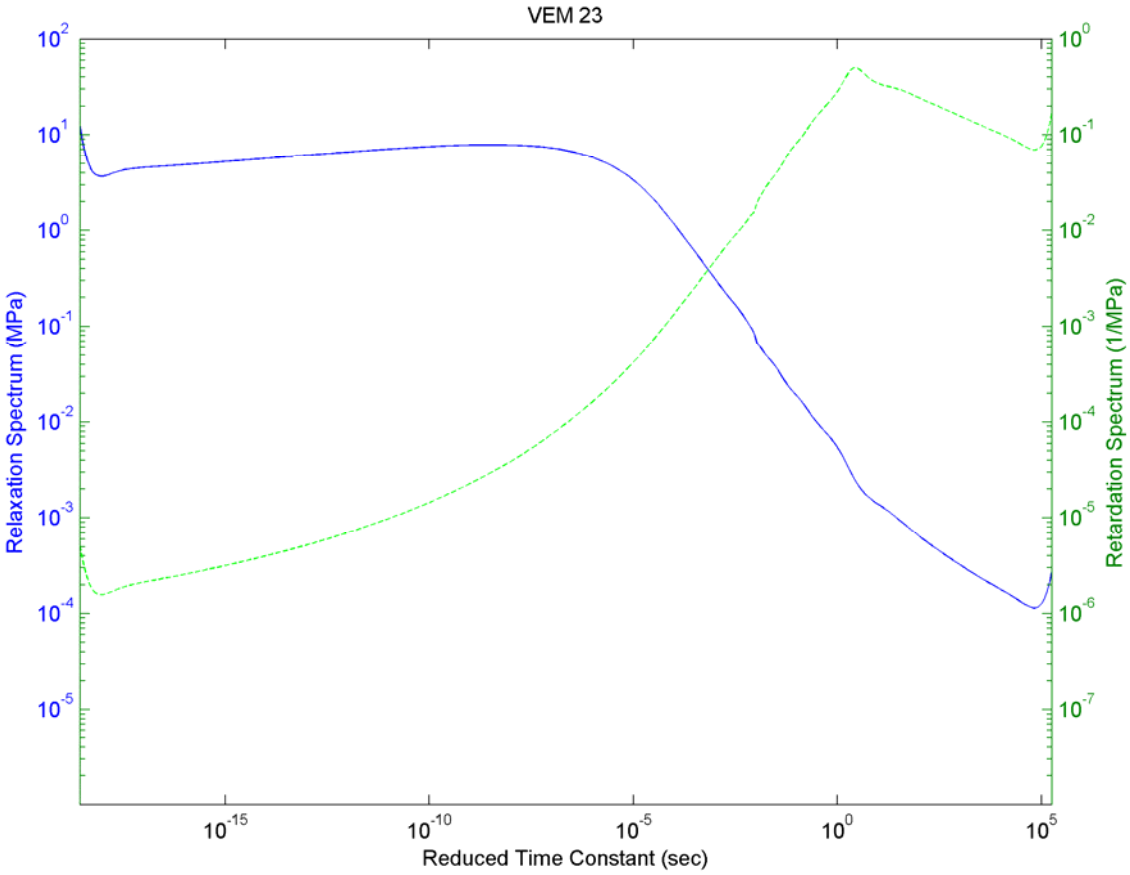

Figure 50: Relaxation and Retardation Spectra for VEM 23

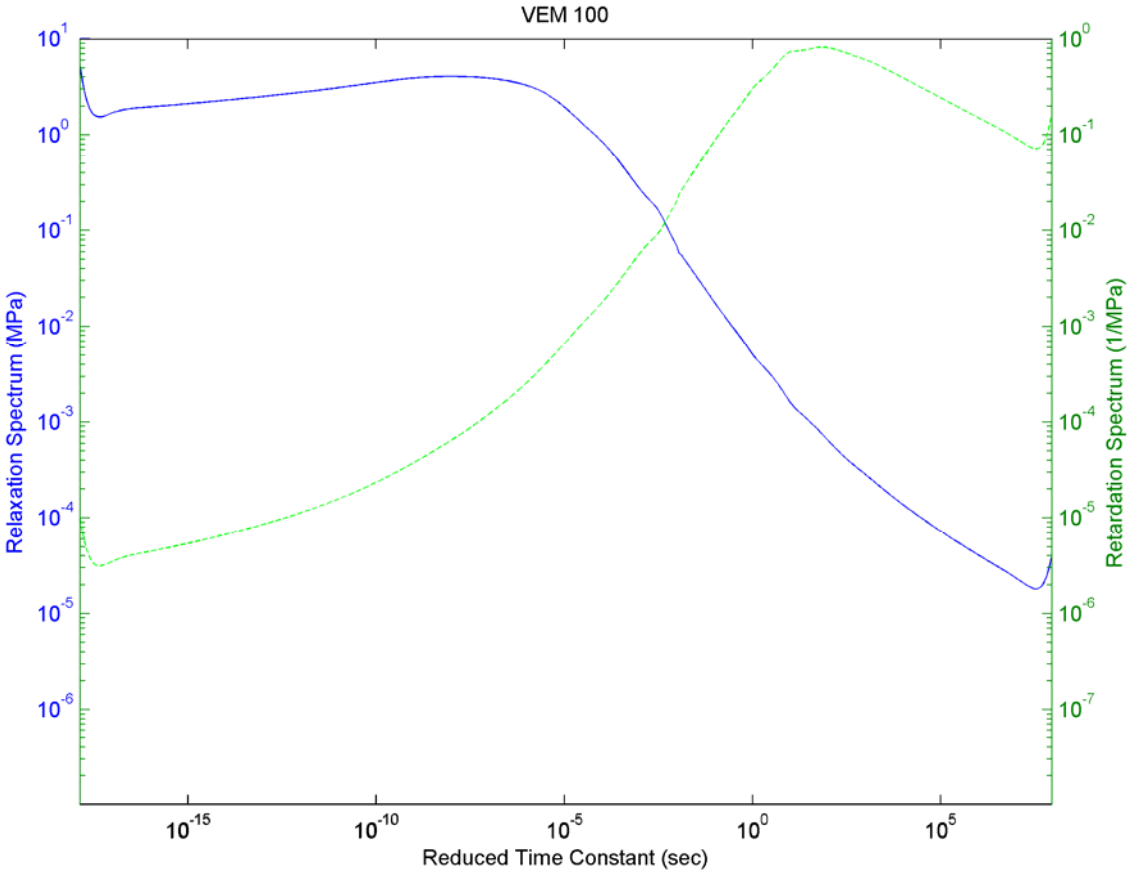

Figure 51: Relaxation and Retardation Spectra for VEM 100

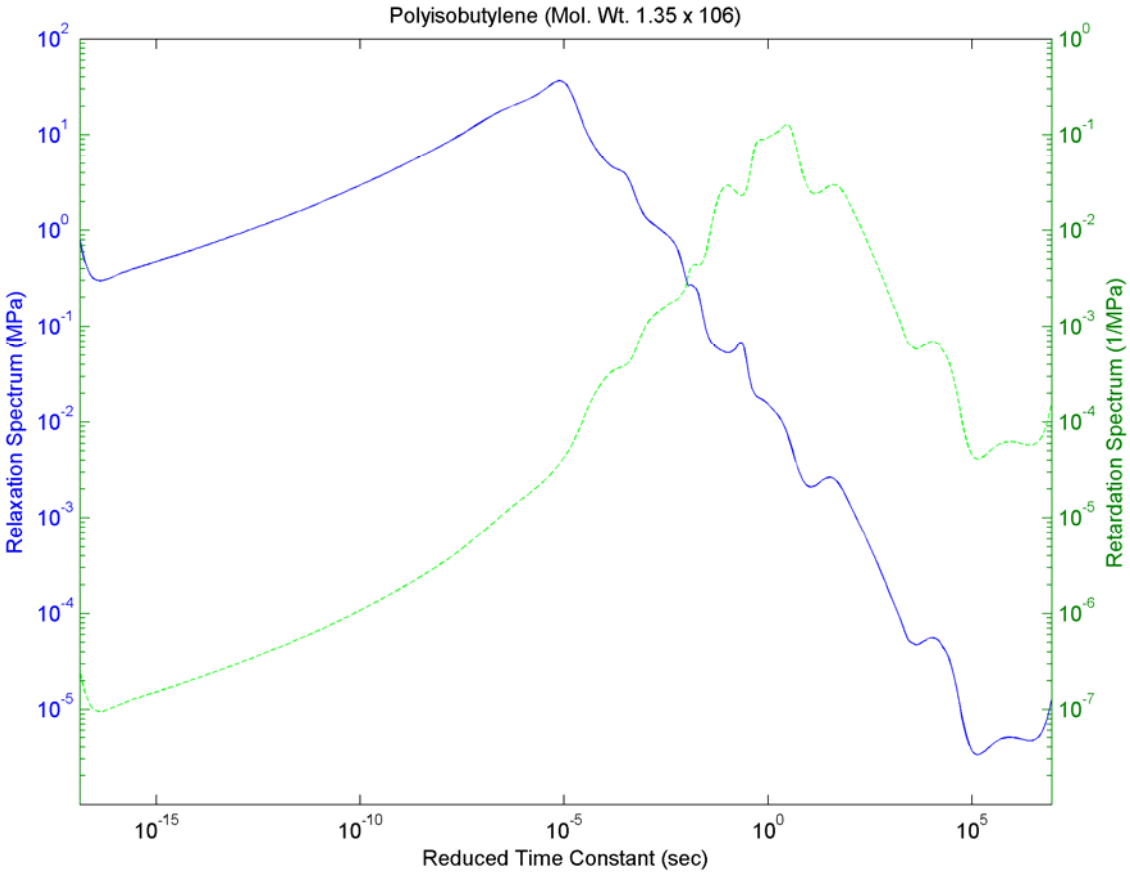

Figure 52: Relaxation and Retardation Spectra for Polyisobutylene

19 REFERENCES

1 B. Fowler, et al., "Viscoelastic Material Plot Database," 4 vols., USAF-WL-TR-93-3069 through -3072, 1993.

2 R.L. Bagley, “Applications of Generalized Derivatives to Viscoelasticity," AF Materials Lab TR-79-4103, November 1979. (Available from Defense Technical Information Center as AD A081131).

3 L. Rogers, “On Modeling Viscoelastic Behavior,” *Shock and Vibration Bulletin,* 51(1) pp. 55-69, May 1981.

4 L. Rogers, “Operators and Fractional Derivatives for Viscoelastic Constitutive Equations,” *J.Rheology,* 27(4), pp. 351-372 (1983).

5 R.L. Bagley and P.J. Torvik, “A Theoretical Basis for the Application of Fractional Calculus to Viscoelasticity,” *J. Rheology*, 27(3), pp. 201-210 (1983).

6 L. Rogers, “Temperature Shift Considerations for Damping Materials,” *Shock and Vibration Bulletin* (56) 1986.

7 L. Rogers, “An Accurate Temperature Shift Function and a New Approach to Modelling Complex Modulus,” *Shock and Vibration Bulletin* (59) 1989.

8 L. Rogers, “A New Algorithm for Interconversion of the Mechanical Properties of Viscoelastic Materials,” AIAA Paper No. 84 - 1038CP, AIAA Dynamic Specialists Conference, Palm Springs, CA, May 17 - 18, 1984.

9 M.L. Williams, “Structural Analysis of Viscoelastic Materials,” *AIAA Journal*, 2(5), pp. 785-808 (1964).

10 L. Rogers, et al., “Graphical Presentation of Damping Material Complex Modulus,” International Standards Organization, Standard No. ISO 10112:1991(E), 1991.

11 J.D. Ferry, *Viscoelastic Properties of Polymers*, 3rd ed., Wiley,1980.

12 A.D. Nashif, D.I.G. Jones, and J.P. Henderson, *Vibration Damping*, Wiley, 1985.

13 K.S. Cole and R.H. Cole, *J. Chem. Phys.*, 9, pp. 341-351 (1941).

14 B. Hartman, G.Lee, and J.Lee, "Loss Factor Height and Width Limits for Polymer Relaxations," *J. Acoust. Soc. Am.* 95 (1), pp. 226-233, January 1994.

15 S. Havriliak and S. Negami, "A Complex Plane Analysis of qqq alpha -dispersions in Some Polymer Systems," in Transactions and Relaxations in Polymers, *J. Polym. Sci.* Part C. No. 14, ed. By R.F. Boyer, (Interscience, NY, 1966), pp. 99-117.

16 Michelle Gobin epouse Salvia, "Proprietes Dynamiques des Propergols Solides Composites," These, L’Universite Claude Bernard Lyon, 1981.

17 C. Huet, Ann. Ponts et Chaussees, 6, 5 (1965).

18 B. Gross, “On Creep and Relaxation II,” *J. Appl. Phys*, V19, pp. 257-264, March 1948.

19 I.M. Horowitz, *Synthesis of Feedback Systems*, Academic Press, 1963, pp. 299-315.

20 H. Chestnut and R.W. Mayer, *Servomechanisms and Regulating System Design*, Vol. I, 2 ed., Wiley, 1959, p.324.

21 J.J. D’Azzo and C.H. Houpis, *Feedback Control System Analysis and Synthesis*, 2nd ed., Mcgraw-Hill, New York, 1966, pp. 175-194.

22 R.L. Bagley and P.J. Torvik, “On the Fractional Calculus Model of Viscoelastic Behavior,” *J. Rheology,* 30(1), pp. 133-155, (1986).

23 D.F. Golla and P.C. Hughes, "Dynamics of Viscoelastic Structures - a Time-Domain, Finite Element Formulation," *J. Appl. Mech.*, Vol. 52, pp. 897-906, December 1985.

24 D.J. McTavish and P.C. Hughes, "Prediction and Measurement of Modal Damping Factors for Viscoelastic Space Structure," *AIAA J.*, Vol. 30, No. 5, pp. 1392-1399, May 1992.
25 S. Wu, "Polymer Molecular Weight Distribution from Dynamic Melt Viscoelasticity," *Polymer Engineering and Science,*, Vol. 25, No. ?, pp. 122-128, February 1985.
26 W.H. Tuminello, “Molecular Weight Distributions of Tetrafluoroethylene-Hexafluoropropylene Copolymers,” *Polymer Engineering and Science,* Vol 29, No 10, pp. 645-653, May 1989.
27 L. Rogers, “An Accurate Temperature Shift Function and a New Approach to Modeling Complex Modulus,” *Shock and Vibration Bulletin*, (59) 1989.
28 D.I.G. Jones, “A Reduced Temperature Nomogram for Characterization of Damping Material Behavior,” *Shock and Vibration Bulletin*, 48(2), pp. 13-22, 1978.
29 D.I.G. Jones, “Results of Recent Analysis of the Frequency Temperature Behavior of Polyisobutylene,” *Damping ’93*, WL-TR-93-3103, June 1993, paper DCB.
30 J. Soovere and M.L. Drake, Aerospace Structures Technology Damping Design Guide Volume III - Damping Material Data, AFWAL-TR-84-3089, December 1985, pp.36-44.